MEIS1: AT THE CROSSROADS BETWEEN METABOLIC AND CELL CYCLE REGULATION

APPROVED BY SUPERVISORY COMMITTEE

Hesham Sadek, MD, PhD (Mentor)

Hiromi Yanagisawa, MD, PhD (Chair)

Eric Olson, PhD

Joseph Garcia, MD, PhD

DEDICATION

To my teachers, my parents and my family

MEIS1: AT THE CROSSROADS BETWEEN METABOLIC AND CELL CYCLE REGULATION

by

FATIH KOCABAS

DISSERTATION

Presented to the Faculty of the Graduate School of Biomedical Sciences

The University of Texas Southwestern Medical Center at Dallas

In Partial Fulfillment of the Requirements

For the Degree of

DOCTOR OF PHILOSOPHY

The University of Texas Southwestern Medical Center at Dallas

Dallas, Texas

August, 2012

MEIS1: AT THE CROSSROADS BETWEEN METABOLIC AND CELL CYCLE REGULATION

FATIH KOCABAS, Ph.D.

The University of Texas Southwestern Medical Center, Dallas, 2012

Mentor: HESHAM A. SADEK, M.D., Ph.D.

Stem cells undergo self-renewal, maintaining themselves in an undifferentiated state while generating differentiated cells that are required for the tissue homeostasis or repair. One intriguing feature of stem cells is their maintenance in their respective hypoxic niche. Survival in this low-oxygen microenvironment requires significant metabolic adaptation. However, little is known about stem cell metabolism, its regulation or its effect on stem cell function. We started our work by focusing on the most comprehensively characterized adult stem cell population, the hematopoietic stem cells (HSCs). We demonstrate that mouse and human HSCs utilize glycolysis instead of mitochondrial oxidative phosphorylation to meet their energy demands. Furthermore, we demonstrate that Meis1 and Hif-1α are markedly enriched in HSCs and that Meis1 functions upstream of the two master redox regulators Hif-1α and Hif-2α, where loss of

Meis1 results in a metabolic shift from glycolysis to mitochondrial oxidative metabolism, and increased oxidative stress, and loss of HSC quiescence. These results underscore the critical link between metabolism and cell cycle regulation of HSCs. We then sought to determine whether other stem cell populations share these unique metabolic characteristics. This strategy enabled us to identify the epicardium and the subepicardium of the heart as the cardiac hypoxic stem cell niche, which houses a metabolically distinct, Hif-1α positive population of glycolytic cardiac progenitors. Moreover, our studies indicate that Meis1, which regulates HSC metabolism and quiescence, also induces post-natal cell cycle exit and quiescence of cardiomyocytes through induction of synergistic cyclin dependent kinase inhibitor families. We demonstrate that both embryonic and adult deletion of Meis1 in cardiomyocytes results in widespread cardiomyocyte proliferation in the adult heart. Overall, our studies identify Meis1 as a critical transcriptional regulator of cell cycle and metabolism.

ACKNOWLEDGEMENTS

This work would not have been possible without the assistance of many. First of all, I thank my mentor, Dr. Hesham A. Sadek, for his invaluable mentorship, his steadfast enthusiasm, his encouragement to the scientific discipline required to be an effective scientist and for allowing me to pursue diverse scientific questions. The scientific environment in Sadek lab has been wonderful and fruitful. I would like to thank my colleagues Ahmed Mahmoud and Dr. Shalini Muradlihar who have provided me with invaluable scientific advice, friendship and support.

The many members of the Hill Lab, Mammen Lab, Garcia Lab, Alec Lab, DeBerardinis Lab, and Olson Lab have been invaluable for good advice that made this a productive experience. Thanks to Drs. Sarvjeet Singh and Diana Canseco at Mammen Lab and Dr. Rui Chen at Garcia Lab for technical advice and friendship. Thanks to the Jessica Sudderth at DeBerardinis Lab for her kindness and help with metabolic assays. I am especially indebted to our collaboration with Dr. Junke Zheng at Alec Lab. Our collaboration has been enjoyable as well as productive, and I have learned a lot from him on how to address scientific problems in hematology. In particular, I would like to thank Drs. Drazen Sosic, Arin Aurora and Enzo Porrello at Olson Lab for their friendship, technical advice and support.

Special thanks to Suwannee Thet for excellent assistance with genotyping and John McAnally for generation of transgenic mice. I am thankful to John Shelton and the histology core members for outstanding histology sections and technical advice with histological analysis and immunohistochemistry. Thanks to Dr. Mahesh Padanad for his careful and critical reading of dissertation.

I am grateful to our collaborators for kindly sharing mice and reagents. Specifically, I would like to thank Dr. Neal Copeland and Dr. Keith Humphries for providing the Meis1 floxed mice, Dr. Joachim R. Goethert at Universitaetsklinikum Essen for providing the Scl-Cre-ER^{T} mice and Dr. Joseph A. Garcia for Hif-1α floxed mice.

I thank the Division of Biomedical Sciences and the Genetics and Developmental Biology program, and the members of my committee, Drs. Eric Olson, Joseph A. Garcia, and Hiromi Yanagisawa for their time and effort. Their insights have been important in completing this work.

Finally, I am indebted to my parents for their love, patience and constant prayers. I am grateful to all my friends in Dallas area for having made these years filled with good memories, to my wife, Hatice, for her unwavering love and support and my daughter Refia for bringing so much joy into my life.

TABLE OF CONTENTS

PRIOR PUBLICATIONS

Fatih Kocabas*, Tugba Simsek* ,Junke Zheng*, Ralph J. DeBerardinis, Ahmed I. Mahmoud, Eric N. Olson, Jay W. Schneider, Cheng Cheng Zhang, Hesham A. Sadek. The Distinct Metabolic Profile of Hematopoietic Stem Cells Reflects Their Location in a Hypoxic Niche. Cell Stem Cell, Volume 7, Issue 3, 380-390, 3 September 2010.

Fatih Kocabas, Ahmed I. Mahmoud, Enzo Porrello, Drazen Sosic, Eric N. Olson, Ralph J. DeBerardinis, and Hesham A. Sadek. The Hypoxic Epicardial and Subepicardial Microenvironment. J Cardiovasc Transl Res. 2012 May 8.
DOI: 10.1007/s12265-012-9366-7.

Fatih Kocabas, Shalini Muralidhar, Hesham A. Sadek. New Frontiers in Cardiac Regeneration. Journal of Biomedicine and Biotechnology (invited review).

Fatih Kocabas*, Junke Zheng*****, Suwannee Thet, Ralph J. DeBerardinis, Chengcheng Zhang, Hesham A. Sadek. Meis1 Regulates the Metabolic Phenotype and Oxidant Defense of Hematopoietic Stem Cells (Under review at Blood).

Fatih Kocabas, Junke Zheng, Ralph J. DeBerardinis, Cheng Cheng Zhang, Hesham A. Sadek. Metabolic Profile of Human Hematopoietic Stem Cells (Submited).

Fatih Kocabas*, Ahmed I. Mahmoud*****, Shalini Muralidhar, Suwannee Thet, Enzo R. Porrello, Eric Olson, Hesham A. Sadek. Meis1 Is a Key Regulator of Post-Natal Cardiomyocyte Cell Cycle Arrest (In Preperation).

Enzo R.Porrello*, Ahmed I. Mahmoud*, Emma Simpson, **Fatih Kocabas**, Young-Jae Nam, David Grinsfelder, Beverly A. Rothermel, Eric N.Olson, Hesham A. Sadek**.** Regulation of Neonatal Heart Regeneration by the miR-15 Family (Submitted to PNAS).

Sheng-Min Shih, **Fatih Kocabas***, Benjamin D. Engel*, Thomas Bilyard*, Arne Gennerich, Wallace F. Marshall, Ahmet Yildiz. Intraflagellar Transport Drives Flagellar Surface Motility in *Chlamydomonas* (Submitted to Cell).

*Equal Contribution.

LIST OF FIGURES

LIST OF ABBREVIATIONS

ALL	Acute lymphoblastic leukemia
AML	Acute myeloid leukemia
Anoxia	Lack of oxygen
CFSE	5-(and-6) carboxyfluorescein succinimidyl ester
CFU	Colony forming unit
DAPI	4,6-diamidino-2-phenylindole
FACS	Fluorescence-activated cell sorting
FS	Fractional shortening
FTC	Fumitremorgin C
GCPs	Glycolytic cardiac progenitors
HIF-1	Hypoxia Inducible Factor-1
High MP	High Mitochondrial Potential
HPSCs	Hematopoietic progenitor/stem cells
Hypoxia	Decreased partial pressure of oxygen
low MP	Low Mitochondrial Potential
LT-HSCs	Long-term Hematopoietic Stem Cells
Meis1	Myeloid ecotropic viral integration site 1
MI	Myocardial infarction

MPB Cells	Mobilized peripheral blood cells
ROS	Reactive oxygen species
WBM	Whole bone marrow

PREFACE

Tissue homeostasis and repair are dependent on stem cells, which maintain themselves in an undifferentiated state by undergoing self-renewal while generating required differentiated cells (Weissman, 2000). One crucial underlying property of stem cells is their potency. Embryonic stem cells, for instance, are considered as pluripotent, which denotes their ability to differentiate into all types of cells required during development. On the other hand, most adult stem cells are considered as multipotent as they have capacity to differentiate into only lineage-restricted family of cells. Stem cells have been extensively studied for treatment of a wide range of diseases including neurological disorders, heart failure, diabetes, spinal cord injury, and leukemia. Hematopoietic stem cells (HSCs) are among the most widely studied adult stem cells due to their incredible potential (Gahrton and Bjorkstrand, 2000; Katzel et al., 2007). HSCs are a rare population of bone marrow cells located in the hypoxic endosteal regions of bone marrow. They are generally quiescent, maintained at G_0 phase of cell cycle and divide only in response to stimulus to replenish blood components. Their maintenance during the life of an organism requires complex interplay between extrinsic and intrinsic factors such as growth factors, transcription factors and cell cycle regulators (Blank et al., 2008; Pietras et al., 2011; Warr et al., 2011; Zon, 2008).

One of the most critical areas of research is regulation of cell cycle, as it has wide implications in regenerative biology and cancer (Funk, 1999; He et al., 2009; Park and Lee, 2003). Cell cycle regulation is a highly complex process that involves hundreds of genes that regulates cell cycle progression through cell cycle checkpoints, namely G1, G2 and Metaphase checkpoints(Malumbres and Barbacid, 2009; Park and Koff, 2001). Lessons learned from the cancer field indicate that dysregulation of cell cycle checkpoints and metabolism occur hand in hand (Malumbres and Barbacid, 2009; Zhou et al., 2010). Cancer cells preferentially metabolize glucose at higher rates using glycolysis, which is known as Warburg effect (Vander Heiden et al., 2009). This provides a short cut to produce enough ATP to meet energy demand. One accepted reason for preferential use of glycolysis by cancer cells *in vivo* is the lack of adequate supply of oxygen (Denko, 2008). The use of anaerobic glycolysis confers survival advantage to cancer cells in this hypoxic environment. Similarly, several stem cells have been reported to reside in hypoxic niches, which suggest presence of unique metabolic adaptations in stem cells (Mohyeldin et al., 2010). However, little is known about metabolic phenotype and its regulation or how metabolism of stem cells is linked to their cell cycle (Aguilar and Fajas, 2010; Buchakjian and Kornbluth, 2010). Therefore, we set out to outline the link between metabolism and cell cycle regulation of stem cells. Part I describes characterization of HSC metabolism, which led us to discover Meis1 as a novel transcriptional regulator of

cell cycle and metabolism in HSCs. Part II elucidates the role of Meis1 in regulation of postnatal cardiomyocyte cell cycle arrest.

PART 1 – UNIQUE METABOLIC PROFILE OF STEM CELLS

CHAPTER 1

INTRODUCTION

Stem cells are distinguished by their ability to remain undifferentiated and capacity to undergo self-renewal, which allow them to proliferate during fetal development and to be maintained throughout adult life (Weissman, 2000). An emerging hallmark of stem cell function relies on the specialized microenvironments, called niche. Stem cell niches are initially described in worms and flies, and later in mammals and defined as a microenvironment that supports the function and maintenance of stem cells trough integration of local and systemic factors (Doetsch et al., 1999a; Doetsch et al., 1999b; Kimble and White, 1981; Mohyeldin et al., 2010; Spradling et al., 1997; Xie and Spradling, 1998). Several adult stem cells has been suggested to reside in niches which show low partial pressure of oxygen, namely hypoxia (De Filippis and Delia; Mastrogiannaki et al., 2009; Mohyeldin et al., 2010; Morrison and Spradling, 2008; Nakada et al., 2011; Parmar et al., 2007; Urbanek et al., 2006). Neuronal stem cell niches, for instance, demonstrate charecteristics of hypoxic niche, where neuronal stem cells located in the subventricular zone (SVZ) of the lateral

ventricles and the subgranular zone (SGZ) of the dentate gyrus in the hippocampus (Mohyeldin et al., 2010; Panchision, 2009; Roitbak et al., 2010; Zhao et al., 2008). Mesenchymal stem cells (MSCs), however, are located in almost all tissues in relatively hypoxic perivascular niches (Crisan et al., 2008; Pasarica et al., 2009). Moreover, hematopoietic stem cells which are among the most widely studied adult stem cells have been shown to reside in the hypoxic endosteal regions of bone marrow(Perry and Li, 2012; Zhang et al., 2003).

Hematopoietic Stem Cells (HSCs)

HSCs are classified by their repopulation ability in lethally irradiated recipients (Weissman, 2000). The cells that can repopulate and maintain hematopoietic system for the rest of life are defined as Long-term HSCs (LT-HSCs). LT-HSCs give rise to short-term HSCs (ST-HSCs), which can only sustain hematopoietic system for several weeks (Zhong et al., 2005). Various markers have been identified that accurately identify HSCs (Weissman, 2000). Surface antigens and vital dyes have been extensively used for isolation of HSCs by fluorescent activated cell sorting (FACS) (Bhatia et al., 1997; Camargo et al., 2003; Conneally et al., 1997; Gothert et al., 2005; Kiel et al., 2005; Majeti et al., 2007; Osawa et al., 1996). Commonly used combination of surface antigens to isolate LT-HSCs are $CD34^{-}CD48^{-}CD150^{hi}Linage^{-}Sca1^{+}c\text{-}Kit^{+}$ and $CD34^{-}$, $Flk2^{-}Linage^{-}$

$Sca1^{+}c\text{-}Kit^{+}$ (Goodell et al., 1996; Huynh et al.; Kiel et al., 2005; Osawa et al., 1996; Wilson et al., 2008; Yilmaz et al., 2006). However, while HSC isolation relies on the expression of surface antigens or transporters, functional properties of HSCs remains to be determined for HSC enrichment protocols.

Hypoxic HSC Niche

HSC are known to reside in specialized niches within the bone marrow (Lilly et al., 2011). Previous studies suggest that the HSC niche in the endosteal regions of the bone marrow has limited perfusion and low levels of partial pressure of oxygen (PO_2) (average fifty-five mmHg) (Arai et al., 2004; Calvi et al., 2003; Draenert and Draenert, 1980; Harrison et al., 2002; Zhang et al., 2003). In addition, cells away from capillaries have been estimated to show 10-fold lower levels of PO_2 (Chow et al., 2001). Moreover, perfusion studies, using a Hoechst staining technique, demonstrated that HSCs predominantly reside in low perfusion compartments in the bone marrow (Parmar et al., 2007). Furthermore, HSCs are sensitive to hypoxic cytotoxin tirapazamine and show staining of hypoxia probe pimonidazole *in vivo* (Parmar et al., 2007). *In vitro* studies also indicate that HSC function and reconstitution ability are well preserved upon culturing in hypoxic conditions (Cipolleschi et al., 1993; Danet et al., 2003; Ivanovic et al., 2004). Finally, several reports also support the role of hypoxia in

the maintenance of HSCs quiescence (Goodell et al., 1996; Hermitte et al., 2006; Kim et al., 2002; Scharenberg et al., 2002; Shima et al., 2010). These findings suggest that HSCs reside in a hypoxic microenvironment and indicates the importance of hypoxia signaling in HSCs.

Hypoxia Signaling

All mammals express a highly conserved transcriptional complex that responds to decreased oxygen levels, namely hypoxia inducible factor (HIF) (Semenza, 2010). Hif-1 belongs to PER-ARNT-SIM subfamily of the basic helix-loop-helix (bHLH) family of transcription factors. It is composed of oxygen regulated Hif-1α subunit and constitutively expressed Hif-1β subunit (Semenza, 2010; Wang et al., 1995a; Wang and Semenza, 1995). Hif-1α initially discovered as the transcriptional regulator of erythropoietin gene (EPO) that controls the erythrocyte production (Semenza and Wang, 1992). Hif-1α activity is inherently dependent on oxygen levels and is unstable at normoxia (20% oxygen) such that its half-life is shorter than five minutes (Jewell et al., 2001; Yu et al., 1998). In normoxia, Hif-1α is hydroxylated by prolyl-hydroxylases (PHDs) and degraded through the ubiquitin-proteasome pathway following interaction with the von Hippel Lindau (VHL) protein (Bruick and McKnight, 2001; Epstein et al., 2001; Semenza, 2001, 2007a). PHDs use oxygen and α-ketoglutarate as substrates to

undergo enzymatic reactions to modify two proline residues (P402 and P564) of Hif-1α (Chowdhury et al., 2008; Kaelin and Ratcliffe, 2008). Hydroxylation of Hif-1α recruits VHL protein, which interacts with Elongin C/E3 ubiquitin-protein ligase for ubiquitination and degradation by proteasome complex. Under hypoxia, however, hydroxylation of prolyl residues is inhibited, which results in stabilization, formation of the Hif-1 complex, nuclear translocation, and transactivation of downstream genes.

Hif-1, which has hundreds of downstream target gene, plays a crucial role in cellular metabolism (Bunn and Poyton, 1996; Caro, 2001; Wang et al., 1995a). Hif-1 induces expression of glucose transporters and glycolytic enzymes such as hexokinase, aldolase, enolase, and lactose dehydrogenase A (Gatenby and Gillies, 2004; Iyer et al., 1998; Marin-Hernandez et al., 2009; Maxwell et al., 1999; Vander Heiden et al., 2009). Moreover, Hif-1 inhibits mitochondrial activity by repressing key enzymes in the Krebs cycle and preventing production of NADH and FADH2 delivered to the electron transport chain (Papandreou et al., 2006; Semenza, 2007c). In addition to preferential induction of glycolyisis and inhibition of mitochondrial respiration, Hif-1 inhibits mitochondrial biogenesis, which results in a metabolic shift from oxidative phosphorylation to anaerobic cytoplasmic glycolysis (Zhang et al., 2007). This metabolic shift may have significant consequences unrelated to metabolism, primarily related to the

production of reactive oxygen species (ROS) by the mitochondria, which is a major mediator of cellular oxidative stress.

Oxidative Stress

Mitochondrial oxidative phosphorylation is a major source of ROS production. It is estimated that about 2% of all electrons flowing through the respiratory chain, through premature transfer of electrons, result in generation of ROS (Turrens, 1997, 2003). ROS can lead to wide spread cellular damage by oxidizing proteins, lipids, and nucleic acids. Regulation of ROS is important for HSC function (Ergen and Goodell, 2010; Jang and Sharkis, 2007). HSCs located in the low ROS flow cytometry compartment show selective repopulation capacity (Jang and Sharkis, 2007). In addition, high levels of ROS is associated with loss of HSC function (Ergen and Goodell, 2010). Cells residing in hypoxic microenvironment gain protection against harmful effects of ROS through inhibition of mitochondrial metabolism by Hif-1α (Papandreou et al., 2006; Semenza, 2007c; Zhang et al., 2007) or induction of antioxidant genes by Hif-2α (Scortegagna et al., 2003a).

Hif-2α (EPAS1) has many similarities with Hif-1α but demonstrates distinct functional roles (Covello et al., 2006; Scortegagna et al., 2003a; Wiesener et al., 2003). While Hif-1α is expressed ubiquitously, expression of Hif-2α limited to

certain tissues (Covello et al., 2006; Scortegagna et al., 2003a; Wiesener et al., 2003). Hif-2α knockout mice show a number of defects in hematopoiesis, metabolism, and regulation of ROS (Scortegagna et al., 2003a; Scortegagna et al., 2005). Increased ROS in Hif-2α knockout mice was associated with lower expression of antioxidant genes such as *Cat*, *Gpx1*, *Sod1* and *Sod2* (Scortegagna et al., 2003a). Moreover, Hif-2α is associated with cardioprotection through transcriptional activation of Abcg2 in cardiac side population progenitors (Martin et al., 2008).

Cardiac Progenitor Cells

Recent reports indicate that the adult mammalian heart is capable of limited, but measurable, cardiomyocyte turnover (Bergmann et al., 2009; Laflamme and Murry, 2011; Laflamme et al., 2002; Loffredo et al., 2011; Segers and Lee, 2008). While the lineage origin of the newly formed cardiomyocytes is not entirely understood, mounting evidence suggest that they may be derived from an unidentified cardiac progenitor population (Laflamme and Murry, 2011; Loffredo et al., 2011). A number of resident cardiac progenitor cells are identified based on the expression of surface markers such as c-kit, Scal-1 and Isl-1, epicardial localization, dye exclusion or in vitro culture (Barile et al., 2007; Bearzi et al., 2007; Chong et al., 2011; Martin-Puig et al., 2008; Matsuura et al., 2004; Oh et

al., 2003; Passier et al., 2008; Segers and Lee, 2008; Slukvin, 2011; van Vliet et al., 2008). Many of these cardiac progenitor cells demonstrate capacity for self-renewal, clonogenicity, can differentiate into cardiomyocyte and vascular lineages *in vitro* and express cardiac genes such as GATA-4, Nkx2.5 and MEF2, which are important for cardiac development (Bearzi et al., 2007; Martin-Puig et al., 2008; van Vliet et al., 2008). Willms` tumor 1 gene (WT1) is another important transcription factor that has been identified in cardiac progenitors (Zhou et al., 2008). Lineage tracing studies demonstrate that WT1 expressing epicardial cells differentiate into cardiomyocytes during cardiac development and contribute to de novo cardiomyocytes following injury in adult mouse hearts (Smart et al., 2011; Zhou et al., 2008). Intriguingly, Hif-1 has been shown to play an important role in the regulating WT1 expression *in vitro* and *in vivo* (Scholz and Kirschner, 2011; Wagner et al., 2002; Wagner et al., 2003).

Several studies suggested presence of cardiac progenitor cell niches based on the staining of surface marker Isl-1 (Laugwitz et al., 2005; Schenke-Layland et al., 2011). However, recent studies on lineage of Isl-1+ cells in adult heart demonstrated that Isl-1+ positive cells are a marker of adult sinoatrial node rather than cardiac progenitors or cardiac stem cell niche (Weinberger et al., 2012). Hypoxia could be considered as common theme for adult stem cell niches, where stem cells preferentially utilize cytoplasmic glycolysis to meet their energy

demands. However, it is unclear if the heart harbors similar hypoxic regions, or whether these regions house metabolically distinct cardiac progenitor populations.

CHAPTER TWO

THE DISTINCT METABOLIC PROFILE OF HEMATOPOIETIC STEM CELLS REFLECTS THEIR LOCATION IN A HYPOXIC NICHE

INTRODUCTION

The microenvironment, or niche, plays a crucial role in self-renewal and differentiation of hematopoietic stem cells (HSCs) (Fuchs et al., 2004; Spradling et al., 2001). One of the hallmarks of the HSC niche is its low oxygen tension, hence the term "hypoxic niche" (Chow et al., 2001; Parmar et al., 2007). This low oxygen environment is not only tolerated by HSC, but also appears to be essential for their function (Bradley et al., 1978; Chow et al., 2001; Cipolleschi et al., 1993; Danet et al., 2003; Eliasson and Jonsson; Katahira and Mizoguchi, 1987; Koller et al., 1992; Kubota et al., 2008; LaIuppa et al., 1998; Lo Celso et al., 2009; Parmar et al., 2007). The mechanism of this hypoxic tolerance of HSCs, while poorly understood, requires significant metabolic adaptation.

Hif-1 is a master regulator of metabolism. It regulates both glycolysis and mitochondrial respiration, inducing a metabolic shift towards anaerobic glycolysis (Hagg and Wennstrom, 2005; Kim et al., 2006b; Marin-Hernandez et al., 2009;

Maxwell et al., 2007; Papandreou et al., 2006; Wang et al., 1995a; Zhang et al., 2007). Hif-1 function is dependant on dimerization of the constitutively active *Hif-1β* subunit and the tightly regulated *Hif-1α* subunit. *Hif-1α* undergoes hydroxylation, followed by ubiquitination and degradation during normoxia in most cells (Ivan et al., 2001; Jaakkola et al., 2001; Kamura et al., 2000; Maxwell et al., 1999; Salceda and Caro, 1997). Upregulation of *Hif-1α* can occur either by transcriptional activation (Hirota et al., 2004; Laughner et al., 2001) or protein stabilization (Li et al., 2005; Nakayama et al., 2004; Qi et al., 2008; Semenza, 2007a). Several studies have demonstrated that *Hif-1α* may play a crucial role in HSCs (Iyer et al., 1998; Kim et al., 2006a; Ryan et al., 1998) , however, the function and mechanism of regulation of *Hif-1α* in HSCs remain largely unknown.

Meis1 belongs to the Hox family of homeobox genes, which is a conserved set of genes that encode DNA-binding transcription factors (Cesselli et al., 2001). *Meis1* is expressed in the most primitive hematopoietic populations and is down regulated upon differentiation (Argiropoulos et al., 2007; Imamura et al., 2002; Pineault et al., 2002a). Moreover, targeted Meis1 knockout causes lethality by embryonic day 14.5 with multiple hematopoietic and vascular defects (Azcoitia et al., 2005; Hisa et al., 2004; Imamura et al., 2002). Despite the clear association of *Meis1* with HSCs, the precise function of *Meis1* in HSCs is not well understood.

In the current study, we outline the unique metabolic characteristics of LT-HSCs and we show that separation of bone marrow cells solely based on their metabolic footprint markedly enriches for HSCs. Finally, we demonstrate that *Meis1* regulates HSC metabolism through transcriptional activation of Hif-1α.

METHODS

LT-HSC Isolation

LT-HSCs were isolated from the bone marrow cells of 4- to 6-month-old C57BL/6 mice by FACS after surface marker staining for Lin, Sca-1, C-Kit, CD34, and Flk2 to identify Lin^-, $Sca\text{-}1^+$ $C\text{-}kit^+$, and $CD34/Flk2^-$ cells (LTHSCs). All antibodies were purchased from BD PharMingen. In studies LT-HSCs were isolated for metabolic analysis, magnetic lineage depletion (autoMACS separator, Miltenyibiotec) was utilized. In these studies, additional control fluorescent surface marker staining was performed, and the cells were evaluated by flow cytometry for ensuring that adequate lineage depletion (>95% lineage depletion) was reproducibly achieved. For metabolic studies, LT-HSCs isolated from 62 mice were pooled, and metabolic studies were performed within 24 hr of isolation.

Metabolic Assays

Oxygen consumption was measured with the BD Oxygen Biosensor System in accordance with the manufacturer's recommendations. A total of 2 to 3 $x10^5$ cells/well were used. Oxygen consumption was determined after 2 hr of culture in the biosensor.

ATP levels were quantified with ATP Bioluminescence Assay Kit HS II (Roche) in accordance with the manufacturer's recommendations. A total of 2 to $3x10^5$ cells/well were used.

Lactate production was measured with gas chromatography-mass spectrometry. Cells were cultured for 12 hr in a medium supplemented with 10 mM D-[1-13C]-glucose (Cambridge Isotope Labs) to allow up to half of the glucose-derived lactate pool to be labeled on C-3. The samples were analyzed for lactate abundance. The final results are presented as nMoles 13C-Lactate/nMol ATP.

Mitochondrial source of NADH was determined with the electron transport chain complex III inhibitor antimycin A (AMA). AMA leads to cessation of electron flow through the respiratory chain resulting in rapid accumulation of NADH from the Krebs cycle. Stock AMA (Sigma Aldrich) was prepared at 1 M in DMSO. A baseline NADH fluorescence gate was set with untreated high and low MP cells. High and low MP cells were then treated with 2 mM AMA for 5 min and profiled for NADH fluorescence. Cells with mitochondrial source of NADH production display an increase in NADH fluorescence following AMA treatment.

Flow Cytometric Profiling and Separation of Cells Based on Mitochondrial Activity

Flow cytometric profiling and separation of BM cells based on their mitochondrial activity was performed with mitotracker dyes and endogenous NADH fluorescence. The metabolic profile of mouse LT-HSCs was determined with concomitant surface marker and mitotracker staining. Mitotracker dyes that accumulate within mitochondria on the basis of mitochondrial proton gradient (MitoTracker deep red 633, MitoTracker Red CMXRos and MitoTracker Red CM-H2XRos) (Poot et al., 1996), as well as nonproton gradient sensitive dyes (MitoTracker Green), were used. Endogenous NADH fluorescence was measured flow cytometrically at 37^{o}C with a UV laser (Ex: 350 nm, Em: 460 nm, Moflo analyzer, Cytomation) as described previously (Chance and Thorell, 1959). Flow cytometric separation of high and low MP cells was carried out by separating cells in the low MP gate (6%–9%) and an equivalent number of cells with high mitochondrial potential.

Stem Cell Assays

Colony forming cell (CFC) assays were performed on high and low MP cells separated solely on the basis of the flow cytometric mitochondrial profile according to recommendations (Methocult, Stem Cell Technologies). For *in vivo* bone marrow reconstitution studies, high and low MP cells were isolated from 8- to 10-week-old C57BL/6 CD45.2 mice. Equal numbers of high and low MP CD45.2 donor cells (5 x10^{4}) were mixed with 5 x 10^{4} freshly isolated CD45.1

competitor bone marrow cells, and the mixture was injected intravenously via the retro-orbital route into each of a group of 6- to 9-weekold CD45.1 mice previously irradiated with a total dose of 10 Gy. For measuring reconstitution of transplanted mice, peripheral blood was collected at the indicated times after transplant and the presence of $CD45.1^+$ and $CD45.2^+$ cells in lymphoid and myeloid compartments were measured as described (Zhang and Lodish, 2004, 2005). Separate studies were performed where LSK cells were depleted from the bone marrow by flow cytometry, followed by equal distribution of LSK cells to high and low MP populations (1500 LSK cells per group). CD45.2 high and low MP donor cells (5×10^4) were mixed with 5×10^4 freshly isolated CD45.1 competitor bone marrow cells.

Gene Profile of Low and High MP Cells

RNA was extracted from high and low MP cells by using TRIzol (Invitrogen) in accordance with the manufacturer's instructions. cDNA was reverse transcribed with an RT-PCR kit (SA Biosciences). Mouse Real-Time Syber Green PCR Mix was purchased from SuperArray. PCR was performed on an ABI Prism 7700 Sequence Detector (Applied Biosystems). HSCs and hypoxia primer sets (SABiosciences) were used. The data were analyzed with the ΔΔCt method. Fold change was calculated as difference in gene expression between high and low MP cells. Additional real-time PCR for Meis1, Hif-1α was performed with the

SyberGreen method (Applied Biosystems) on ABI Prism 7700 Sequence Detector (Applied Biosystems) and primers specific for the selected genes.

Intracellular Detection of Hif-1α and Meis1 Proteins

Hif-1α and Meis1 proteins were detected by immunocytochemistry as follows; fresh bone marrow cells underwent fixation with 4% paraformaldehyde for 10 min at room temperature. After permeabilization (0.01% Triton) and serum block, cells were incubated overnight with primary antibodies (1:50 dilution anti-Hif-1α and 1:50 dilution anti-Meis1). Staining was assessed by flow cytometry after incubation with corresponding fluorophore-conjugated secondary antibody.

Isolation of mouse bone marrow cells

Mouse bone marrow was extracted from the femurs and tibias of C57BL/6 mice (Jackson Labs) following euthanasia by flushing the marrow space with PBS. Following RBC lysis, the cells were pelleted, washed and resuspended at 2-3 x 10^6 cells/ml in DMEM media with 10% fetal bovine serum in preparation for flowcytometric analysis.

ABCG2 blocking

To exclude the possibility that dye efflux plays a role in the mitotracker profile observed, we used Fumitremorgin C (FTC), which is a specific blocker of the ABCG2 transporter. Cells were pretreated with 10 μM FTC prior to staining with mitotracker dyes. The percentage of cells in the low mitotracker gate were compared +/- FTC.

Bone marrow reconstitution

High and low MP cells were isolated from 8-10 week old C57BL/6 CD45.2 mice. Equal numbers of high and low MP CD45.2 donor cells (5×10^4) were mixed with 1×10^5 freshly isolated CD45.1 competitor bone marrow cells, and the mixture was injected intravenously via the retro-orbital route into each of a group of 6-9 week old CD45.1 mice previously irradiated with a total dose of 10 Gy. To measure reconstitution of transplanted mice, peripheral blood was collected at the indicated times post-transplant and the presence of $CD45.1^+$ and $CD45.2^+$ cells in lymphoid and myeloid compartments were measured. Briefly, for analyzing repopulation of mouse HSCs, peripheral blood cells of recipient CD45.1 mice were collected by retro-orbital bleeding, followed by lysis of red blood cells and staining with anti-CD45.2-FITC, and anti-CD45.1-PE, and anti-Thy1.2-PE (for T-lymphoid lineage), anti-B220-PE (for B-lymphoid lineage), anti-Mac-1-PE, anti-Gr-1-PE (cells co-staining with anti-Mac-1 and anti-Gr-1 were deemed to be of the myeloid lineage). The “Percent repopulation” shown in all Figures was based

on the staining results of anti-CD45.2-FITC and anti-CD45.1-PE. In all cases FACS analysis of the above listed lineages was also performed to confirm multilineage reconstitution.

Real time PCR for *Meis1*, *Hif1*−α

Total RNA was isolated using TRIzol reagent (Invitrogen). cDNA was generated by following the recommended protocol for SuperScript II Reverse Transcriptase (Invitrogen) using 2 ug total RNA. Real time PCR was performed with SyberGreen (Applied Biosystems) on ABI Prism 7700 Sequence Detector (Applied Biosystems) using primers as follows:

M-*Hif-1* α-F AAA CTT CAG ACT CTT TGC TTC G

M-*Hif-1*α-R CGG GCA GAA CGA GAA GAA

M-*Meis1*-F ACG CTT TTT GTG ACG CTT TT

M-*Meis1*-R TCA CAC AGT GGG GAC AAC AG

Hypoxic and anoxic stress

In order to evaluate susceptibility to hypoxic and anoxic stress, high and low MP cells were cultured in DMEM media (supplemented with 10% FBS and penicillin and streptomycin) under severe hypoxia (1% oxygen for 12 hours) or anoxia (0% oxygen for 12 hours). Viability was assessed immediately using trypan blue.

Three separate culture plates were used for each cell type for each experimental condition. Viability was calculated as percent of total cell count.

Western Blot

Whole protein extracts (15 μg/well) were used in all assays. Primary monoclonal mouse anti Hif1-α antibody (BD Transduction Laboratories #610958) was used at 1:1000 dilution (overnight incubation 4°C). Secondary anti- mouse IgG HRP linked antibody (Cell Signaling Technology #7076) was used at 1:2000 dilution (3 hours incubation at 4°C). Relative Optical Density analysis was carried out using Adobe Photoshop software (corrected for beta actin).

Generation of Hif-1α Reporter vectors

An 818 bp long DNA fragment from the first intronic region of Hif1-α containing the conserved Meis1 binding site (+1799 bp from ATG start site, chr14:61,232,973-61,233,790) was amplified from mouse genomic DNA using 5`-CGTGCGGGTTTGGTTGTAATCT-3` and 5`-GCCCATCATTTCATCAAAAGCA-3` primers and subcloned into pCR2.1-TOPO vector (Invitrogen). Both the TOPO vector with PCR fragment and pGL2-EIb vector were digested with XhoI and KpnI. Then the PCR fragment was cloned into Elb-pGL2 to generate Hif1-α-pGL2 luciferase reporter vector. To test Meis1 site specificity, the Meis1 binding site (TGAC) was mutated using

QuikChange® II Site-Directed Mutagenesis Kit (Stratagene) from Hif1-α-pGL2 vector with the following primers: Sense: 5'-CAT AAC GTCTGGGCTCTCCTAAAAGGTGATGCAAACACA A-3' and Antisense: 5'-TTGTGTTTGCATCACCTTTTAGGAGAGCCCAGACGTTATG-3' and mut-TGAC-Hif1-α-pGL2 was generated.

Luciferase reporter assays

Transcriptional activation of Hif-1α by Meis1 was evaluated using Hif-1α-pGL2 and del-TGAC-Hif1-α-pGL2 vectors. 0.8 μg of Hif1-α-pGL2 was cotransfected with 50 ng, 100 ng, 200 ng and 400 ng of the Meis1 expression vector pCMV-SPORT6-Meis1 (OpenBiosystems) and 0.2 μg of pCMVLacZ (internal control) into COS cells using lipofectamine transfection reagent (Invitrogen). At 48 h after transfection, cell lysates were prepared and quantified for firefly luciferase activity using a luciferase reporter system (Promega). Luciferase measurements were calculated as firefly luciferase units versus β-gal units. Transcriptional activation was compared to basal luciferase levels in cells transfected with Hif1-α-pGL2 and empty pGL2-EIb.

Meis1 Knockdown

LT-HSCs were incubated in HSC media as previously described (Zhang et al., 2006; Zhang et al., 2008) during siRNA knockdown for 20 hours.

siRNA sequence:

Sense sequence (5`->3`): GAUUUGGUGAUAGACGAUAtt

Antisense sequence (5`->3`): UAUCGUCUAUCACCAAAUCga

Chromatin immunoprecipitation assay (ChIP)

ChIP assays were performed to evaluate the *in vivo* binding of Meis1 to its consensus sequence in the Hif-1α gene. The assays were done using the ChIP kit (Upstate, cat#17-295) according to the manufacturer's instructions. 1.5 $\times 10^6$ Kasumi-1 cells were crosslinked in 1% formaldehyde for 10 min at 37^{o}C. After two washes with PBS, cells were spun down for 4 min at 2000g. Then, cell pellets were lysed in 200 µl of SDS Lysis Buffer with 1mM PMSF (Sigma P7626) and 1X Protease inhibitor cocktail (Roche, 11836170001). Sonication was carried out in 1.5 ml tubes with the settings; 5 s on, 5 s off and repeated for 4 times on ice (550 Sonic Dismembrator, Fisher Scientific). The resulting DNA lengths were 200–1000 bp in length. 200 µl of sonicated sample was used for each assay. Meis1 antibody (Santa Cruz Biotechnology, sc-10599) and normal goat IgG (Santa Cruz Biotechnology, sc-2028) were used. The DNA isolated from input chromatin fragments and from the precipitated chromatin fragments by anti-Meis1 antibody or control IgG was subjected to real time PCR using primers flanking the consensus Meis1 binding site (TGAC):

5’-TTGAAAAACTTGCCTAGACTGAGAGT-3’ and

5’-CAGTATCATTAAAACTGCCTAAATTT-3’.

Animal Care

All experiments using animals were previously approved by the Institutional Animal Care and Use Committee at UT Southwestern Medical Center.

Statistical Analysis

Significance levels were calculated with a Student’s *t* test. P values smaller than 0.05 considered significant.

RESULTS

Metabolic Profile of Mouse LT-HSCs

Lin^-, $Sca\text{-}1^+$, $c\text{-}Kit^+$, $CD34^-$, and $Flk2^-$ (LT-HSCs) cells have low rates of mitochondrial respiration (Figure 1A) and low levels of ATP (Figure 1B). Lower rates of mitochondrial respiration can be attributed to lower energy requirements (i.e., quiescence) and/or utilization of glycolysis instead of oxidative phosphorylation. Therefore, we examined the overall glycolytic flux as determined by the rate of ^{13}C lactate production (derived from glucose). As shown in Figure 1C, the rate of glucose derived ^{13}C lactate production was higher in LT-HSCs compared to whole bone marrow. This method determines the source of lactate and not only the amount of lactate produced. This is important because cells can produce lactate from the metabolism of glutamine rather than glucose (DeBerardinis et al., 2007). Next, we determined the metabolic profile of LT-HSCs by flow cytometry. Whole mouse bone marrow underwent lineage depletion, then was concomitantly stained for $Sca\text{-}1^+$, $c\text{-}Kit^+$, $CD34^-$, and $Flk2^-$ surface expression and for mitotracker incorporation. Cells were also assessed for endogenous NADH fluorescence.

These techniques allow profiling of cells based on their mitochondrial proton gradient in the case of mitotracker (Poot et al., 1996) and endogenous NADH fluorescence (Chance and Thorell, 1959) as an index of overall mitochondrial

respiration (as the majority of cellular NADH is derived from mitochondrial respiration). The majority of LT-HSCs were localized to a well-defined flow cytometry gate, which contained 6%–9% of total bone marrow cells. Cells in this gate were characterized by low mitochondrial potential (MP) (Figures 1D and 1E) and low NADH fluorescence (Figure 2A). This low MP population contained >80% of LT-HSCs (Figure 1F). Lineage characterization of the low MP population demonstrated that LT-HSCs and Lineage, Sca-1^{+}, c-Kit^{+} (LSK) cells are the only two populations that are largely localized to the low MP gate, whereas all other lineages had mostly high mitochondrial potential (Figure 1F).

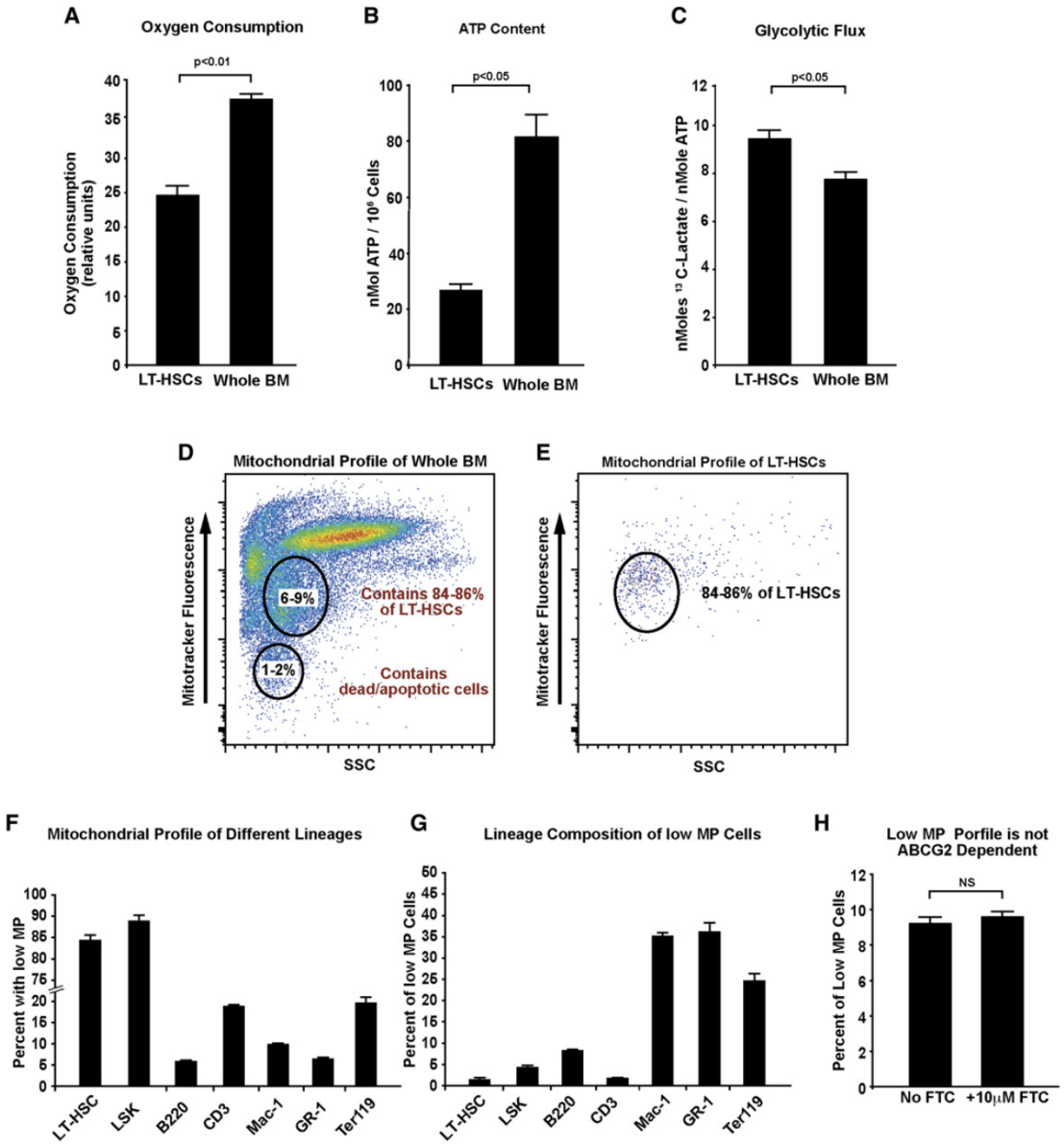

Figure 1. Metabolic Profile of Mouse HSCs: (A) Oxygen consumption of Lin^-, $SCA\text{-}1^+$, $c\text{-}Kit^+$, $CD34^-$, and $Flk2^-$ cells (LT-HSCs) and whole bone marrow demonstrating lower rates of oxygen consumption by LT-HSCs (n = 3). (B) ATP

level of LT-HSCs and whole bone marrow demonstrating lower ATP levels in LT-HSCs (n = 3). (C) Glycolytic flux of LT-HSCs and whole bone marrow demonstrating higher rates of glycolysis in LT-HSCs (n = 3). (D) Flow cytometry profile of whole mouse bone marrow stained with mitotracker. Note the distinct populations with different mitotracker fluorescence. (E) Mitotracker profile of LT-HSCs. The majority of LT-HSCs (84%–86%) are localized to a distinct population (6%–9% of total bone marrow cells) with low mitochondrial potential (MP cells). (F) Mitotracker profile of different bone marrow lineages. Note that whereas the majority of LT-HSCs and LSK cells are localized to the low mitochondrial potential gate, the majority of all other lineages have high mitochondrial potential (n = 4). (G) Lineage composition of the low MP cells. Note that whereas the low MP gate is markedly enriched in LT-HSCs and LSK cells, it also contains all other bone marrow lineages (n = 4). (H) Percentage of cells in the low MP gate following pretreatment with FTC (a specific blocker of the ABCG2 transporter). Note that FTC had no effect on the percentage of cells in the low MP gate (n = 3). This indicates that the low MP profile is not secondary to dye efflux. Data presented as mean ± SEM.

Moreover, this low MP gate, although markedly enriched in LT-HSCs and LSK cells, contains all other bone marrow lineages (Figure 1G). To exclude the possibility that this low mitotracker profile is secondary to dye efflux, we used

Fumitremorgin C (FTC), a specific blocker of the ABCG2 transporter. The ABCG2 transporter is responsible for dye efflux by the side population (SP) stem cells (Goodell et al., 1997; Scharenberg et al., 2002;Zhou et al., 2001). As shown in Figure 1H, FTC had no effect on the percentage of cells in the low MP gate.

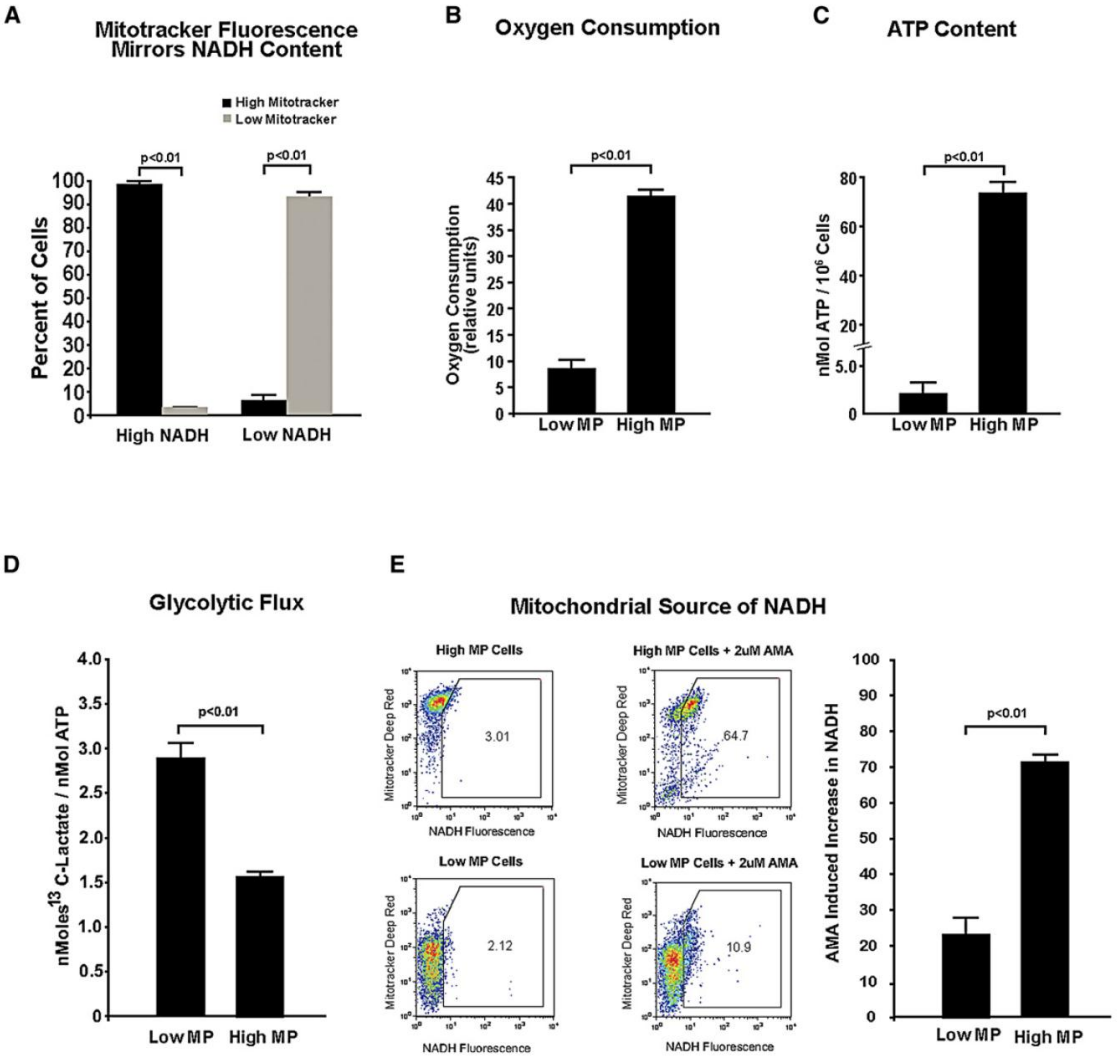

Figure 2. Low MP Cells are glycolytic: (A) Comparison between mitotracker fluorescence and endogenous NADH fluorescence of both high MP and low MP cells. Note the direct correlation between mitotracker fluorescence and NADH fluorescence, which provides further proof of the metabolic state of these two populations (n = 4). (B) Oxygen consumption of high and low MP cells. Note the

significantly lower rates oxygen consumption in the low MP cells (n = 3). (C) ATP content of high and low MP cells demonstrating a significantly lower levels of ATP in the low MP cells (n = 3). (D) Measurement of glycolytic flux of high and low MP cells as determined by ^{13}C-Lactate production. The low MP cells displayed significantly higher rates of glycolysis/nMol ATP compared to the high MP cells (n = 3). (E) Determination of cellular source of NADH: flow cytometry profiles of high (upper) and low (lower) MP cells before (left) and after (right) treatment with antimycin A (AMA). Note the significant shift of most of the high MP cells after AMA treatment (upper right panel) and the minimal shift of low MP cells in response to AMA (lower right panel). The bar graph shows quantification of the percentage of cells with increased NADH fluorescence in response to AMA (n = 3). This indicates that the majority of NADH in the low MP cells is derived from nonmitochondrial source(s). Data presented as mean ± SEM.

Metabolic Characteristics of High and Low MP Cells

We next characterized the metabolic properties of cells in the low MP gate as they compare to cells with high MP. First, we directly correlated endogenous NADH fluorescence with mitotracker fluorescence. NADH fluorescence is an index of mitochondrial oxidative phosphorylation given that oxidative metabolism yields a significantly higher amount of NADH for each molecule of glucose oxidized when compared to glycolysis (eight molecules NADH compared to two

molecules, respectively) (Chance and Thorell, 1959). As shown in Figure 2A, high and low mitotracker cells displayed high and low NADH fluorescence cells, respectively.

This result is supported by measurement of oxygen consumption, where the high MP cells displayed significantly higher oxygen consumption rates compared to the low MP cells (Figure 2B). Low MP cells also preferentially utilized glycolysis for their metabolic needs. As shown in Figure 2D, the rate of ^{13}C lactate production was significantly higher in the low MP cells. We further confirmed this finding by using a specific mitochondrial electron transport chain inhibitor. Inhibition of the electron transport chain complex III by antimycin A (AMA) results in NADH accumulation only in cells that rely on mitochondrial respiration for NADH production. We used this principle to evaluate the source of NADH in high and low MP cells. As shown in Figure 2E, only a small percentage of the low MP cells displayed increased NADH after AMA treatment compared to high MP cells, indicating that mitochondrial respiration is not the main source of NADH in low MP cells. Taken together, these results indicate that the low MP cells do not rely on mitochondrial respiration for energy production, but rather on cytoplasmic glycolysis.

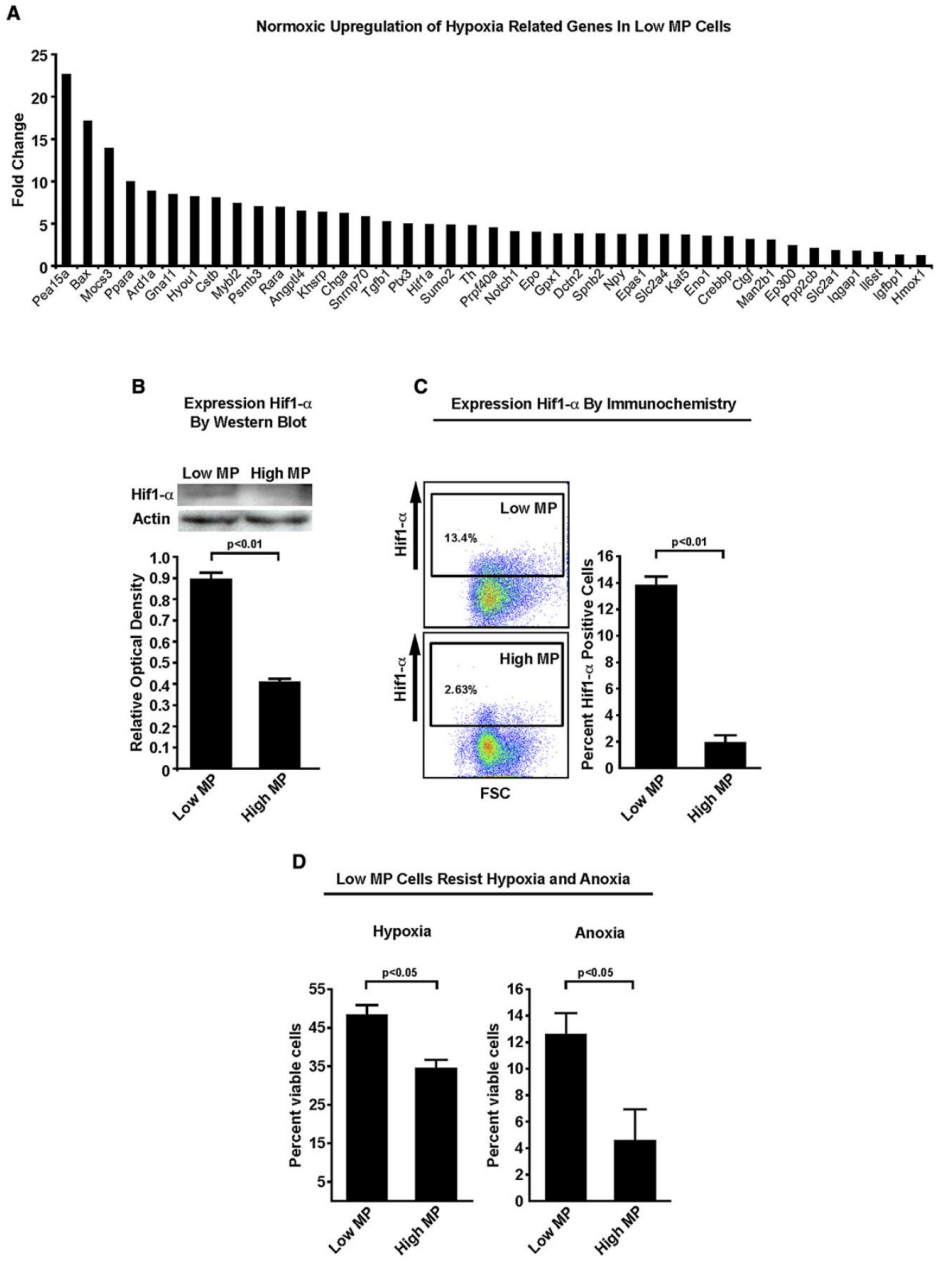

Figure 3. Normoxic Upregulation of Hif-1α in Low MP Cells: (A) Hypoxia real-time PCR array profile of low MP cells compared to high MP cells. Note the significant normoxic upregulation of hypoxia inducible genes in low MP cells under normoxic conditions (5–6 hr after isolation). (B) Upper panel(s) show

western blot analysis of high and low MP cells with Hif-1α antibody and actin as loading control. The lower panel shows densitometry analysis demonstrating higher Hif-1α protein expression in the low MP cells (n = 3). (C) Immunocytochemistry staining demonstrating a higher percentage of low MP cells expressing Hif-1α compared to high MP cells (n = 3). (D) Viability of low and high MP cells followed low-oxygen stress. The left panel shows the percentage of viable low and high MP cells after 12 hr of severe (1%) hypoxia. The right panel shows the percentage of viable low and high MP cells after 12 hr of anoxia (n = 3). Viability was assessed with trypan blue. Note the significantly higher viability in the low MP population after both hypoxia and anoxia. Data presented as mean ± SEM.

Low MP Cells Are Primed for Hypoxia Resistance

We performed a PCR array for hypoxia related gene expression on freshly isolated high and low MP cells. Under normoxic conditions, the low MP cells displayed significant upregulation of numerous hypoxia-inducible genes and regulatory glycolysis genes (Figure 3A) compared to high MP cells. This was further confirmed by upregulation and stabilization of Hif-1α protein (RNA in Figure 3A and protein in Figures 3B and 3C) in the low MP cells. These results not only provide a mechanistic explanation of the metabolic phenotype of low MP cells but also suggest that the low MP cells are primed for adaptation to low-

oxygen environment. This was corroborated by the significantly higher viability of low MP cells following both severe hypoxic and anoxic stresses (Figure 3D).

Collectively, these results indicate that cells in the low MP gate utilize glycolysis instead of mitochondrial respiration for their energy demands. This metabolic phenotype is associated with normoxic upregulation of Hif-1α and its downstream target genes.

Stem Cell Characteristics of Metabolically Sorted Cells

Given the unique metabolic characteristics of LT-HSCs cells, we tested whether isolation of bone marrow cells solely based on their metabolism enriches for HSC. After flow cytometric separation of high and low MPcells, we evaluated their gene expression profile with PCR array. Figure 4A demonstrates that low MP cells express higher levels of numerous HSC-associated transcripts.

Furthermore, we utilized *in vitro* and *in vivo* hematopoietic progenitor and HSC assays to characterize the stem cell properties of low MP cells. Low and high MP cells were cultured in Methocult medium and the colonies were evaluated after 12 days. Low MP cells displayed a much higher colony forming capacity compared to high MP cells (Figure 4B). Further characterization of colony types revealed

that the low MP cell produced a higher percentage of CFU-GEMM type (mixed colonies) with lower percentages of BFU-E and CFU-GM colonies compared to high MP cells (Figures 4C–4E), although the low MP population had significantly higher number of all types of colonies.

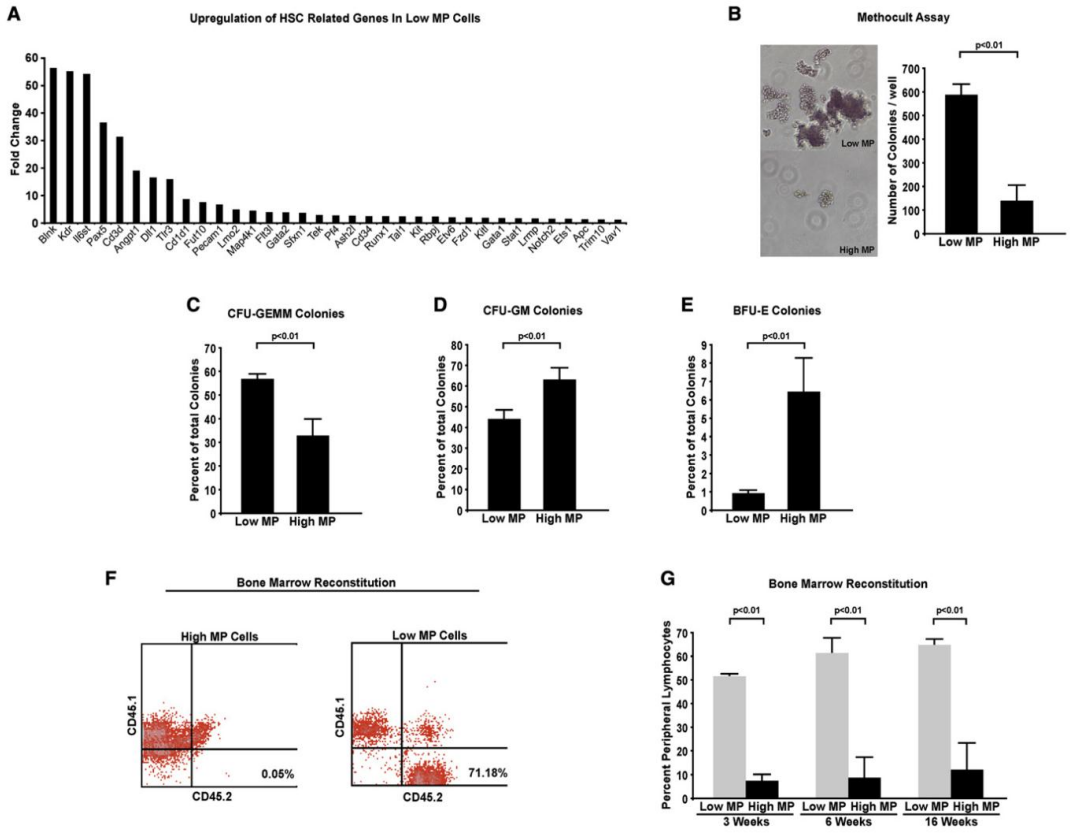

Figure 4. Low MP Cells Are Enriched for HSCs: (A) PCR array profile of low MP cells compared to high MP cells demonstrating enrichment of a number of HSCs associated genes in the low MP population.(B) The left panel shows a representative bright field microscopic image of colonies obtained from low and

high MP cells. The right panel shows quantification of colonies derived from low and high MP cells in methocult after 12 days. (C) GFU-GEMM colonies. (D) CFU-GM colonies. (E) BFU-E colonies (n = 3). Note the significantly higher number of colonies derived from the low MP population. These results indicate that the low MP population is markedly enriched for hematopoietic progenitor cells. (F) Representative flow cytometry profiles of peripheral blood of bone marrow recipient mice after staining with anti-CD45.2-FITC antibody (x axis) and anti-CD45.1-PE antibody (y axis), demonstrating higher engraftment in the recipient of low MP cells. (G) Time course analysis of bone marrow reconstitution with low and high MP cells (n = 5 animals/group). Note the significantly higher bone marrow repopulation capacity of the low MP cells at all time points. This result indicates that the low MP population is enriched for long term repopulating HSCs. Data presented as mean ± SEM.

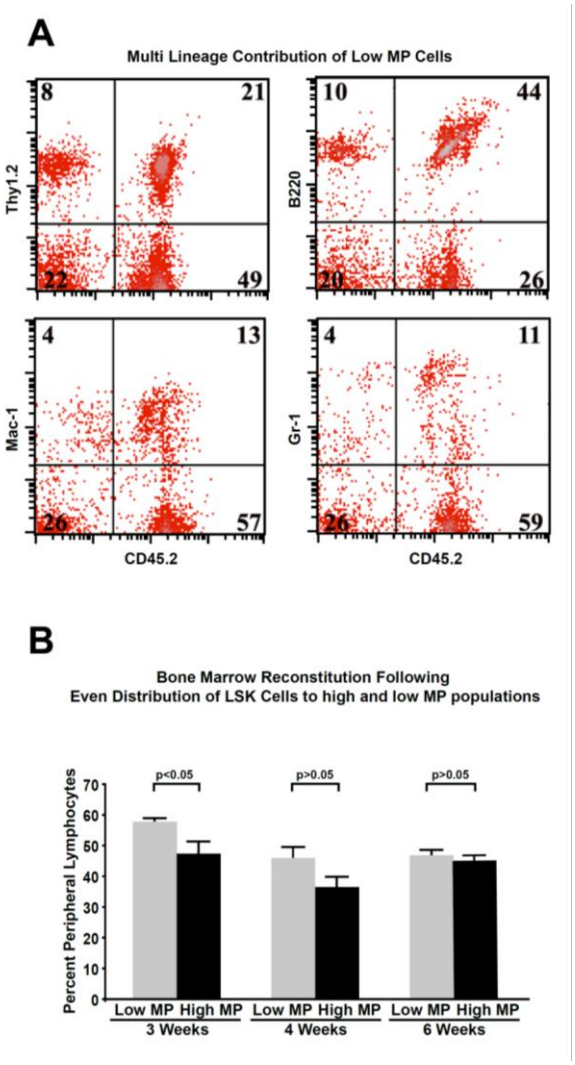

Figure 5: Multi-lineage contribution of Low MP cells A) Flowctometry plots of peripheral blood mononuclear cells to demonstrate the multi-lineage contributions of HSCs in the low MP population in a mouse at 4-months post-transplant. B) Bone marrow reconstitution using high and low MP cells following depletion of LSK cells and equal distribution of LSK cells amongst high and low MP populations. Note the lack of significant difference in bone marrow reconstitution

between the two populations following equal distribution of LSK cells. (n=3). Data presented as mean ± SEM.

These results indicate that low MP cells are enriched for hematopoietic progenitor cells. *In vivo* bone marrow reconstitution studies following lethal irradiation were undertaken to determine the long-term repopulation capacity of low MP cells. Serial analysis of the peripheral blood of the recipient mice demonstrated a significantly higher percentage of engraftment with the low MP cells compared to high MP cells at all time points (Figures 4F and 4G). Moreover, peripheral blood cells were collected and analyzed by flow cytometry with lineage markers to determine the capacity of low MP cells to repopulate different hematopoietic lineages. As shown in Figure 5A, the low MP cells repopulated all tested lymphoid ($CD45.2^+Thy1.2^+$, $CD45.2^+B220^+$) and myeloid lineages ($CD45.2^+Mac\text{-}1^+$, $CD45.2^+Gr\text{-}1^+$). Additional studies were undertaken in which the bone marrow was depleted of HSCs by flow cytometric separation of LSK cells, followed by equal distribution of LSK cells to the high and low MP populations. Bone marrow reconstitution studies using these high and low MP populations with equal numbers of HSCs demonstrated no difference in transplantation efficiency (Figure 5B). This confirms that the enhanced reconstitution capacity by the low MP population is due to localization of LT-HSCs to the low MP gate. Collectively, these results confirm that the low MP cell

fraction of the bone marrow is highly enriched in both hematopoietic progenitors and long-term repopulating HSCs.

Expression of Hif-1α in LT-HSCs

In order to determine the mechanism of the glycolytic metabolic phenotype of LT-HSCs, we evaluated the expression pattern of Hif-1α in LT-HSCs and WBM. Upregulation of Hif-1α mRNA was confirmed by real-time PCR as shown in Figure 6. WBM and LT-HSCs underwent fixation followed by permeabilization and immunocytochemical staining for Hif-1α. Here, we show that the majority (89%) of LT-HSCs express Hif-1α, whereas less than 30% of the WBM cells are Hif-1α positive (Figure 7A).

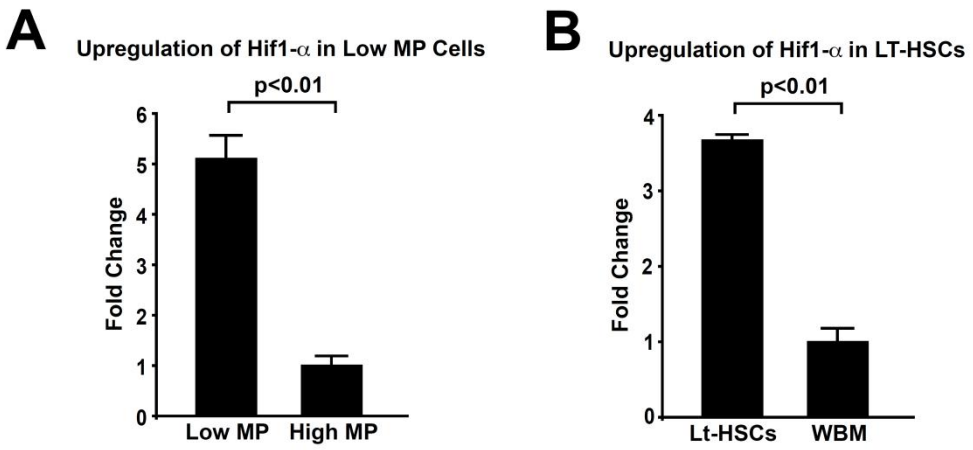

Figure 6: Upregulation of Hif-1α in Low MP and LT-HSCs. Real Time PCR demonstrating: A) Upregulation of Hif-1α in low MP cells, and B) Upregulation

of Hif-1α in LT-HSCs compared to whole bone marrow. (n=3). Data presented as mean ± SEM.

Meis1 is a Transcriptional Activator of Hif-1α

Meis1 is a HSC-associated transcription factor required for definitive hematopoiesis; however, its precise role in HSCs is not well understood. We determined that whereas only a small percentage of WBM cells express Meis1 protein (1.4%), the vast majority of LT-HSCs are Meis1 positive (96.2%) (Figure 7B).

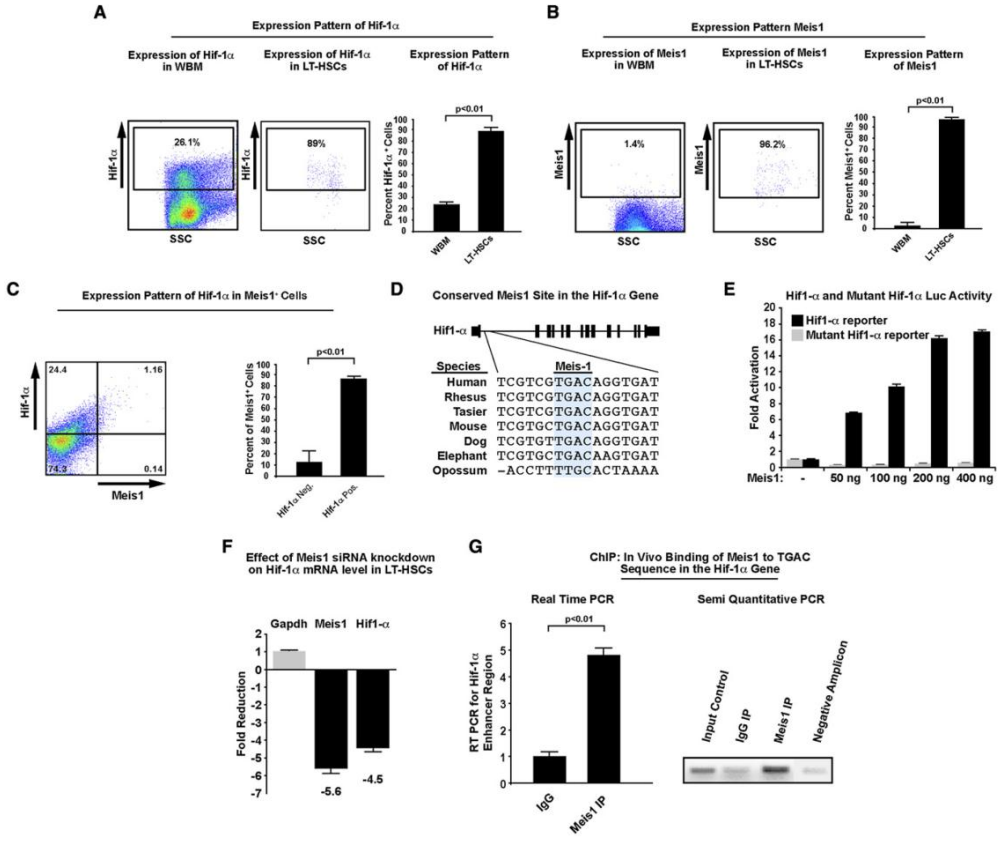

Figure 7. Transcriptional Regulation of Hif-1α by Meis1: (A) Expression pattern of Hif-1α. The left panel shows expression of Hif-1α in WBM. The middle panel shows expression of Hif-1α in LT-HSCs. The right panel shows quantification of Hif-1α expression. Note that whereas less than 25% of the unfractionated bone marrow cells express Hif-1α, the vast majority of LT-HSCs express Hif-1α protein (n = 3). (B) Expression pattern of Meis1. The left panel shows expression of Meis1 in WBM. The middle panel shows expression of Meis1 in LT-HSCs. The right panel shows quantification of Meis1 expression.

Note that whereas less than 2% of the unfractionated bone marrow cells express Meis1, almost all the LT-HSCs express Meis1 protein (n = 3). (C) Colocalization of Hif-1α and Meis1 in the WBM. The left panel shows a representative flow cytometry profile of the expression of Hif-1α and Meis1. The right panel shows quantification of Hif-1α and Meis1 expression. Note that although only a small percentage of WBM cells express Meis1, the majority of these $Meis1^{+}$ cells also coexpress Hif-1α (n = 3). (D) Schematic of the conserved Meis1 binding domain in the first intronic region Hif-1α. (E) Luciferase assay demonstrating dose dependent increase in Hif-1α luciferase activity after transfection with Meis1 expression vector. Mutation of the four nucleotides in the Meis1 seed region completely abolishes the luciferase activity (n = 3). (F) Real-time PCR following siRNA knockdown of Meis1 in freshly isolated LT-HSCs. Knockdown of Meis1 in LT-HSCs (5.6-fold) resulted in marked downregulation of Hif-1α mRNA levels (4.5-fold), (n = 3). (G) ChIP assay demonstrating *in vivo* binding of Meis1 to its consensus binding sequence in the Hif-1α first intron. The left panel shows real-time PCR with primers flanking the consensus Meis1 binding sequence compared to control IgG after immunoprecipitation. The right panel shows PCR products showing input control and negative amplicon (n = 3). Data presented as mean ± SEM.

Moreover, we colocalized Hif-1α and Meis1 proteins by immunocytochemistry and found that the majority of Meis1 positive cells were also positive for Hif-1α (85.2%) (Figure 7C). This expression pattern of Hif-1α and Meis1 remained unchanged hours after isolation of bone marrow cells, indicating that the expression of Hif-1α may not be simply secondary to the *in vivo* environment in the bone marrow.

These findings led us to examine whether Hif-1α expression by LT-HSCs is downstream of the HSC-associated transcription factor Meis1. We identified a conserved Meis1 consensus binding sequence in the Hif-1α first intronic region (Figure 7D). Luciferase assays were carried out with wild-type Hif-1α expression vector (Hif1-a-pGL2) and a Hif-1α expression vector harboring a mutated Meis1 binding sequence (mut-TGAC-Hif-1a-pGL2). Increasing concentrations of Meis1 expression vector (CMV-M-Meis1) resulted in dose-dependent transcriptional activation of Hif-1α. This activation was dependent on binding of Meis1 to its consensus binding sequence in the Hif-1α first intronic region because mutation of the seed sequence completely abolished the activation of Hif-1α by Meis1 (Figure 7E).

To determine whether Meis1 is required for Hif-1α expression, we utilized siRNA to knockdown Meis1 in freshly isolated LT-HSCs. Scrambled Meis1 siRNA was

used as control. Transfection with Meis1 siRNA resulted in diminution of Meis1 mRNA levels. This was associated with a marked downregulation of Hif-1α mRNA (Figure 7F). Taken together, these results indicate that Meis1 is required for optimal transcriptional activation of Hif-1α in LT-HSCs.

To confirm the *in vivo* binding of Meis1 to its conserved sequence in the Hif-1α gene, we performed ChIP assays in Kasumi1 cells. The results confirmed that Meis1 binds *in vivo* to its conserved sequence in the Hif-1α first intronic region as determined by real-time PCR following immunoprecipitation with Meis1 antibody (Figure 7H). PCR products are shown in the right panel.

DISCUSSION

Stem cell separation techniques generally rely on the pattern of expression of specific membrane proteins. As a result, isolation of HSCs requires the combination of several antibodies such that stem cells are defined by the presence or absence of certain epitopes or markers (Challen et al., 2009; Goodell et al., 1996; Kiel et al., 2007; McCune et al., 1988; Murray et al., 1995; Peault et al., 1993). While several reports have indicated that HSCs are resistant to hypoxia (Cipolleschi et al., 1993) and reside within hypoxic niches in the bone marrow (Chow et al., 2001; Li and Li, 2006; Parmar et al., 2007), these characteristics have not been exploited for identification of unique metabolic properties of HSCs, or for HSC enrichment.

In the current study, we define the metabolic phenotype of mouse HSCs. We demonstrate that LT-HSCs cells are localized to a distinct population of cells characterized by low mitochondrial potential (low MP). This population represents only 6-9% of the total bone marrow, but contains >80% of LT-HSCs, based on surface marker expression. We show that both LT-HSCs and low MP cells have low ATP levels and utilize cytoplasmic glycolysis instead of mitochondrial oxidative phosphorylation. This metabolic phenotype is associated with upregulation of *Hif-1α*, at both the transcript and the protein levels. Separation of cells solely based on this metabolic profile markedly enriches for

HSCs as determined by *in vitro* colony forming assays and *in vivo* long-term repopulation assays. Finally, we show that the HSC-associated transcription factor *Meis1* regulates HSC metabolism through transcriptional activation of *Hif-1α.*

Hif-1α is a master regulator of metabolism known to regulate various aspects of cellular response to hypoxic stress. While the mechanism of oxygen dependent post-translational regulation of Hif-1α is well understood, little is known about its transcriptional regulation. A number of reports indicate that Hif-1α is regulated at the transcriptional level both during hypoxia and normoxia (Belaiba et al., 2007; Blouin et al., 2004; Hirota et al., 2004; Jiang et al., 1997; Laughner et al., 2001; Liu et al., 2004). In the current study, we show that *Meis1* activates Hif-1α transcription in LT-HSCs through binding to its conserved consensus binding sequence in the Hif-1α first intronic region.

The metabolic phenotype of HSCs outlined here is supportive of the adaptability of HSCs to the physiologic low oxygen tension in the bone marrow hypoxic niches. Under these hypoxic conditions, glycolytic metabolism predominates and can provide sufficient amounts of ATP to sustain HSCs. This metabolic phenotype also confers a survival advantage on HSCs during severe hypoxic or anoxic insults that would invariably eliminate differentiated cells that rely on

oxidative metabolism. Importantly, the transcriptional regulation of Hif-1α by *Meis1* highlights the involvement of stem cell-associated transcription factors in regulation of HSC metabolism, and indicates that the glycolytic phenotype of HSCs is not merely a product of their hypoxic environment.

CHAPTER THREE

UNIQUE METABOLIC FOOTPRINT OF HUMAN HEMATOPOIETIC STEM CELLS

INTRODUCTION

HSCs are defined by their inherent capacity to self-renew and to differentiate into all blood cell types. HSCs reside in regions of the bone marrow challenged by low oxygen tension (hypoxic), which is termed "hypoxic niche" (Eliasson and Jonsson; Wang and Wagers, 2011). We recently demonstrated that mouse HSCs in this hypoxic niche adopt an anaerobic metabolic profile, in which HSCs manifest lower rates of oxygen consumption, lower ATP content, and increased cytoplasmic glycolysis (Simsek et al., 2010). In addition, we and others showed that mouse HSCs demonstrate increased HIF-1α levels (Kim et al., 2006a; Simsek et al., 2010; Takubo et al., 2010).

Hif-1 regulates various aspects of metabolism from the oxidant stress response to regulation of glycolysis and mitochondrial respiration (Kim et al., 2006a; Marin-Hernandez et al., 2009; Papandreou et al., 2006; Semenza, 2009a, b, 2010; Zhang et al., 2007). HIF-1, a major mediator of transcriptional response to hypoxia, is composed of O_2 sensitive HIF-1α and constitutively active HIF-1β subunits (Semenza, 2001, 2007a; Wang et al., 1995a). Moreover, conditional deletion of

HIF-1α in bone marrow results in various defects such as loss of quiescence and progressive decline in HSC number following bone marrow transplantations and aging (Takubo et al., 2010). It has been shown that hypoxic cultures promote the production of hematopoietic progenitors and enhance HSC expansion (Eliasson and Jonsson; Koller et al., 1992; Parmar et al., 2007). HIF-1α protein is mainly stabilized at hypoxia but normoxic upregulation of HIF-1α has also been reported (Belaiba et al., 2007; BelAiba et al., 2006; Hagg and Wennstrom, 2005; Ivan et al., 2001; Jaakkola et al., 2001; Pedersen et al., 2008; Qi et al., 2008; Salceda and Caro, 1997; Semenza, 2007a). We recently demonstrated that Meis1 transactivates HIF-1α expression via a conserved Meis1 binding motif located in the first intron of HIF-1α (Simsek et al., 2010)

.

Several reports suggest that homeobox protein Meis1 plays important roles in hematopoietic progenitors and stem cells (HPSC) biology (Argiropoulos et al., 2007; Becker and Jordan, 2011; Eppert et al., 2011; Pineault et al., 2002b; Wang et al., 2005, 2006). Homozygous mutant mice for Meis1 die during gestation with defects in hematopoiesis which results in decline in myeloid, lymphoid, and multipotent progenitors (Azcoitia et al., 2005; Hisa et al., 2004; Imamura et al., 2002). Meis1 is also associated with leukemogenesis in humans with a frequent up-regulation in primary acute myeloid leukemia (Becker and Jordan, 2011;

Eppert et al., 2011) and acute lymphoblastic leukemia samples (Kawagoe et al., 1999). We recently showed that mouse LT-HSCs express Meis1 where a great majority of Meis1^{+} HSCs coexpress Hif-1α (Simsek et al., 2010). Meis1 is known to interact with the cofactors Pbx1 and HoxA9 which are known regulators of hematopoiesis (Argiropoulos et al., 2007; Calvo et al., 1999; Cvejic et al., 2011; Ferrell et al., 2005; Ficara et al., 2008; Gwin et al., 2010; Hu et al., 2009; Huang et al., 2011; Kirito et al., 2004; Lawrence et al., 2005; Pillay et al., 2010; Pineault et al., 2002a; Thorsteinsdottir et al., 2002; Yan et al., 2006). However, functions of Meis1 and its cofactors in relation to HIF-1 have not been determined in human HPSCs.

In the current report, we demonstrate that human mobilized HPSCs have a metabolic profile characterized by low mitochondrial oxidative phosphorylation, dependence on glycolytic metabolism, and upregulation of Hif-1α and its downstream target genes. We provide evidence that the metabolic phenotype of human HPSCs is mediated in part transcriptional activation of Hif-1α by Meis1 and its cofactors Pbx1 and HoxA9.

METHODS

Isolation of human mobilized peripheral blood (MPB) cells

Human G-CSF mobilized peripheral blood (MPB) was obtained from bone marrow transplant donors by plasmapheresis. Human cells were diluted and separated using ficoll to obtain the MPB mononuclear cell fraction. Then cells were suspended at 2-3 x 10^6 cells/ml in DMEM media with 10% fetal bovine serum for flow cytometry

Flow cytometric profiling and separation of cells based on mitochondrial potential

Flow cytometric profiling and separation of human MPB cells based on their mitochondrial activity were performed by using mitotracker dyes as described previously (Simsek et al., 2010). Briefly, human MPB cells were enriched by lineage depletion using the BD IMag™ Human Lineage Cell Depletion Set (BD Biosciences) according to manufacturer's instructions. The whole MPB fraction and $Lin^-CD34^+CD38^-CD90^+$ cells (30 minutes incubation on ice) were then profiled based on their mitochondrial activity after 15 minutes staining with mitotracker dyes (MitoTracker Red FM Cat# M22425 and MitoTracker Green Cat# M7514, Invitrogen) at 37^{o}C (2 x 10^6 cells/ml, 200 nM mitotracker). Cell sorting based on high and low mitochondrial activity was performed using gates that separated the cells with those with the lowest 7-9% of mitochondrial activity

and equivalent number of cells with the high mitochondrial activity (named low and high mitochondrial potential (MP) cells).

Colony forming assay

Based on mitochondrial profile, colony forming cell (CFC) assays were performed on human G-CSF MPB cells. Same numbers of human high and low MP cells (3 x 10^4 cells) were plated in each methocult plate (MethoCult® GF H4434, Stem Cell Technologies, USA). Viability was assessed with trypan blues as this is crucial that low MP gate often have dying cells with low mitochondrial activity. To minimize cell attachment, plates were precoated with 1% agarose. After twelve days of culture, the total number of colonies (per plate) was counted and the types of colonies were quantified. Note CFU-GEMM colonies indicate mixed colonies whereas BFU-E and CFU-GM are measure of erythroid and myeloid progenitors, respectively.

Oxygen consumption

Oxygen consumption was determined using the BD Oxygen Biosensor System, 384 well (Cat#353834) according to manufacturer's recommendations. MPB Cells and human HPSCs were separated as described above. Equal numbers of cells (5 x 10^4 cells/well in 50 μl volume) were incubated up to 6 hours in the provided 384 well plate prior to measurement at Fluostar Optima plate reader

(BMG Labtech). Culture media lacking cells was used as a negative control and sodium sulfite (100 mM) was used as a positive control. Oxygen consumption is presented as relative units.

ATP assay

HPSCs from human MPB Cells were isolated as described. Fifty thousand cells were used for each measurement. HPSCs and MPB Cells were centrifuged at 1200g for 10 min. ATP standard curves were prepared using ATP concentrations between 10^{-6}-10^{-12}M. Then, 50 µl of ATP standards and 50 µl cell lysates were quantified using ATP Bioluminescence Assay Kit HS II (Roche) using Fluostar Optima plate reader (BMG Labtech) following manufacturer instructions. Finally, data were normalized to cell count.

Measurement of ^{13}C Lactate Production

Cells were cultured in DMEM (Sigma D5030) supplemented with L-glutamine (4 mM), $NaHCO_3$ (42.5 mM), HEPES (25 mM), dialyzed fetal calf serum (10% v/v), Penicillin/Streptomycin and no glucose per well of 96-well plate. The medium was supplemented with double labeled 10 mM D-[1-^{13}C, 6-^{13}C]-glucose (Cambridge Isotope Labs) to allow all of the glucose-derived lactate pool to be labeled on C-3. Fifty thousand cells/well were cultured in 40 µl of medium for 12 hours. After the culture, the cells were pelleted and an aliquot of 25 µl of the

medium was transferred to a glass test tube with the internal standard (17.9 nmol of Sodium L-[$^{13}C_3$]-Lactate, Cambridge Isotope Labs). Lactate was extracted by sequential addition of 1 mL of methanol, chloroform and water followed by vortexing and centrifugation at 2000 rpm for 5 minutes. The aqueous phase was evaporated, derivatized with 100 µl Tri-Sil reagent (Pierce) for 30 minutes at 42^{o}C, and analyzed by gas chromatography-mass spectrometry. A three-point standard curve was also prepared using mixtures of un-enriched lactate and L-[3-$^{13}C_3$]-lactate (Cambridge Isotope Labs). Lactate abundance was determined by monitoring m/z at 117 (un-enriched), 118 (lactate containing ^{13}C from glucose) and 119 (internal standard). The areas of 117 and 118 were summed and corrected against the 119 area to calculate total lactate abundance. To determine the atom percent excess (APE), the 117 and 118 areas were first corrected against the 119 abundance to account for inter-sample variability of extraction. Then the corrected ratio of 118/(117+118) was determined and compared to the standard curve. Finally, the APE was multiplied by the total nmoles lactate to determine the nmoles of ^{13}C-lactate produced. The final results were corrected for total cellular ATP concentration.

Meis1 knockdown

Meis1 siRNA knockdown was carried out in Kasumi-1 cells (human myeloid progenitor cell line known to express Hif-1α at normoxic conditions (Pedersen et

al., 2008)). Upregulation of Meis1 in low MP cells and Kasumi-1 cells compared to human MPB cells were confirmed by real time PCR. Kasumi-1 cells were diluted to a density of 200,000 cells per ml in RPMI media supplemented with 20% FBS and antibiotics. The cells were centrifuged for 10 minutes at 1200g at 4°C and suspended in OPTIMEM (Invitrogen). The cells were then plated into 6-well plates. 12 µl of Hiperfect (Qiagen) and siRNA (50nM of siRNA per 750,000 cells/well) were incubated in 200 µl of OPTIMEM (Invitrogen) for 20 min at RT. Silencer Select Pre-designed siRNAs (Applied Biosystems, Ambion) for Meis1 were diluted into 50nM stocks (siRNA ID# s8662: 5'-GGCAUCUACUCGUUCAGGAtt-3' and 5'-UCCUGAACGAGUAGAUGCCgt-3'). siRNA were added to cells dropwise and incubated for 6 hours. After 6 hours incubation, 2.5 ml RPMI medium was added (20%FBS and antibiotics) and plates were incubated under normal growth conditions for 48 hours.

Expression profile of Low and High MP cells

PCR arrays (HSC and hypoxia primer sets, SABiosciences) were performed to study HPSC and hypoxia inducible gene expression profile of low and high MP cells. RNA was isolated from low and high MP cells by TRIzol method (Invitrogen, Carlsbad, CA) following manufacturer instructions. cDNA was generated by using an RT-PCR kit (SA biosciences, Maryland, USA). Real-Time PCR was performed using Human Real-Time Syber Green PCR Mix

(SuperArray) on an ABI Prism 7700 Sequence Detector (Applied Biosystems). The data was analyzed using the ΔΔCt method. Fold change was calculated as difference in gene expression between low and high MP cells.

Real time PCR for Meis1, Hif-1α and Hif-1α related genes

Total RNA was isolated using TRIzol reagent (Invitrogen). cDNA was generated by following the recommended protocol for SuperScript II Reverse Transcriptase (Invitrogen) using 2 µg total RNA. Real time PCR was performed with SyberGreen (Applied Biosystems) on ABI Prism 7700 Sequence Detector (Applied Biosystems) using primers as follows:

Table 1: Primers used in this study

Gene	Forward Primer	Reverse Primer
Meis1	5'-ACGCTTTTTGTGACGCTTTT-3'	5'-TCACACAGTGGGGACAACAG-3'
Hif-1α	5'-GAAGTGGCAACTGATGAGCA-3'	5'-GCGCGAACGACAAGAAA-3'
LDHA	5'-GGAGATCCATCATCTCTCCC-3'	5'-GGCCTGTGCCATCAGTATCT-3'
SLC2A1	5'-GGCATTGATGACTCCAGTGTT-3'	5'-ATGGAGCCCAGCAGCAA-3'
PFKL	5'-GATGATGTTGGAGACGCTCA-3'	5'-GGTGCCAAAGTCTTCCTCAT-3'
SIAH2	5'-GTTTCTCCGTATGGTGCAGG-3'	5'-TCAGGAACCTGGCTATGGAG-3'
PHD2	5'-GTTCCATTGCCCGGATAAC-3'	5'-CGACCTGATACGCCACTGTA-3'
VDU2	5'-TAGGGGTCTGGAGTGAGTGG-3'	5'-CTCTGAGCATTGGCGACC-3'

Intracellular Detection of Hif-1α and Meis1 in HPSC

Human MPB cells and human HPSCs underwent fixation with 4% paraformaldehyde for 10 min at room temperature. After permeabilization (0.01% Triton) and serum block, cells were incubated overnight with primary antibodies; 1:50 dilution of anti-Hif-1α (Cat#610958, BD Transcduction Laboratories) and 1:50 dilution of anti-Meis1 (sc-10599, Santa Cruz Biotechnology). Staining was assessed by flow cytometry after incubation with corresponding fluorophore-conjugated secondary antibody.

Luciferase assays:

Transcriptional activation of Hif-1α reporter by Meis1 (pCMV-SPORT6-Meis1, Cat#MMM1013-7512739,Openbiosystems), HoxA9 (pCMV-SPORT6-HoxA9, Cat# MMM1013-9200573,Openbiosystems), and Pbx1 (pCMV-SPORT6-Pbx1, Cat# MMM1013-63227,Openbiosystems) were evaluated using Hif1a-pGL2 (as previously described at (Simsek et al., 2010)) or PbxMutHif1a-pGL2 (having Pbx1 binding site mutated) or HoxMutHif1a-pGL2 (having HoxA9 binding site mutated) reporter constructs as indicated in the figures. 0.8 ug of Hif1a-pGL2 or PbxMutHif1a-pGL2 or HoxMutHif1a-pGL2 reporter construct were co-transfected with different doses of the Meis1, HoxA9 and Pbx1 expression vectors and 0.2 ug of pCMV-LacZ (internal control) into COS cells using lipofectamine transfection reagent (Invitrogen). At 48 h after transfection, cell

lysate were prepared and quantified for firefly luciferase activity using a luciferase reporter system (Promega). Luciferase measurements were calculated as firefly luciferase units versus β-gal units. Transcriptional activation were compared to basal luciferase levels in cells transfected with Hif1a-pGL2 or PbxMutHif1a-pGL2 or HoxMutHif1a-pGL2 and empty pGL2. To test Pbx1 site specificity, Pbx1 binding site TGAT at Hif-1a-pGL2 reporter were mutated using site directed mutagenesis kit (Strategene) from Hif-1α-pGL2 vector with the following primers: PbxMut-Hif1a-F:5'-CAATTTCTACAAACTTGTGTTTGCCG ACCCTGTCAGGAGAGCCCAGACGTTA-3' and PbxMut-Hif1a-R: 5'-TAACGTCTGGGCTCTCCTGACAGGGTC GGCAAACACAAGTTTGTAGAAATTG-3' . Similarly, to test HoxA9 site specificity, HoxA9 binding site ATAA at Hif-1α reporter using site directed mutagenesis kit from Hif-1α-pGL2 vector with the following primers: HoxMut-Hif1a-F: 5'-CCTGTCAGGAGAGCCCAGACGCCGCGTATCAATATGTGGCTG CCTC-3' and HoxMut-Hif1a-R: 5'-GAGGCAGCCACATATTGATACGCGGCGTCTG GGCTCTCCTGACAGG-3'.

Statistical Analysis

Results are expressed as mean ± SEM and a 2-tailed Student *t* test was used to determine the level of significance. $p<0.05$ was considered statistically different.

RESULTS

Metabolic profile of human HPSC

HSCs have been reported to reside in hypoxic niches and this suggested that HSCs require adopting unique metabolic properties. Here, we demonstrate that human progenitor/hematopoietic stem cells (HPSCs) ($Lin^-CD34^+CD38^-CD90^+$ cells) from G-CSF mobilized peripheral blood (MPB) have lower rates of mitochondrial respiration. The overall oxygen consumption by HPSCs is significantly lower compared to MPB mononuclear cells (Figure 8A). Consistently, human HPSCs have lower ATP content (Figure 8B). In addition, Figure 8C shows that the rate of glycolysis is significantly higher in HPSCs compared to the MPB mononuclear cells, suggesting that human HPSCs rely primarily on glycolytic metabolism instead of mitochondrial oxidative phosphrylation.

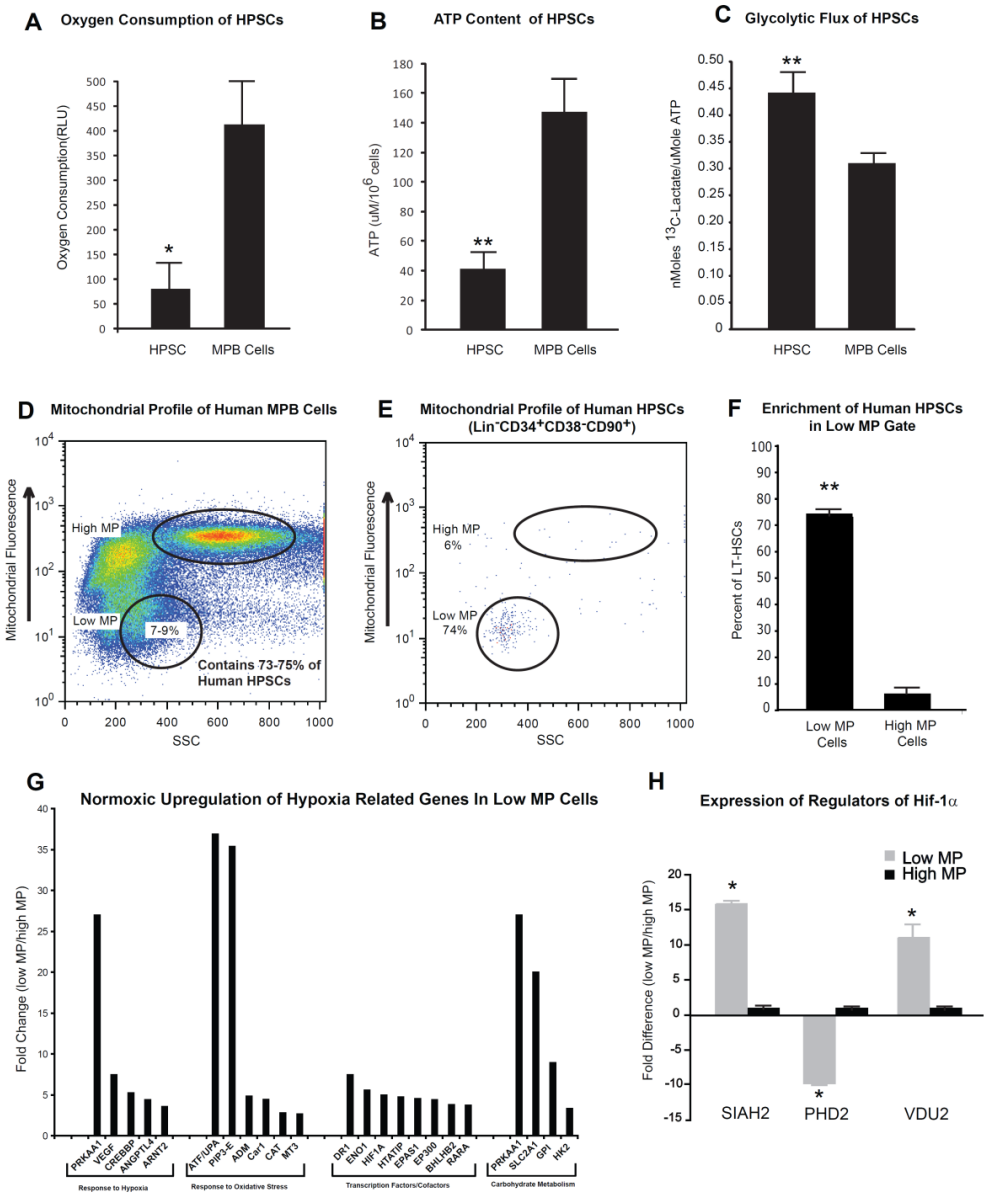

Figure 8: Metabolic Profile of Human HPSC: A) Oxygen consumption of $Lin^-CD34^+CD38^-CD90^+$ (HPSC) and human mobilized peripheral blood cells (MPB Cells) demonstrating lower rates of oxygen consumption by HPSC (n = 3). B)

ATP level of HPSC and MPB Cells demonstrating lower ATP levels in HPSC (n = 3). C) Glycolytic flux of HPSC and MPB Cells demonstrating higher rates of glycolysis in HPSC (n = 3). D) Flow cytometry profile of MPB mononuclear cells stained with mitotracker. Note populations with different mitotracker fluorescence E) Mitotracker profile of human HPSC. The majority of human HPSC (73-75%) are localized to a unique population (7-9%) of total human MPB mononuclear cells with low mitochondrial potential (low MP) F) Quantification of the percent of human HPSC reside in low MP cells and high MP cells demonstrates significant enrichment of human HPSCs in low MP gate. G) Real-time PCR array of low MP cells compared to high MP cells shows significant upregulation of a number of hypoxia inducible genes in the low MP cells at normoxia. H) Expression of regulators of Hif-1α in low and high MP cells by RT-PCR. Note the significant downregulation of the Hif-1α destabilizing enzyme PHD2 and the upregulation of two Hif-1α stabilizing enzymes SIAH2 and VDU2 in the low MP cells (n =3).*$p<0.05$, **$p<0.01$

Next we sought to profile human MPB HPSCs based on their mitochondrial proton gradient as an index of overall mitochondrial respiration. Similar to mouse HSCs, the vast majority of the human $Lin^{-}CD34^{+}CD38^{-}CD90^{+}$ cells (74%) fell within a defined flow-cytometry gate which corresponds to 7-9% of total G-CSF mobilized human peripheral blood cells (Figure 8D). Cells in this gate were

characterized by low mitochondrial potential (low MP) while the majority of the remaining MPB populations fell within a high mitochondrial potential (high MP) (Figure 8E-F).

To characterize the metabolic properties of cells in the low and high MP gates, we performed a PCR array for hypoxia related gene expression in freshly isolated low and high MP cells. Under normoxic conditions, the low MP cells were characterized by significant upregulation of numerous hypoxia-inducible genes and regulatory glycolysis genes including Hif-1α (Figure 8G). These results are not only supportive of the metabolic phenotype of low MP cells, but also suggest that the low MP cells are primed to handle hypoxic stresses. In addition, expression profile of the Hif-1α regulatory genes is in favor of stabilization of Hif-1α protein in low MP cells (Figure 8H). PHD2, which is responsible for hydroxylation of Hif-1α resulting in its ubiquitination and degradation, was significantly ($p<0.05$) downregulated in the low MP cells. Conversely, SIAH2 and VDU2, two stabilizers of Hif-1α were significantly ($p<0.05$) upregulated in low MP cells compared to high MP cells. These results support the higher levels of Hif-1α and the higher expression of Hif-1α target genes in low MP cells.

Together, these results indicate that low MP cells are characterized by baseline upregulation of glycolytic and hypoxia inducible genes, which suggests the

dependence of human HPSCs on glycolysis as the major source of energy production.

Characterization of Stem Cell Profile of Metabolically Sorted Cells

Given HSCs demonstrate distinct metabolic properties, we tested if this metabolic footprint could enrich for HPSCs. Following flow cytometric separation of low and high MP cells, we utilized colony formation analysis as a surrogate assay to test HPSC properties of low MP cells. Equal numbers of low and high MP cells were plated in methocult media for 12 days. Then, number and type of colonies were evaluated. Low MP cells had significantly ($p<0.001$) higher colony formation compared to high MP cells (Figure 9A). Additional classification of colony types showed that the low MP cells produced a higher percentage of CFU-GEMM type (mixed colonies) (Figure 9B) with lower percentages of BFU-E (Figure 9C) and CFU-GM (Figure 9D) colonies than high MP cells. Furthermore, we evaluated the gene expression profile of low and high MP cells by PCR array. Similar to their mouse counterparts, low MP cells were characterized by enrichment of HPSC associated stem cell markers and diminished lineage differentiation markers when compared to high MP cells (Figure 9E and 9F respectively). These results indicate that low MP cells are enriched for human HPSCs.

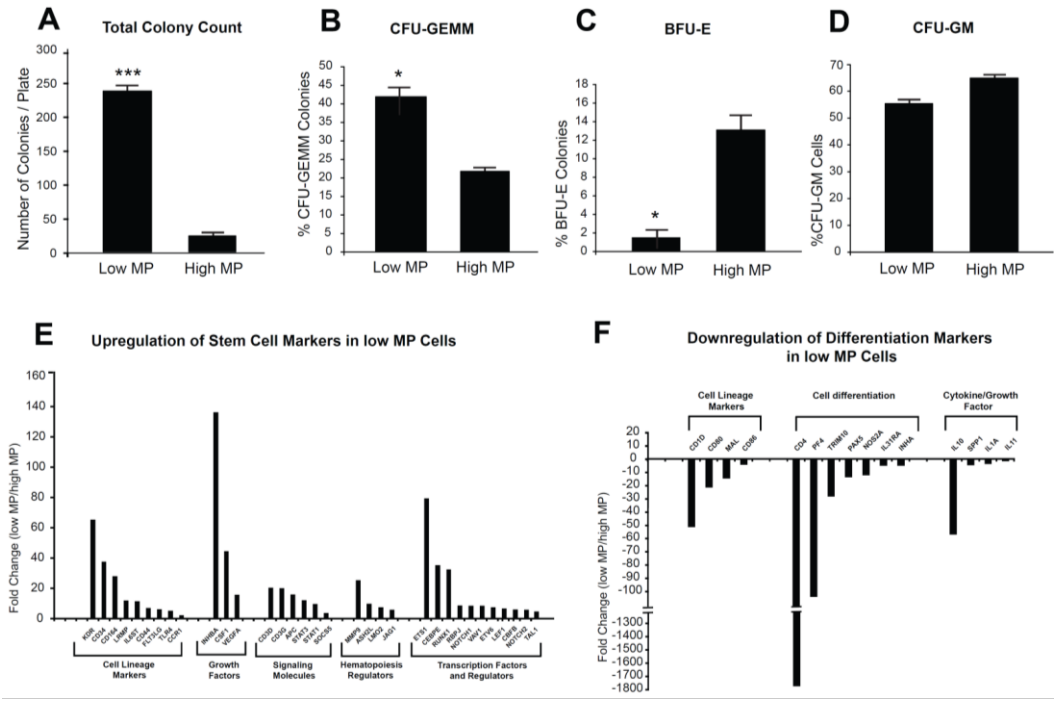

Figure 9: Low MP Cells are enriched for hematopoietic stem cells: *In vitro* colony forming assay using low and high human MPB cells. Panel A-D shows the number of colonies derived from low and high MP cells after 12 days in methocult medium. Note the significantly higher number of colonies derived from the low MP population. (n=3, $p<0.001$) Different types of colonies derived from low and high MP cells were analyzed. B, C and D are the percentages of CFU-GEMM, BFU-E and CFU-GM respectively. E) Real Time PCR array of HPSC markers comparing low MP cells to high MP cells. F) Real Time PCR array of differentiation markers comparing low MP to high MP cells. Note the enrichment

of a number of markers for HPSCs and the downregulation of differentiation markers. *p<0.05, **p<0.01, ***p<0.001

Expression of Hif-1α and Meis1 in human HPSCs

In order to determine the molecular mechanism behind glycolytic phenotype of human HPSCs and the expression of Hif-1α in low MP MPB cells, we evaluated the expression pattern of Hif-1α and Meis1 in human MPB mononuclear cells and HPSCs. Meis1 is a transcription factor required for definitive hematopoiesis. We demonstrated that Meis1 transcriptionally regulates Hif-1α expression in mouse LT-HSCs (Simsek et al., 2010). However, whether Meis1 plays any role in the regulation of Hif-1α in human hematopoiesis was unknown. To address this question, we first determined the expression of Meis1 in human MPB mononuclear cells and HPSCs. Cells were fixed, permeabilized, and intracellularly stained by antibodies against Hif-1α and Meis1 followed by flow cytometry analysis. While about 5% and 6% of MPB mononuclear cells express Hif-1α and Meis1, respectively (Figure 10A and Figure 10D), a significantly higher percent of HPSCs express Hif-1α (47%) (Figure 10B-C) and Meis1 (48%) (Figure 10 E-F). In addition, approximately 80% of $Meis1^{+}$ MPB cells are Hif-1α positive (Figure 10G-H). This expression pattern was obtained after hours of MPB harvest, which suggest that expression of Hif-1α in the MPB cells is not secondary to the *in vivo* hypoxic niche in the bone marrow.

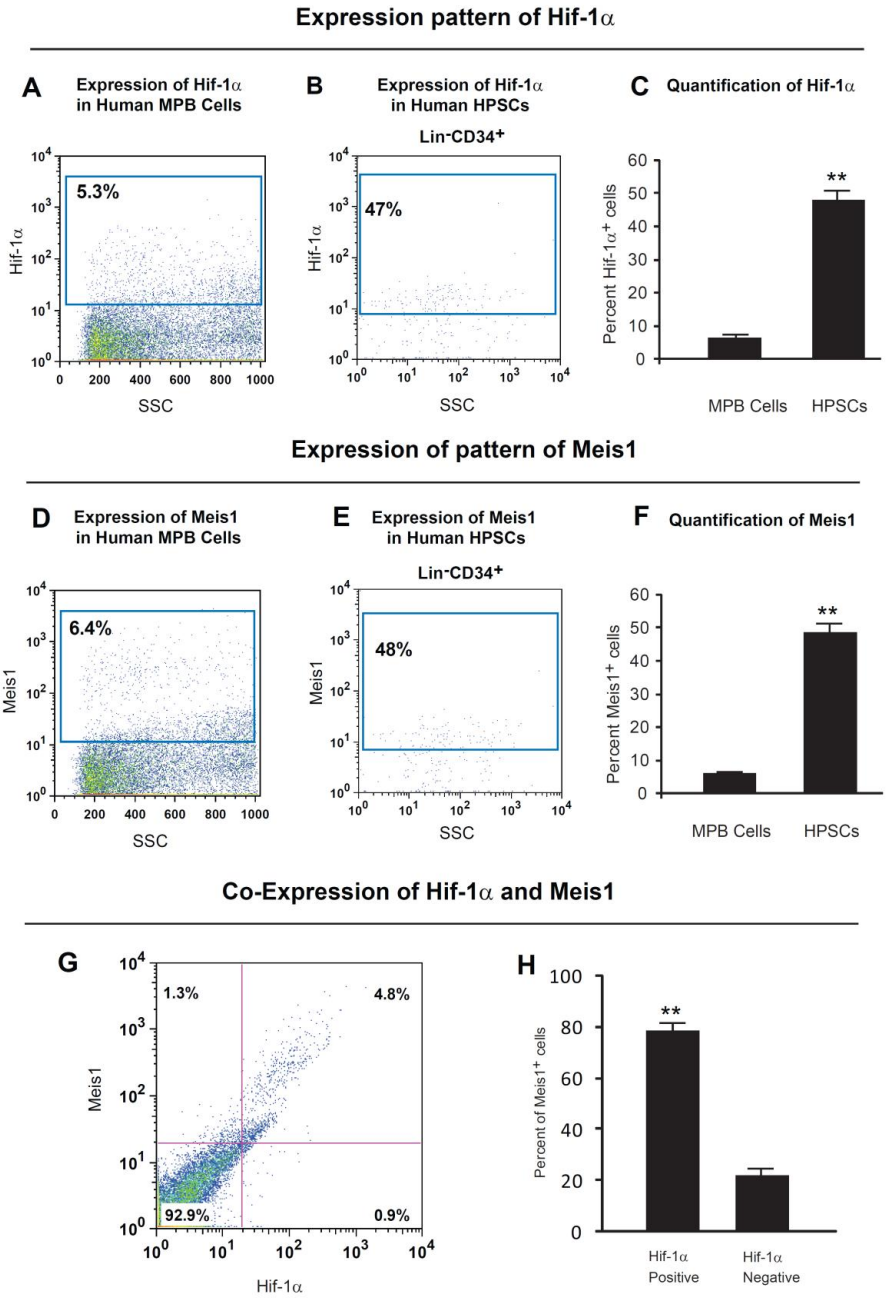

Figure 10: Expression profile of Hif-1α and Meis1 in Human HPSCs: Expression pattern of Hif-1α A) The left panel shows expression of Hif-1α in human MPB cells. B) Expression of Hif-1α in human HPSCs. C) Quantification of Hif-1α expression. Note that while 5.3% of the human MPB cells express Hif-1α, the significantly higher percentage (47%) of HPSCs express Hif-1α (~9 fold)

(n = 3). **Expression pattern of Meis1** D) The left panel shows expression of Meis1 in human MPB cells. E) Expression of Meis1 in HPSC. F) The right panel shows quantification of Meis1 expression. Note that while 6.4% of the human mobilized peripheral blood cells express Meis1, 48% of HPSCs express Meis1 (n = 3) (~7.5 fold). Co-expression of Hif-1α and Meis1 G) Flow cytometric colocalization of Hif-1α and Meis1 in the human MPB cells. Left panel shows a representative flow cytometry profile of Hif-1α and Meis1 expression. E) Quantification of the percent of $Meis1^{+}$ cells. Note the majority of $Meis1^{+}$ cells coexpress Hif-1α. **$p<0.01$

Regulation of Hif-1α by Meis1

Given the confirmed conserved Meis1 consensus binding sequence in the Hif-1α intron and the Meis1 expression in HSCs, we sought to determine whether Meis1 is required for Hif-1α expression in human hematopoietic cells. To this end, we used siRNA to knockdown Meis1 in Kasumi-1 cells (a human myeloid progenitor cell line known to express Hif-1α at normoxic conditions (Pedersen et al., 2008)). Upregulation of Meis1 and Hif-1α in low MP cells and in Kasumi-1 cells was confirmed by real time PCR (Figure 11A-B and 11C respectively) prior to siRNA experiments. Scrambled Meis1 siRNA was used as control. 50 nM Meis1 siRNA resulted in significant decrease of Meis1 mRNA levels (5.2 +/- 1.0 fold reduction) ($p<0.05$). This was associated with a significant downregulation of Hif-1α mRNA

(Figure 11D), as well as reduced expression of glycolytic genes downstream of Hif-1α including lactate dehydrogenase (LDHA), Glut1 (SLC2A1), and phosphofructokinase (PFKL) (Figure 11E) ($p<0.05$). These results demonstrate that Meis1 is required for optimal expression of Hif-1α and its downstream target genes in human hematopoietic cells.

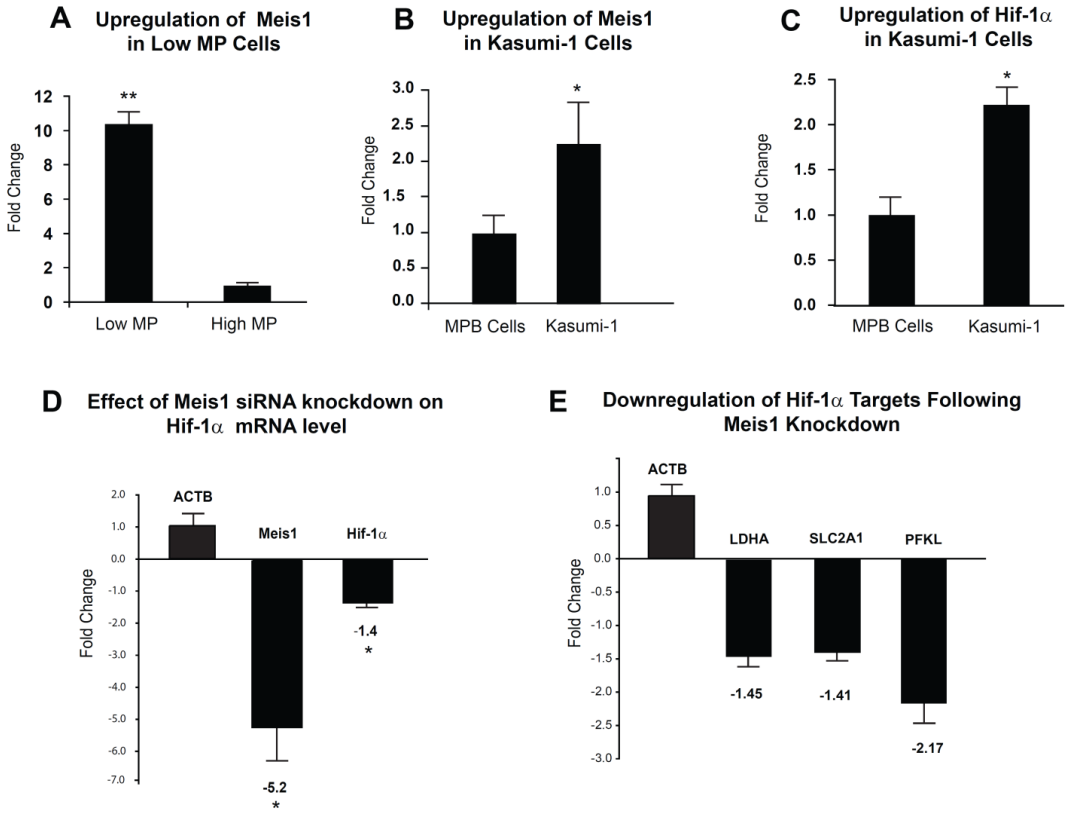

Figure 11: Transcriptional regulation of Hif-1α by Meis1: A) Real Time PCR of Meis1 in low and high MP cells shows significantly higher levels of Meis1 expression in low MP cells. B) Upregulation of Meis1 in Kasumi-1 cells compared to human MPB Cells and C) Upregulation of Hif-1α in Kasumi-1 cells compared to human MPB Cells. D) Real time PCR of Meis1 and Hif-1α in Kasumi-1 cells following siRNA knockdown of Meis1. E) Real time PCR of lactate dehydrogenase (LDHA), Glut1 (SLC2A1) and phosphofructokinase (PFKL) following siRNA knockdown of Meis1. Note the significant downregulation of Hif-1α mRNA and Hif-1α target genes following siRNA knockdown of Meis1. n = 3,*$p<0.05$, **$p<0.01$

Cooperation of Meis1 with Pbx1 and HoxA9 in the regulation of Hif-1α expression

In addition to Meis1 binding motif in the Hif-1α intron, we identified conserved putative Pbx1 ("TGAT") and HoxA9 ("ATAA") binding motifs in close proximity to consensus Meis1 binding site (Figure 12A). Meis1, Pbx1 and HoxA9 pose interaction domains or motifs that facilitate cooperation in gene activation. Given that Meis1 is known to cooperate with Pbx1 and HoxA9 in gene activation, we tested the role of Pbx1 and HoxA9 in the activation of Hif-1α. Using Hif-1α-pGL2 luciferase reporter which includes conserved Meis1, Pbx1 and HoxA9 sites, we demonstrate a dose dependent activation of Hif-1α by Pbx1 (Figure 12B) and HoxA9 (Figure 12C) in addition to Meis1 as we showed earlier (Simsek et al., 2010). This activation demonstrates dependence on binding of Pbx1 or HoxA9 to its consensus binding sequences in the Hif-1α reporter as mutation of the seed sequences (PbxMut-Hif-1α-pGL2 or HoxMut-Hif-1α-pGL2 reporters, respectively) completely abolished the activation of Hif-1α by Pbx1 or HoxA9 respectively. To test co-operation of Meis1 with Pbx1 and HoxA9 in the Hif-1α expression, we performed further luciferase assays using different combinations of Meis1, Pbx1, and HoxA9 vectors. Here we demonstrate that Meis1, Pbx1 and HoxA9 cooperate in the activation of Hif-1α (Hif-1α-pGL2 reporter) (Figure 12D).

In summary, Hif-1α expression is orchestrated by cooperative activation of Meis1, Pbx1 and HoxA9 (Figure 12E). This activation is dependent on consensus binding motifs located at Hif-1α intronic enhancer.

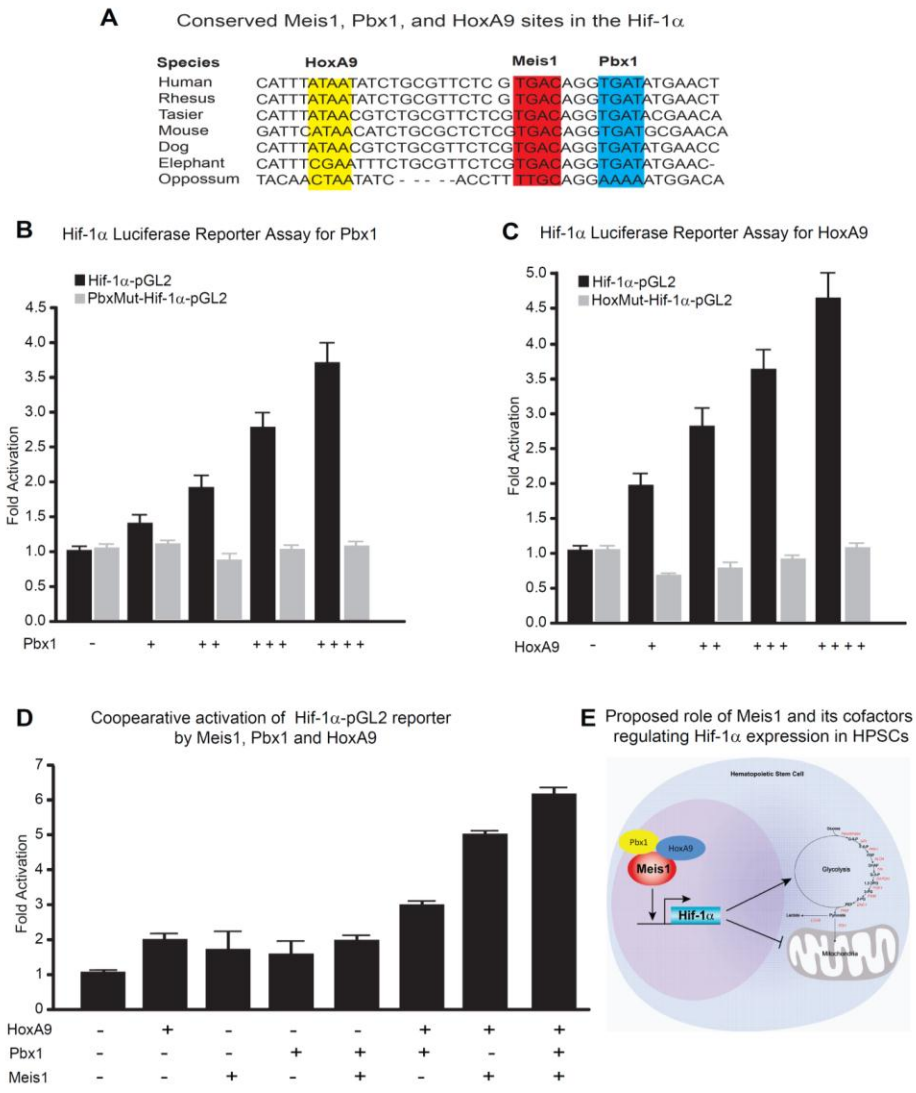

Figure 12: Cooperative role of Pbx1, HoxA9, and Meis1 for transcriptional regulation of Hif-1α: A) Figure shows conserved consensus Meis1, Pbx1, and HoxA9 motifs found on Hif-1α gene. Note the binding motifs found next to each

other in close proximity and highly conserved. B) Luciferase reporter assays demonstrate dose-dependent transcriptional activation of Hif-1α (Hif-1α-pGL2 reporter) by Pbx1 and mutation of Pbx1 bindings sites abolished Hif-1α activation (PbxMut-Hif-1α-pGL2 reporter) C)Luciferase reporter assays demonstrate dose-dependent transcriptional activation of Hif-1α (Hif-1α-pGL2 reporter) by HoxA9 and mutation of HoxA9 bindings sites abolish Hif-1α activation (HoxMut-Hif-1α-pGL2 reporter) D) Luciferase reporter assays with different combinations of Meis1, Pbx1, and HoxA9 demonstrates (additive) cooperation of Meis1, Pbx1 and HoxA9 for activation of Hif-1α (Hif-1α-pGL2 reporter) E) Schematic of proposed model showing regulation of Hif-1α expression by a complex of Meis1/Pbx1/HoxA9 proteins in hematopoietic stem cells.

DISCUSSION

Several studies indicated that bone marrow HPSCs are reside in hypoxic niches and capable of surviving upon hypoxic stress (Eliasson and Jonsson; Koller et al., 1992; Parmar et al., 2007). However, it is unclear if HPSC are endowed with distinct metabolic properties that confer this hypoxic tolerance. In the current report, we show that human mobilized HPSC are localized to a flow cytometry gate characterized by low mitochondrial potential (low MP). This population represents only 7-9% of the G-CSF mobilized human peripheral blood cells, but is enriched for more than 70% of human HPSCs as $Lin^{-}CD34^{+}CD38^{-}CD90^{+}$ cells. Moreover, we confirm this metabolic profile by demonstrating that human HPSCs have lower ATP content, lower rates of oxygen consumption, and use cytoplasmic glycolysis instead of mitochondrial oxidative phosphorylation as the major energy producing pathway. This unique metabolic profile is associated with upregulation of Hif-1α levels.

Because we found that human HPSCs are localized to the low MP gate even after G-CSF mobilization to the peripheral blood, it suggests that HPSCs may have intrinsic mechanism for the regulation of their metabolic properties. This is supported by our finding that transcription factors Meis1 and Hif-1α are highly enriched HPSCs.

Hif-1α as a master regulator of metabolism plays an essential role in various aspects of adaptation to hypoxic stress. Hif-1α is very well studied in terms of its posttranslational stabilization during hypoxia. However, little is known about transcriptional regulation of Hif-1α. Some reports indicate that Hif-1α is regulated at the transcription level not only at hypoxia but also normoxia (BelAiba et al., 2006; Laughner et al., 2001). Here we show that, the transcription factor Meis1 plays an important role in HPSC metabolism through transcriptional regulation of Hif-1α in cooperation with its cofactors Pbx1 and HoxA9. The transcriptional regulation of Hif-1α by Meis1 and its cofactors suggests that the metabolic profile of human HPSCs may be an intrinsic characteristic and not only a product of their hypoxic microenvironment. Investigation on metabolic profile of human bone marrow or cord blood HPSCs and leukemia cell lines will be attractive to further address these unique metabolic characteristics.

CHAPTER FOUR

THE CARDIAC HYPOXIC NICHE AND GLYCOLYTIC CARDIAC STEM CELLS

INTRODUCTION

The adult mammalian heart is incapable of any meaningful functional recovery after significant cardiomyocytes loss, which leads to irreversible contractile dysfunction (reviewed in (Laflamme and Murry, 2011; Segers and Lee, 2008)). However, limited cardiomyocyte turnover does occur in the adult heart, albeit insufficient for restoration of contractile function (Bergmann et al., 2009; Laflamme et al., 2002; Loffredo et al., 2011). Although the lineage origin of new cardiomyocytes in the adult heart is not well understood, they appear to be derived from an unidentified cardiac progenitor population (Laflamme and Murry, 2011; Loffredo et al., 2011).

A number of cardiac progenitors have been identified based on expression of certain epitopes, such as C-Kit (Oh et al., 2003), or Sca-1(Matsuura et al., 2004), dye exclusion (reviewed in (Barile et al., 2007)), ex-vivo culture conditions (reviewed in (Passier et al., 2008; Segers and Lee, 2008)), or epicardial localization (Chong et al., 2011; Slukvin, 2011). In zebrafish, the epicardium is

activated in response to injury (Lepilina et al., 2006), and the subepicardium houses a population of cardiomyocytes that replenish the injured myocardium (Kikuchi et al., 2010). In mammals, the epicardium is also activated following injury (Zhou et al., 2011). Recent reports indicate that the Wt1 epicardial cells modulate the cardiac injury response through paracrine signaling to the subepicardium, and contribute to cardiomyocyte formation after priming with thymosin beta-4 (Smart et al., 2011) . Therefore, despite the localization of a number of cardiac regeneration events to the epicardium and subepicardium, the anatomical and functional properties that make this region a bona fide cardiac stem or progenitor niche (Popescu et al., 2009; Urbanek et al., 2006; Walker et al., 2009), remain unclear.

Several organ-specific adult stem cells reside in specialized niches in the adult organism ((Urbanek et al., 2006) and Reviewed in (Morrison and Spradling, 2008; Nakada et al., 2011)). These niches are characterized by their low oxygen tension (Mohyeldin et al., 2010; Parmar et al., 2007), therefore favoring anaerobic glycolytic metabolism, which may play a protective role against reactive oxygen species (ROS) (Nakada et al., 2011). We recently demonstrated that hematopoietic stem cells (HSCs) utilize cytoplasmic glycolysis instead of mitochondrial respiration to meet their energy demands. This low mitochondrial footprint is associated with upregulation of Hif-1α, and can be used for HSC

enrichment in the absence of antibody based enrichment methods (Simsek et al., 2010).

In the current report, we identify the epicardium and subepicardium as the cardiac hypoxic niche. We utilize metabolic footprinting and differential perfusion techniques to identify a hypoxia resistant progenitor population that preferentially utilize glycolytic metabolism, which we call glycolytic cardiac progenitors (GCPs). Finally, we demonstrate that Hif-1α regulates the metabolic phenotype, proliferative rate, and maintenance of undifferentiated state of these glycolytic cardiac progenitors.

METHODS

Capillary quantification:

Adult heart sections were stained with the endothelial marker endomucin, and detected using DAB chromogen. Images of 4 chamber-view adult stained heart sections were quantified for capillaries for 3 cell layers in 5 different zones in the coronal plane (base to apex), and 7 different zones in the horizontal plane (endocardium to epicardium).

For endomucin staining, which labels endothelial cells, slides were deparaffinized, blocked in 5% goat serum (Invitrogen, CA) and incubated with a rat anti-mouse endomucin antibody (1:250 dilution in PBS clone# eBioV.7C7 (V.7C7), eBioscience, CA, USA) overnight at 4ºC. The following day, slides were washed 3 times in PBS and then incubated for 30 min at room temperature with a biotinylated rabbit anti-rat secondary antibody (1:500 dilution, Vector Labs, CA). Slides were next washed 3 times in PBS and then incubated for 30 minutes at room temperature with horseradish peroxidase streptavidin (1:500 dilution, Vector Labs, CA). Slides were then washed 4 times in PBS, incubated in the dark for 10 min at room temperature with diaminobenzodine (Dako, CA) and counterstained with hematoxylin. Sections were then dehydrated in ethanol twice for 3 min each, before being cleared with xylene (2 x 3 min) and mounted in Permount (Fisher Scientific, IL).

Immunostaining of Hif-1α:

Paraffin embedded heart sections deparaffinized and rehydrated. Antigen retrieval with 10mM Na-Citrate (pH6.1) in boiling water for 20 min was performed. Sections were cooled down for 30 min by adding 1/5 of distilled water (room temperature) every 5 minutes. Following 30 min blocking with 10% goat serum, sections incubated with Hif-1α (SC-10790 Santa Cruz, 1:50 dilution) and Tnnt (Thermoscientific, MS-295-P1, 1:50 dilution) antibodies overnight at 4^{o}C. Sections washed with PBS and incubated with corresponding secondary antibodies.

Isolation of non-cardiomyocytes from adult mouse heart:

Whole adult mouse hearts (8-12 weeks old) were anticoagulated with 10 IU/kg of IP heparin sodium, and the hearts were harvested and quickly rinsed in ice-cold saline. Retrograde perfusion digestion using collagenase was performed as previously described (O'Connell et al., 2007). Cardiomyocytes were discarded following centrifugation at 50g for 5 minutes. Non-cardimyocytes in the supernatant were isolated by centrifugation at 1200g for 10 minutes.

Flow cytometric profiling and characterization of heart cells with low mitochondrial footprint:

Flow cytometric profiling and separation of non-cardiomyocytes based on their mitochondrial footprint was performed with mitotracker dyes. Non-cardiomyocytes were incubated for 15 minutes with Mitotraker Green (Cat#M7514, Invitrogen) at 37^{o}C. Cells with the lowermost mitochondrial potential (0.5% of total number of cells) were sorted and cultured in embryonic stem cell (ESC) medium. These cells were referred to as glycolytic cardiac progenitors (GCPs). To determine the lineage of these cells, surface marker staining was performed for the following epitopes prior to flowcytometry profiling: 1) Stem cell markers: c-Kit (Cat#553356, BD Biosciences), and Sca-1 (Cat#553335, BD Biosciences). 2) Endothelial marker CD31 (BD Biosciences), and 3) Hematopoietic lineage marker CD45 (BD Biosciences). Additional characterization for Nkx2.5 (T6074, Sigma), Gata4 (#SC-1237, Santa Cruz), WT1 (#SC-192, Santa Cruz), and Tbx18 (#SC-17869, Santa Cruz) was performed. GCPs that were positive for cardiac and epicardial progenitor markers were quantified by immunofluorescence. Three-four images per staining were taken at 40X and percent of positive cells were determined [(number of positive cells/image)*100/(total number cells/field)].

***In vivo* perfusion based on Hoechst fluorescence intensity:**

Adult mice (6-8 weeks) were injected intraperitoneally with 100µl of 1.2 mg/ml Verapamil (Sigma-Aldrich) solution in PBS, to prevent dye exclusion by the ABCG2 transporter. Hoechst 33342 (Invitrogen) was used to determine *in vivo* perfusion based on Hoeschst fluorescence intensity following systemic administration, as described previously (Parmar et al., 2007). Mice were retro orbitally injected under isoflurane anesthesia with one dose of Hoechst dye (1.5 mg/mouse) 10 minutes before heart perfusion. Non-cardiomycytes were isolated as described. Non-cardiomyocytes were then stained at 37^{o}C for 15 minutes with Mitotraker Green (200 nM), and profiled by flow cytometry for Hoescht and MT Green.

Real time PCR:

Total RNA was isolated using TRIzol reagent (Invitrogen). cDNA was generated by following the recommended protocol for SuperScript II Reverse Transcriptase (Invitrogen) using 2 ug total RNA. Real time PCR was performed with SyberGreen (Applied Biosystems) on ABI Prism 7700 Sequence Detector (Applied Biosystems) using primers as follows from qPrimer Depot (http://mouseprimerdepot.nci.nih.gov/) :

Table 3. Primer list

Gene	Forward	Reverse
Nkx-2.5	GTC CAG CTC CAC TGC CTT C	CAA GTG CTC TCC TGC TTT CC
Gata4	CAG GCA TTG CAC AGG TAG TG	CTG GAA GAC ACC CCA ATC TC
WT1	CCC GTG GGT GTG TAT TCT GT	ACC TTA AAG GGA ATG GCT GC
Tbx18	CTT GAT GGG GGA CAG ATC AT	AAT GAG CTG GAT GAC CAA GG
Siah2	CAC CAG GAC AAG GAC AGG A	TGT AAG TAT GCT ACC ACG GGC
PHD2	CAT GTC ACG CAT CTT CCA TC	GAT AAA CGG CCG AAC GAA A
VDU2	AGT ACT TCA CGC CAT TCC GA	AAG ACT GCC TTG CTG CTT TC
FIH1	GTGTCA TTG AGT GTC TGC TGC	AGG TCC AAC AGG GAG GAA AT
HSP90	ATT GGT TGG TCT TGG GTC TG	GCC AGT TGC TTC AGT GTC CT
FSP1	TTT GTG GAA GGT GGA CAC AA	CAG CAC TTC CTC TCT CTT GG
Hif-1α	CGG CGA GAA CGA GAA GAA	AAA CTT CAG ACT CTT TGC TTC G
SMαA	GTT CAG TGG TGC CTC TGT CA	ACT GGG ACG ACA TGG AAA AG
SM22a	GAC TGC ACT TCT CGG CTC AT	CCG AAG CTA CTC TCC TTC CA
Calponin1	TGG TGC CAG TTC TGA GTT GA	ATG TAT GGC CTC AAA GAC GG

Flk1	TCC AGA ATC CTC TTC CAT GC	AAA CCT CCT GCA AGC AAA TG
VWF	CCG TCT TCA GTA GCT GGC AT	GTG TAA ACG GGC ATC TCC TC
Tie2	TTT CGG CAT CAG ACA CAA GA	CCG GCT TAG TTC TCT GTG GA
Tnnt2	ACC CTC AGG CTC AGG TTC A	GTG TGC AGT CCC TGT TCA GA
Myh6	CTT CAT CCA TGG CCA ATT CT	GCG CAT TGA GTT CAA GAA GA
Col1a1	TAG GCC ATT GTG TAT GCA GC	ACA TGT TCA GCT TTG TGG ACC
Col3a1	TAG GAC TGA CCA AGG TGG CT	GGA ACC TGG TTT CTT CTC ACC
TnnI	CTC GGT AGT TGG CAG AGG AG	GCC TCT GGA GAT CAT CAT GG
Actc1	GCT CTG GGC TTC ATC ACC TA	AGC TGT CTT CCC GTC CAT C

Hypoxic and anoxic stress:

GCPs and cardiac fibroblasts were exposed to hypoxia (1% oxygen) and anoxia (0% oxygen) for 12 hours. Viability was assessed by trypan blue for three separate plates and presented as percent of total cell count.

Western Blot:

Whole protein extracts (150 μg/well) were collected from GCPs and cardiac fibroblasts in Cytobustor protein extraction reagent (Novagen, #71009-50mL)

with protease inhibitor cocktail and PMSF. Western blot was performed using rabbit anti Hif1-α antibody (#sc-10790, Santa Cruz) at 1:500 dilution overnight incubation at 4°C. Secondary anti- rabbit IgG HRP linked antibody (Cell Signaling Technology, #7074) was used at 1:1000 dilution for 1 hour incubation at RT. Relative Optical Density analysis was carried out using Adobe Photoshop software (corrected for tubulin).

Metabolic Assays:

Oxygen consumption was measured by the BD Oxygen Biosensor System (BD, CA, USA) according to manufacturer's recommendations. Equal numbers of cells (5×10^4 cells/well) were incubated for 1 hour in the provided 96 well plate prior to measurement. Culture media lacking cells was used as a negative control and sodium sulfite (100 mM) was used as a positive control. Oxygen consumption is presented as relative units.

Measurement of ATP Content: 5×10^4 GCPs and Cardiac Fibroblasts were used for each ATP assays. ATP standard curve was plotted with 10^{-6}-10^{-12}M ATP standards. 50 ul of cell lysates and ATP standarts were quantified by ATP Bioluminescence Assay Kit HS II (Roche) using Fluostar Optima plate reader (BMG Labtech). Finally, data were normalized to cell count.

Lactate production was measured with gas chromatography-mass spectrometry. In summary, 2 x 10^5 cells were cultured for 12 hr in 160µl of medium supplemented with 10 mM D-[1-^{13}C]-glucose (Cambridge Isotope Labs). The samples were analyzed for lactate abundance. The results are presented as nMoles ^{13}C-Lactate.

Colony formation:

To assess the colonegenicity of GCPs, we sorted single cells into 96 well plates by flowcytometry. One week later, the wells were examined for colony formation.

Differentiation assays

Endothelial lineage differentiation was assessed by angiogenesis assay using *In vitro* Angiogenesis Assay Kit (Cat#ECM625, Milipore) according to manufacturer's instructions. 5 x10^3 GCPs were plated on ECMatrix gel with ES or endothelial differentiation medium. Tube formation and CD31 expression were assessed after 12 days. To induce smooth muscle lineage differentiation, GCPs were cultured in DMEM supplemented with 5%FBS (low serum) for 1 week. For cardiomyocyte differentiation, GCPs were isolated from a ROSA YFP reporter mouse and used for co-culture experiments with neonatal rat cardiomyocytes (Arminan et al., 2010) for 1 month following *in vitro* reporter activation (Cre

transfection). Subsequently, YFP^{+}GCPs were isolated by flowcytometry. Cells were then re-cultured on coverslips and used for immuno staining for Tnnt2 (1:100, MS-295-P1, Thermo Scientific, IL), GFP (Cat#11122, Invitrogen) and α-actinin (1:100, A7811, Sigma), or used for RNA isolation and real time PCR quantification of cardiac transcripts. In addition, GCPs were also exposed to other cardiogenic stimuli (1%DMSO and 5-AzaC) as previously described (Matsuura et al., 2004; Qian et al., 2011).

Hif-1α knockdown and generation of retroviruses:

Hif-1α knockdown was carried out in GCPs by using retroviruses. 293T cells were plated 5 $x10^{6}$ cells the day before transfection in DMEM media supplemented with 10% FBS and antibiotics. 34 µg of Hif-1α shRNAmir retroviral vector(Cat# RMM1766-96744026, Open Biosystems) or Non-silencing pSM2 shRNAmir retroviral control (Cat#RHS1707, Open Biosystems) and 17 µg of pCL-Eco Retrovirus packaging vector (Imgenex, CA) were incubated in 1.5 ml µl of DMEM for 5 min. 90 µl of Lipofectamine 2000 (Invitrogen) was added to vector mixture and incubated for 20 min at room temperature. Medium was replaced with fresh medium after four hours. Retroviruses collected from medium after 48 hours. GCPs were treated with retroviruses and selected with puromycin.

Downreguation of Hif-1α in GCP Hif1-α-shRNA cells compared to GCP control-shRNA cells was confirmed by real time PCR and western blot.

Proliferation assay:

GCPs infected with control shRNA retrovirus and Hif-1α shRNA retrovirus plated into 6-well plates at same number (10 $x10^3$). After 48hrs, cells are trypsinized and counted with trypan blue.

Statistical analysis:

Significance levels were calculated using a student's *t* test. $P<0.05$ was considered significant.

RESULTS

The epicardial/subepicardial hypoxic niche

In order to determine the anatomical location of the hypoxic niche in the heart, we performed a series of experiments to characterize the differential capillary density, and hypoxia marker expression in the uninjured mouse heart. We found that the mouse ventricular epicardium/subepicardium (outermost 3 cell layers) has the lowest capillary density (Figure 13A and Figure 14) compared to the rest of the ventricular myocardium and endocardium. Moreover, we found that Hif-1α expression in the uninjured mouse heart is localized to the epicardium/subepicardium (Figure 13B), which is a strong indicator of the hypoxic nature of this niche. Moreover, we show that over 50% of epicardial cells, and a much lower percentage of subepicardial cardiomyoytes, and non-cardiomyocytes express Hif-1α (Figure 15). In contrast to the strict epicardial/subepicardial localization of Hif-1α in the ventricles, we found that the majority of atrial cells expressed Hif-1α (Figure 16), perhaps owing to the thin atrial wall

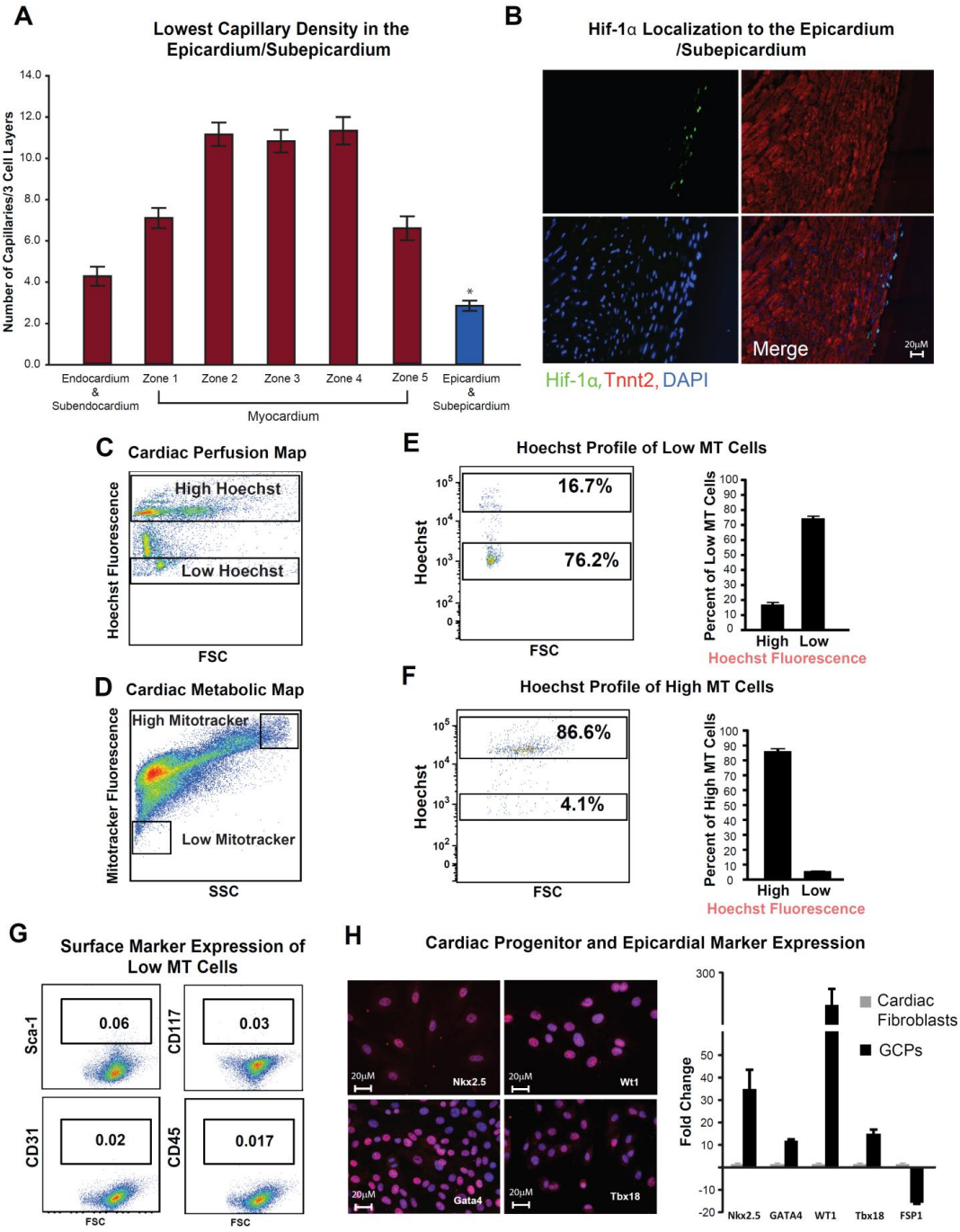

Figure 13: Characterization of the Cardiac Hypoxic Niche

A) Lowest capillary density in Epicardium/Subepicardium zone compared to the rest of the heart. **B)** Hif-1α immunostaining demonstrating localization of Hif-1α to the epicardium and subepicardium of the uninjured heart. **C)** Flowcytometry

profile of non-cardiomyocytes following retro-orbital injection of Hoechst dye. Note the distinct populations with different Hoechst fluorescence reflecting differential perfusion. **D)** Metabolic profile of non-cardiomyocytes. **E)** The majority of non-cardiomyocytes with low mitochondrial potential are localized to a distinct population with low Hoechst fluorescence, and vise versa. **G)** Cells in Low MT Gate are negative for the stem cell marker c-Kit and Sca-1, the endothelial marker CD31, and the hematopoietic marker CD45. **H)** Left panels: Cultured GCPs express cardiac progenitor and epicardial markers. Right Panel: Real time PCR confirmation. Data presented as mean ± SEM, n=3, *$p<0.05$.

Metabolic and perfusion selection of epicardial cells

To confirm the differential perfusion of the epicardium and subepicardium compared to the rest of the heart, we utilized a previously published protocol for *in vivo* perfusion quantification using Hoechst dye. We coupled this assay with metabolic profiling (using mitotracker) to co-localize perfusion with metabolic footprint. We found that the majority of the non-cardiomyocytes with the lowest mitotracker staining (low mitochondrial content), also had the lowest Hoechst fluorescence (reside in low perfusion zone), and vice versa (Figure 13C-F). We then sorted and cultured non-cardiomyocytes with the lowest mitochondrial content (0.5% of total number of cells-referred to as glycolytic cardiac progenitors or GCPs, which represents a heterogeneous cell population) to characterize their

marker expression. We found that these cells are clonogenic (following single cell sorting) and self-renewing (currently over 80 doubling passages in culture). Moreover, we found that these GCPs do not express stem (c-Kit or Sca-1), endothelial (CD31) or hematopoietic (CD45) markers at baseline (Figure 13G), but rather express cardiac progenitor and epicardial markers ($Nkx2.5^+$ (>95%), $GATA4^+$ (>65%), $WT1^+$ (>85%), and $Tbx18^+$.(>60%)(Cai et al., 2008)). These results were confirmed by real time PCR (Figure 13H).

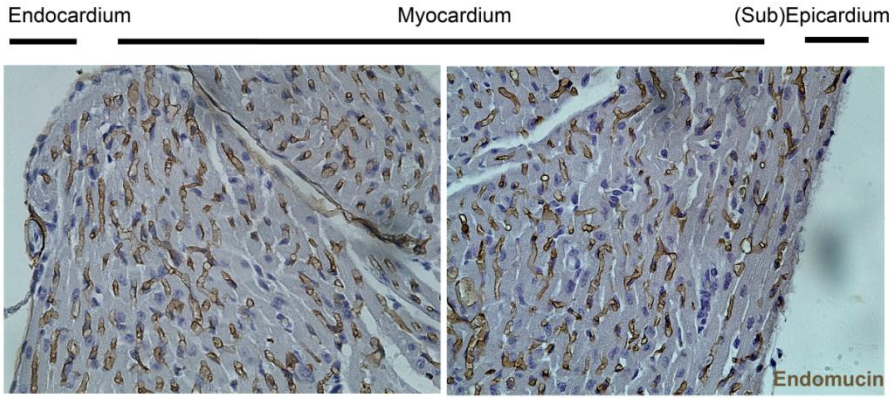

Figure 14. Endomucin Staining : Adult heart sections were stained with the endothelial marker endomucin, and detected using DAB chromogen. Images of 4 chamber-view adult heart sections were quantified for capillaries for in cell layers at 5 different zones in the coronal plane (base to apex), and 7 different zones in the horizontal plane (endocardium to epicardium).

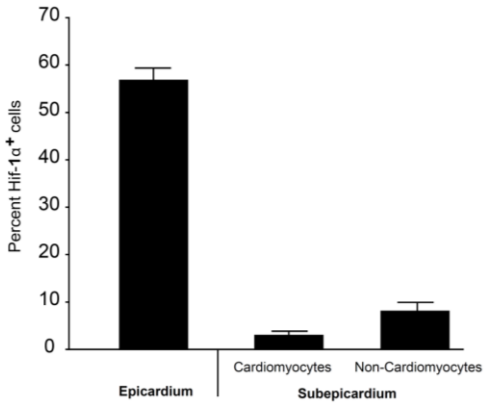

Figure 15. Quantification of Hif-1α expression in ventricular epicardium and subepicardium: The number of Hif-1 α expressing cells in the epicardium and subepicardium were quantified. The majority of ventricular epicardial cells expressed Hif-1α, while only a small percentage of subepicardial and myocardial myocytes and non myocytes expressed Hif-1α.

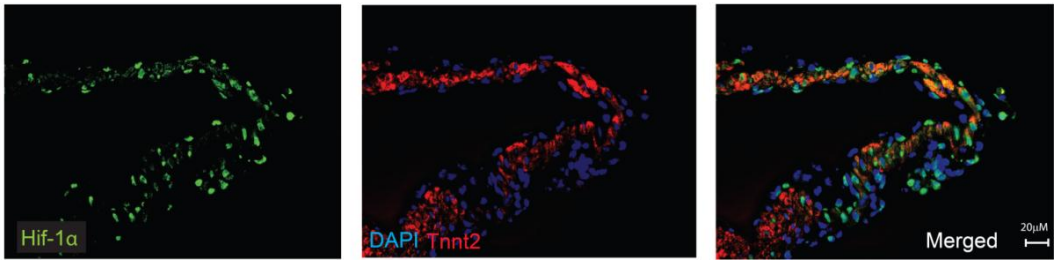

Figure 16. Atrial Hif-1α expression: The majority of atrial cells express Hif-1α. Hif-1α (green), Tnnt2 (red) and DAPI (blue)

Metabolic characteristics of GCPs

To determine if GCPs utilize glycolysis, rather than mitochondrial oxidative phosphorylation (akin to other stem cell populations), we measured oxygen consumption, glycolytic flux, and ATP content of GCPs compared to cardiac fibroblasts. We found that GCPs displayed significantly lower oxygen consumption rates (Figure 17A) and ATP content (Figure 17B) compared to the

cardiac fibroblasts. Moreover, GCPs have significantly higher glycolytic flux (Figure 17C). Taken together, these results indicate that GCPs rely on cytoplasmic glycolysis, rather than mitochondrial oxidative phosphorylation to meet their metabolic demands.

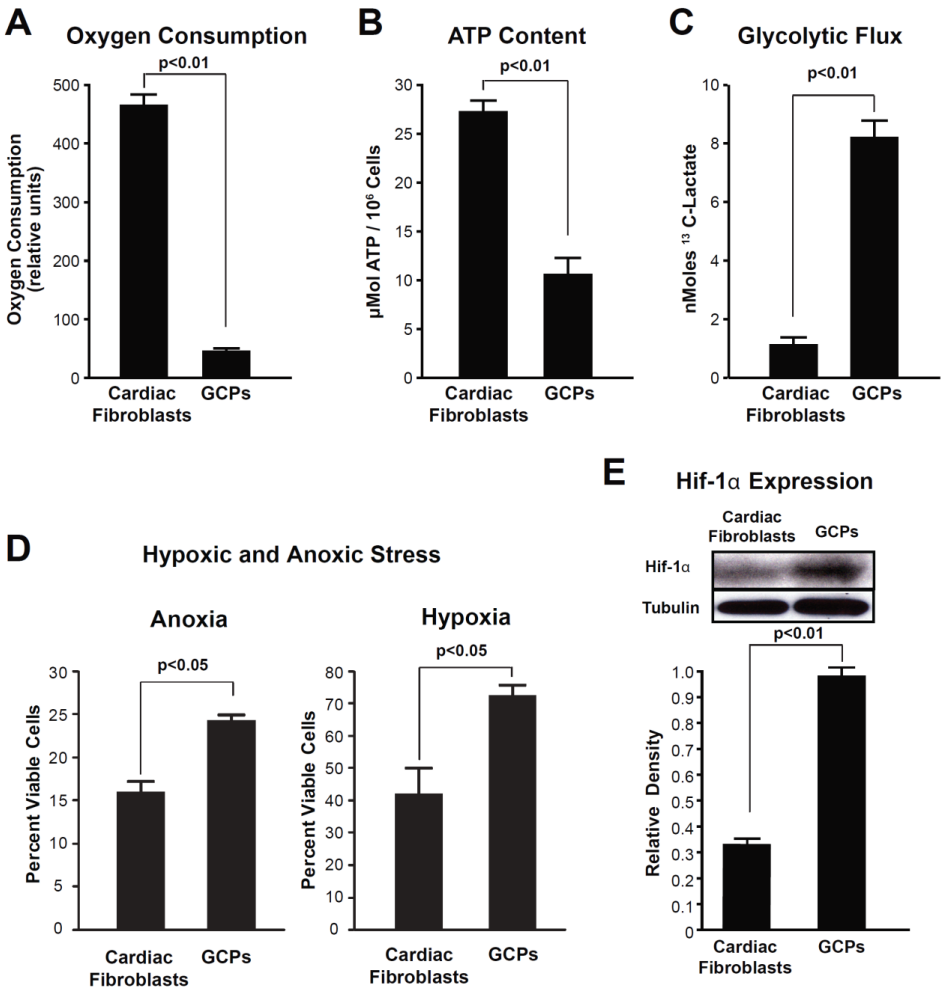

Figure 17: Metabolic Profile of GCPs: A) Lower oxygen consumption of GCPs compared to cardiac fibroblasts **B)** Lower ATP content of GCPs compared to cardiac fibroblasts. **C)** Higher glycolytic flux of GCPs compared to cardiac

fibroblasts. **D)** Viability of GCPs and cardiac fibroblasts at low-oxygen stress. The left panel shows the percentage of viable GCPs and cardiac fibroblasts after 12 hours of severe (1%) hypoxia. The right panel shows the percentage of viable GCPs and cardiac fibroblasts after 12 hours of anoxia. **E)** Western blot showing significantly higher expression levels of Hif-1α in GCPs compared to cardiac fibroblasts. Bottom panel is the quantification of relative band density. Data presented as mean ± SEM, n=3.

Low oxygen stress and Hif-1α expression

One of the major protective mechanisms against hypoxia is the ability to generate ATP in the absence of oxygen. This is typically carried out by enhanced rates of cytoplasmic glycolysis, rather than the oxygen dependent mitochondrial oxidative phosphorylation. Since we determined that GCPs utilize glycolysis, rather than mitochondrial oxidative phosphorylation for their energy demands, we wanted to determine if this glycolytic metabolic phenotype is associated with resistance to low oxygen stress. Here we show that a significantly higher number of GCPs survived both hypoxic and anoxic stresses compared to cardiac fibroblasts (Figure 17D), which is consistent with their glycolytic metabolic phenotype. In order to determine the mechanism of metabolic regulation and hypoxia resistance of GCPs, we examined their Hif-1α expression and determined that GCPs display

significant upregulation of Hif-1α protein compared to cardiac fibroblasts (Figure 17E).

Differentiation potential of GCPs

One of the hallmarks of stem, or progenitor cells, is their ability to differentiate to multiple lineages. In the next set of experiments, we set out to determine whether GCPs are capable of acquiring different cardiac lineages, through *in vitro* differentiation. Our results indicate that GCPs can differentiate into endothelial lineage as determined by matrigel tube formation by GCPs (Figure 18A), CD31 surface marker expression (Figure 18B), and expression of other endothelial markers by real time PCR (Figure 18C). Moreover, we found that at baselines, GCPs display rare Smooth Muscle α Actin (SMαA) positive cells (<6%), which increases to >45% upon culture in differentiation conditions (Figure 18D). This smooth muscle lineage differentiation is also supported by the increased expression of other smooth muscle markers such as SM22α, and Calponin1 (Figure 18E). Finally, we show that YFP^+ GCPs express cardiomyocyte markers following various cardiogenic stimuli as determined by mRNA and protein expression (about 10%$TnnT^+$ and 2.5% α-$Actinin^+$ YFP^+ GCPs) (Figure 18F-H).

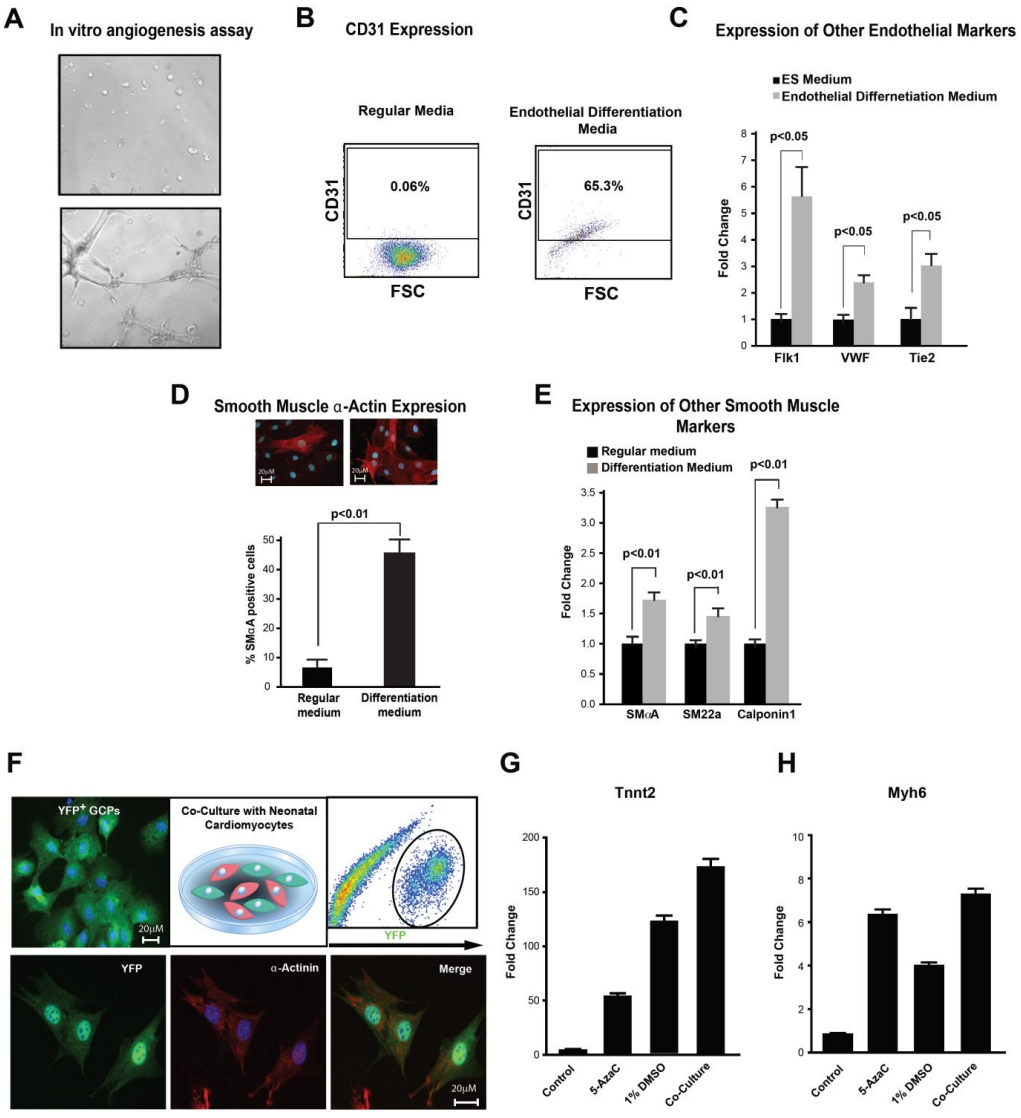

Figure 18: Differentiation Potential of GCPs: A) Lack of tube formation in GCPs cultured under normal condition (upper panel), and robust tube formation of GCPs cultured under endothelial differentiation conditions. **B)** Lack of CD31 expression in GCPs cultured under normal conditions (left panel), and robust expression of CD31 in GCPs cultured under endothelial differentiation conditions (right panel). **C)** Real time PCR of GCPs following induction of endothelial

differentiation demonstrating upregulation of endothelial markers (FLK1, VWF, and TIE2). **D)** Upper left panel: Rare Smooth Muscle α-Actin (SMαA) immunostaining of GCPs in non-differentiation conditions. Upper right panel: Significant increase in the number of SMαA cells following differentiation. Bar graph: Quantification of Smooth Muscle α-Actin positive cells**. E)** Real time PCR demonstrating increased expression of smooth muscle genes following culture of GCPs in differentiation conditions. **F)** Upper left: YFP^+ GCPs isolated from Rosa YFP reporter mouse hearts, showing positive YFP immunostaining (green). Upper middle: Cartoon illustrating co-culture with neonatal cardiomyocytes. Upper right: Flowcytometry profile showing sorting of YFP^+ GCPs following co-culture with neonatal cardiomyocytes. Lower panels: α-actinin expression in YFP^+ GCPs, and **H)** Real time PCR for Tnnt2 and Myh6 expression of GCPs following various cardiogenic stimuli. Data presented as mean ± SEM, n=3

Hif-1α regulates metabolic phenotype and differentiation of GCPs

To determine whether the metabolic phenotype of GCPs is regulated by Hif-1α, we performed knockdown studies. Knockdown of Hif-1α in GCPs resulted in marked downregulation of Hif-1α mRNA (Figure 19A) and protein levels (Figure 19B). This resulted in a metabolic shift from glycolysis to mitochondrial oxidative phosphorylation (Figure 19C-E). In addition, this metabolic switch was associated with a decrease in proliferation rates (Figure 19F), and loss of undifferentiated

state. Interestingly, this spontaneous differentiation appeared to favor an increase in cardiomyocyte (Tnnt2, TnnI, Actc1, and Myh6) and endothelial (Flk1, Vwf, Tie1, and TIE2), lineage markers, but not smooth muscle (SMαA, SM22a, and Cnn1) or fibroblast (Col1a1 and FSP1) (Figure 19G).

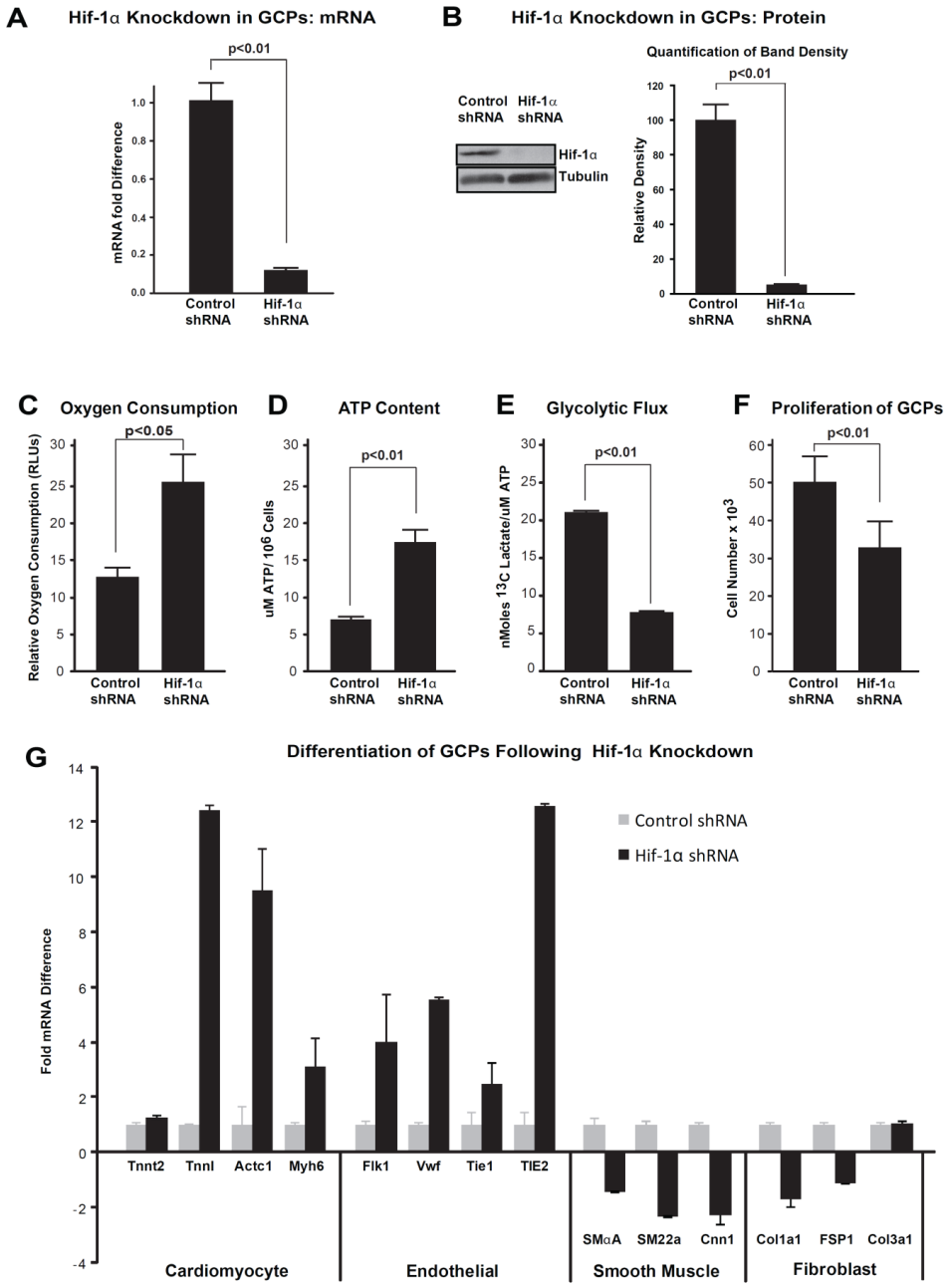

Figure 19. Role of Hif-1α in the regulation of metabolism and differentiation of GCPs : A) Real-time PCR following retroviral knockdown of Hif-1α in GCPs showing marked downregulation of Hif-1α mRNA levels. B) Western blot showing knockdown of Hif-1α in GCPs following infection with control and Hif-

1α shRNA retroviruses. Right panel is the quantification of relative band density of western blot, normalized to Tubulin. **C, D and E)** Showing metabolic switch from glycolytic metabolism to mitochondrial oxidative phosphorylation. **F)** Decreased GCP proliferation following Hif-1α knockdown **G)** Differentiation of GCPs Following Hif-1α Knockdown: Real Time PCR profile of GCPs following Hif-1α knockdown showing induction of a number of cardiomyocyte and endothelial markers, and downregulation of smooth muscle and fibroblast markers. Data presented as mean ± SEM, n=3.

DISCUSSION

The epicardium displays a unique response to myocardial injury, where it undergoes epithelial to mesenchymal transition (EMT), thereby contributing to various cardiac lineages, and even exerting a protective paracrine effect (Kikuchi et al., 2010; Lepilina et al., 2006; Limana et al., 2007; Olivey and Svensson, 2010; Smart et al., 2007; Zhou et al., 2011). This unique injury response of the epicardium may be partially explained by its distinct cell types, and developmental origin (Dettman et al., 1998; Mikawa and Gourdie, 1996). However, why the underlying subepicardial layers display a distinct injury response, characterized by resistance to ischemia (Reimer et al., 1977), contains cardiac progenitor cells (Popescu et al., 2009; Walker et al., 2009), and contributes to new cardiomyocyte formation (Kikuchi et al., 2010), is not clear. In the current report, we propose that the outermost layers of the heart (the epicardium and subepicardium) represent the cardiac hypoxic niche, characterized by the lowest capillary density across the entire ventricular thickness, localization of Hif-1α expression, and housing a hypoxia resistant progenitor population.

Hif-1α, which is the master regulator of hypoxic stress response, is stabilized during hypoxia (Li et al., 2005; Nakayama et al., 2004; Qi et al., 2008; Semenza, 2007a), and rapidly degraded under normoxic conditions (Kamura et al., 2000; Maxwell et al., 1999). It regulates various aspects of the adaptive response to

hypoxia, resulting in a metabolic switch from aerobic mitochondrial metabolism, to anaerobic cytoplasmic glycolysis (Hagg and Wennstrom, 2005; Maxwell et al., 2007), thereby enhancing the cellular ability to produce ATP in the absence of oxygen. Therefore, the localization of Hif-1α to the epicardium and subepicardium is a strong evidence of the hypoxic nature of this niche, and highlights a previously unexplored role of Hif-1α in the uninjured heart.

We have previously shown that profiling of the bone marrow cells, solely based on their metabolic footprint, markedly enriches for HSCs (Simsek et al., 2010). Using a similar strategy, we now show that cardiac cells with lowest mitochondrial footprint reside in the lowest perfusion areas of the heart and express cardiac progenitor and epicardial markers. Similar to the hypoxic HSC compartment, these GCPs preferentially utilize cytoplasmic glycolysis, and resist hypoxic and anoxic stress. Moreover, our results indicate that Hif-1α regulates the metabolic phenotype, and progenitor properties of GCPs. These results highlight a novel role of Hif-1α in regulation of cardiac progenitor cell function. Previous reports also support the role of hypoxia signaling in cardiac progenitor function, where Hif-2α was shown to transcriptionally regulate ABCG2 in cardiac side population cells (Martin et al., 2004; Meissner et al., 2006). Therefore, it would be important for future studies to outline novel downstream targets regulated by Hif-1α in cardiac progenitor cells.

The cardiac regeneration field witnessed a flurry of monumental discoveries over the past decade. Several groups identified a number of cardiac progenitor populations, based on *in vitro* expansion (Smith et al., 2007) epicardial localization (Zhou et al., 2008), surface marker (Beltrami et al., 2003; Oh et al., 2003), or transcription factor expression (Laugwitz et al., 2005; Zhou et al., 2008) (Martin-Puig et al., 2008), and dye exclusion (Martin et al., 2008). Therefore, instead of adding yet another cardiac progenitor population to the list, we propose that metabolic profiling enriches for cardiac progenitor cells that reside in the epicardial/subepicardial hypoxic niche based on their distinct metabolic phenotype. The discrepancy of surface marker expression in the current report may be in part due to *in vitro* expansion, which is known to alter stem cell surface marker expression (Zhang and Lodish, 2005).

The next era of cardiac progenitor cell research requires a broader understanding of *in vivo* regulation of the cardiac progenitor microenvironment, and the signaling cascades involved in cell fate decision, and progenitor cell function. Our results uncover a previously unrecognized hypoxic property of the epicardium and subepicardium, and highlight the role of hypoxia signaling in regulation of cardiac progenitors. Future studies will focus on identifying other cellular components of this hypoxic niche, and how they influence cardiac progenitor function.

CHAPTER FIVE

MEIS1 IS A TRANSCRIPTIONAL REGULATOR OF STEM CELL METABOLISM AND CELL CYCLE

INTRODUCTION

HSCs are defined by their abilities to self-renew and to differentiate into all blood-cell types (Abramson et al., 1977; Jordan et al., 1990; Morrison et al., 1995; Till and Mc, 1961). Much of the advancement in HSC therapy is credited to decades of pioneering work that led to the development of mouse and human HSC enrichment techniques based on staining of cell-surface antigens or vital dyes followed by fluorescence-activated cell sorting (FACS) (Bhatia et al., 1997; Camargo et al., 2003; Conneally et al., 1997; Gothert et al., 2005; Kiel et al., 2005; Majeti et al., 2007; Osawa et al., 1996). However, little is known about metabolic characteristics of HSCs, its regulation, or how the metabolic phenotype may influence HSC function.

In 1978, the concept of the special microenvironment-or niche- of hematopoietic stem cells was introduced (Schofield, 1978). Since then, it has become clear that the niche plays a crucial role in self-renewal and differentiation of HSCs(Fuchs et al., 2004; Spradling et al., 2001). One of the hallmarks of the HSC niche is its low oxygen tension, hence the term “hypoxic niche” (Eliasson and Jonsson).

Numerous studies indicate that this low oxygen environment is not only tolerated by HSCs, but is also essential for their function (Bradley et al., 1978; Cipolleschi et al., 1993; Danet et al., 2003; Katahira and Mizoguchi, 1987; Koller et al., 1992; Kubota et al., 2008; LaIuppa et al., 1998; Lo Celso et al., 2009; Parmar et al., 2007). We recently demonstrated that HSCs rely on glycolysis and have lower rates of oxygen consumption (Simsek et al., 2010), which may be crucial for survival of HSCs within hypoxic bone marrow niches.

In the mitochondria, oxygen is used as the terminal electron acceptor for the respiratory chain, and in the absence of oxygen the proton gradient formed by the respiratory chain collapses and mitochondrial ATP production declines. Under these hypoxic or anoxic conditions, energy production is derived from cytoplasmic glycolysis through the fermentation of glucose, and in the final step of anaerobic glycolysis, pyruvate is converted to lactate to replenish NAD^+. Anaerobic glycolysis produces 18 times less ATP that mitochondrial oxidative phosphorylation (Semenza, 2007b), which may be well suited for quiescent cells, but certainly can not sustain cells with high energy demands.

The energy advantage of mitochondrial oxidative phosphorylation over glycolysis is, unfortunately, not without deleterious consequences, as the mitochondrion is considered a major source of ROS production(Harman, 1972; Miquel et al., 1980;

Nohl, (1978); Turrens, 1997, 2003). ROS are believed to be important mediators of aging, and of numerous degenerative diseases, including HSC dysfunction and senescence (Ergen and Goodell, 2010). In fact, within the HSC compartment, the repopulation capacity is localized to only those HSCs with low levels of free radicals (Jang and Sharkis, 2007). Therefore the glycolytic metabolic phenotype of HSCs may not only protect them against hypoxic insults, but may also serve to minimize oxidant damage that result from mitochondrial oxidative phosphorylation.

Hypoxia inducible factor-1α (Hif-1α) is a major transcriptional regulator of hypoxic response. Hif-1α mediates the metabolic switch from aerobic mitochondrial metabolism, to anaerobic cytoplasmic glycolysis (Elvidge et al., 2006; Hagg and Wennstrom, 2005; Maxwell et al., 2007) by increasing both the expression(Wang et al., 1995b), and kinetic rate (Marin-Hernandez et al., 2009) of key glycolysis enzymes. Moreover, Hif-1α inhibits the utilization of pyruvate by the mitochondria (Kim et al., 2006b; Papandreou et al., 2006), and inhibits mitochondrial biogenesis (Zhang et al., 2007). Takubo and colleagues (Takubo et al., 2010)recently demonstrated that Hif-1α is enriched in HSCs, and that loss of Hif-1α results in HSC dysfunction (Takubo et al., 2010), while our group recently

showed that Meis1 is required for transcriptional activation of Hif-1α in HSCs (Simsek et al., 2010).

Meis1, which is a three-amino-acid loop extension homeodomain protein, plays an important role in leukemogenesis as well as normal hematopoiesis. Meis1 was first identified as a common viral integration site in myeloid leukemic cells of BXH-2 mice (Moskow et al., 1995), and it is also frequently up-regulated in human primary acute myeloid leukemia (AML) and acute lymphoblastic leukemia (ALL) samples (Imamura et al., 2002; Rozovskaia et al., 2001). Moreover, overexpression of Meis1 accelerates the initiation of AML in murine models (Fischbach et al., 2005; Pineault et al., 2004; Pineault et al., 2003). In normal hematopoiesis, Meis1 is expressed in the most primitive hematopoietic populations and is downregulated upon differentiation (Argiropoulos and Humphries, 2007; Argiropoulos et al., 2007; Imamura et al., 2002). Targeted Meis1 knockout causes lethality by embryonic day 14.5 with multiple hematopoietic and vascular defects (Azcoitia et al., 2005; Hisa et al., 2004; Imamura et al., 2002). Pbx-1, a cofactor of Meis1, has been shown to regulate self-renewal of HSCs by maintaining their quiescence (Ficara et al., 2008). However, the role of Meis1 regulating the function and metabolism if HSCs remain poorly understood.

Here we show that Meis1 regulates both HSC metabolism and oxidant stress response, through transcriptional regulation of Hif-1α and Hif-2α respectively. Meis1$^{-/-}$ HSCs had higher rates of oxygen consumption, lower rates of glycolysis, and increased ROS, which resulted in loss of HSC quiescence, and apoptosis.

METHODS

Mouse breeding and genotyping

The original Meis1 floxed mice were kindly provided by Dr. R. Keith Humphries. Mice were genotyped with Meis1 For1: 5'-CCAAAGTAGCCACCAATATCATGA-3' and Meis1 Rev: 5'-AGCGTCACTTGGAAAAGCAATGAT-3' primers. WT allele is determined by a 332bp-long PCR product and mutant allele determined by a 440bp long PCR product on 1.2% agarose gel. HSC specific deletion of Meis1 was achieved by following crosses of $Meis1^{f/f}$ with Scl-Cre-ER^{T} mice (Gothert et al., 2005). Scl-Cre mice were genotyped using Scl-Cre-ER primer 1; 5'-GAACCTGAAGATGTTCGCGAT-3 and Scl-Cre-ER primer 2; 5'-ACCGTCAGTACGTGAGATATC-3. To generate $Meis1^{-/-}$ mice, $Meis1^{f/f}$;Scl-Cre-ER^{T}+ mice were injected intraperitoneally with Tamoxifen (40 mg/kg) (T5648-1G, Sigma-Aldrich) daily for 14 days. We used age-matched Tamoxifen injected $Meis1^{+/+}$;Scl-Cre-ER^{T}(+) or $Meis1^{f/f}$;Scl-Cre-ER^{T}(-) mice as controls ($Meis1^{+/+}$ mice). Genotyping of Cre-deleted Meis1 locus (Meis1 exon8 deleted) was performed using Meis1 For2: 5'- CATTGACTTAGGTGTATGGGTGTC-3' and Meis1 Rev: 5'-AGCGTCACTTGGAAAAGCAATGAT-3' primers. Cre-deleted Meis1 locus gives rise to a 261 bp product while wt and mutant (non-deleted) shows no amplicon.

The Hif-1α floxed mice were kindly provided by Dr. Joseph A. Garcia, UT Southwestern Medical Center at Dallas. Mice were genotyped with Hif1a-For: 5'-GCAGTTAAGAGCACTAGTTG-3' and Hif1a-Rev: 5'-GGAGCTATCTCTCTAGACC-3' primers and PCR product run on 1.5% agarose gel (WT band ~ 260 bp and mutant allele ~270bp). HSC specific deletion of Hif-1α was achieved by following crosses of Hif-1$\alpha^{f/f}$ with Scl-Cre-ER^{T} mice and tamoxifen injections (40mg/kg for 14 days). We used age-matched Tamoxifen injected Hif-1$\alpha^{+/+}$;Scl-Cre-ER^{T}(+) or Hif-1$\alpha^{f/f}$;Scl-Cre-ER^{T}(-) mice as controls (Hif-1$\alpha^{+/+}$ mice).

Flow cytometry

Donor bone marrow (BM) cells were isolated from 8-12 week old Meis1$^{+/+}$ or Meis1$^{-/-}$ mice (or Hif-1$\alpha^{+/+}$ and Hif-1$\alpha^{-/-}$ mice). Lin^{-}Sca1^{+}Kit^{+}Flk2^{-}CD34^{-} cells (LT-HSCs) were isolated by staining with a biotinylated lineage cocktail (anti-CD3, anti-CD5, anti-B220, anti-Mac-1, anti-Gr-1, anti-Ter119; Stem Cell Technologies) followed by streptavidin-PE/Cy5.5, anti-Sca-1-FITC, anti-Kit-APC, anti-Flk-2-PE, and anti-CD34-PE. For analyzing repopulation of mouse HSCs, peripheral blood cells of recipient CD45.1 mice were collected by retro-orbital bleeding, followed by lysis of red blood cells and staining with anti-CD45.2-FITC, anti-CD45.1-PE, anti-Thy1.2-PE (for T-lymphoid lineage), anti-B220-PE (for B-lymphoid lineage), anti-Mac-1-PE, or anti-Gr-1-PE (cells co-

staining with anti-Mac-1 and anti-Gr-1 were deemed to be of the myeloid lineage) monoclonal antibodies (BD Pharmingen). The "percent repopulation" shown in all figures was based on the staining results of anti-CD45.2-FITC and anti-CD45.1-PE. In all cases FACS analysis of the above listed lineages was also performed to confirm multi-lineage reconstitution as previously described (Simsek et al., 2010).

For analyzing of LT-HSCs in the peripheral blood by flow cytometry, peripheral blood of $Meis1^{-/-}$ or $Meis1^{+/+}$ mice were collected by retro-orbital bleeding, followed by lysis of red blood cells and staining with LT-HSCs markers $Lin^{-}Sca1^{+}Kit^{+}Flk2^{-}CD34^{-}$ as described above.

The cell cycle analysis with Hoechst 33342 and pyronin Y staining was performed as we described (Zheng et al., 2011). Briefly, the $Lin^{-}Sca\text{-}1^{+}Kit^{+}Flk2^{-}CD34^{-}$ cells or $Lin^{-}Sca\text{-}1^{+}Kit^{+}CD150^{+}CD48^{-}$ cells were collected in Hank's buffered salt solution medium containing 10% FBS, 1 g/liter glucose, and 20 mM Hepes (pH 7.2). Cells were washed, Hoechst 33342 (20 μg/ml, Invitrogen) was added, and cells were incubated at 37°C for 45 min after which Pyronin Y (1 μg/ml, Sigma) was added. Cells were incubated for another 15 min at 37°C, washed, and resuspended in cold PBS. Samples were immediately analyzed by flow cytometry (BD Biosciences, FACSAria). To examine the apoptosis, Lin^{-}

$Kit^{+}Sca\text{-}1^{+}$ cells were stained with PE-conjugated anti-Annexin V and 7AAD according to manufacturer's manual (BD Pharmingin). To study the apoptosis in LT-HSCs, bone marrow cells were stained for HSC markers Sca-1-PE/Cy5.5, C-Kit-APC, CD34-PE and Flk2-PE following lineage depleting as described above and stained with FITC-conjugated anti-Annexin V according to manufacturer's manual (BMS500FI/20, Ebioscience).

Competitive reconstitution analysis

The indicated numbers of CD45.2 donor cells from $Meis1^{+/+}$ or $Meis1^{-/-}$ mice were mixed with 1 x 10^5 freshly isolated CD45.1 competitor BM cells and the mixture was injected intravenously via the retro-orbital route into each of a group of 6-8 week old CD45.1 mice previously irradiated with a total dose of 10 Gy. To measure reconstitution of transplanted mice, peripheral blood was collected at the indicated time points post-transplant and the presence of $CD45.1^{+}$ and $CD45.2^{+}$ cells in lymphoid and myeloid compartments were measured as described.

Homing

BM Lin^{-} cells were labeled with 5-(and -6) carboxyfluorescein succinimidyl ester (CFSE), and $3x10^6$ cells were transplanted into indicated strains of lethally irradiated mice. After 16 hours, the total number of $CFSE^{+}$ cells in the BM, spleen or liver was determined by flow cytometry. When $CFSE^{+}$ LSK ($CFSE^{+}Lin^{-}$ $Sca1^{+}Kit^{+}$) cells (HSCs) were analyzed, the BM cells were stained with a

biotinylated lineage cocktail followed by streptavidin-PE/Cy5.5, anti-Sca-1-PE, and anti-Kit-APC before analysis, as described (Zheng et al., 2011).

Colony-forming assays

Normal BM cells were diluted to the indicated concentration in IMDM with 2% FBS, and were then seeded into methylcellulose medium M3434 (StemCell Technologies), for CFU-GM and BFU-E colony formation according to the manufacturer's instructions.

Real-Time PCR

Total RNA was isolated from $Meis1^{-/-}$ and $Meis1^{+/+}$ HSCs ($Lin^{-}Sca1^{+}Kit^{+}Flk2^{-}CD34^{-}$cells) using Qiagen`s RNeasy Mini Kit (cat# 74104) according to manufacturer's instructions. cDNA was synthesized using SuperScript II RT (Invitrogen). Predesigned primers (table 3) from NIH mouse primer depot (http://mouseprimerdepot.nci.nih.gov/) ordered from Integrated DNA Technologies. Real time PCR was performed with SyberGreen (Applied Biosystems) on ABI Prism 7700 Sequence Detector (Applied Biosystems). β-actin was used as control to normalize results.

Table 3: List of primers used for real time PCR

Gene	Forward Primer	Reverse Primer
β-actin	GAACCCTAAGGCCAACCGTGAAAGAT	ACCGCTCGTTGCCAATAGTGATG
p16 (Xu et al., 2011)	GGGTTTCGCCCAACGCCCCGA	TGCAGCACCACCAGCGTGTCC
p19 (Xu et al., 2011)	GTTTTCTTGGTGAAGTTCGTGC	TCATCACCTGGTCCAGGATTC
Meis1	GTTGTCCAAGCCATCACCTT	ATCCACTCGTTCAGGAGGAA
Hif-1α	CGGCGAGAACGAGAAGAA	AAACTTCAGACTCTTTGCTTCG
Hif-2α	ATCACGGGATTTCTCCTTCC	GGTTAAGGAACCCAGGTGCT
Hif-3α	TGTGAACTTCATGTCCAGGC	GCAATGCCTGGTGCTTATCT

Generation of Luciferase Reporter vectors

Conserved Meis1 motifs in Hif-2α gene were determined using genome browser (http://genome.ucsc.edu/). 779bp long DNA fragment containing conserved Meis1 sites (located next to start codon sequence, human chr2:46,525,052-46,525,064) from Hif-2α promoter was amplified by PCR from mouse genomic DNA with following primers. Conserved Meis1 Site: pHif-2α-F; 5'-GGGCTAAACGGAACTCCAGG-3' and pHif-2α-R: 5'-CATAGGAACGCTCTCGGAAAGAC-3'. PCR fragments were subcloned into pCR2.1-TOPO vector (Invitrogen) according to manufacturer's instructions. pHif2a-TOPO and E1b-pGL2 vectors were digested with XhoI and KpnI. Then

the PCR fragments containing conserved Meis1 sites were cloned into E1b-pGL2 to generate pHif2a-pGL2 luciferase reporter vector. To test Meis1 site specificity, Meis1 binding sites (TGAC) at "**TGAC**AGC**TGAC**AA" sequence were mutated to "**TGGC**GGC**CGCC**AA" (NotI site insertion) using iProof High-Fidelity DNA Polymerase (Bio-Rad) from Hif-2α-pGL2 vector with the following primers: Mut-Hif2a-F: 5'-AAgcggccgcCAAGGAGAAAAAAAGGTAAGCGGG-3' and Mut-Hif2a-R: 5'-AAgcggccgcCATTGTCGCCGTGGCCCTC-3'. Hif-2α-Mut-pGL2 reporter was generated following NotI digestion and ligation of PCR product. Transcriptional activation of Hif-2α by Meis1 was evaluated using a luciferase reporter system (Promega) as described previously (Simsek et al., 2010).

Metabolic Assays

Metabolic assays are carried out as described previously (Simsek et al., 2010) with some modifications.

Oxygen Consumption Assays: $Meis1^{+/+}$ and $Meis1^{-/-}$ HSCs were separated flowcytometrically as described above. Equal numbers of cells (5-10 $x10^4$ cells/well) were incubated for 6 hour in the provided 384 well plate (BD Oxygen Biosensor System, CA, USA) and sealed to prevent air exchange prior to measurement. Culture media lacking cells was used as a negative control and

sodium sulfite (100 mM) was used as a positive control. Oxygen consumption is presented as relative units.

ATP Assays: Meis1$^{+/+}$ and Meis1$^{-/-}$ HSCs were sorted as described and centrifuged at 1200g for 10 min. At least fifty thousand cells were used for each single ATP measurement. 50 µl of ATP standards (10^{-6}-10^{-12}M) and 50 µl cell lysates were quantified using ATP Bioluminescence Assay Kit CLS II (Roche, cat# 11699695001) using Fluostar Optima plate reader (BMG Labtech). Finally, data were normalized to cell count and protein content.

Glycolytic Flux Assay: ^{13}C-Lactate production, end product of glycolysis, were measured as described previously (Simsek et al., 2010) using glycolytic flux medium supplemented with 10 mM D-[1-6-^{13}C]-glucose (Cambridge Isotope Labs) to allow up to all of the glucose-derived lactate pool to be labeled on C-3. Minimum fifty thousand cells were cultured in 40 µl of flux medium overnight. Then, the cells were pelleted and supernatant collected and prepared for gas chromatography-mass spectrometry. Lactate abundance was determined by monitoring m/z at 117 (un-enriched), 118 (lactate containing ^{13}C from glucose) and 119 (internal standard). To determine the atom percent excess (APE), the 117 and 118 areas were first corrected against the 119 abundance to account for inter-sample variability of extraction. Then the corrected ratio of 118/(117+118) was

determined and compared to the standard curve. Finally, the APE was multiplied by the total nmoles lactate to determine the nmoles of ^{13}C-lactate produced. The final results were corrected for total cellular ATP concentration as described previously (Simsek et al., 2010).

Measurement of Reactive Oxygen Species

Bone marrow cells from Meis1$^{+/+}$ and Meis1$^{-/-}$ mice were isolated as described above. Following lineage depletion (Lineage depletion kit, BD Imag, BDbiosciences), cells were incubated with 1 µM 5-(and-6)-carboxy-2',7'-dichlorofluorescein diacetate (carboxy-DCFDA) (C-369, Invitrogen) for 30 min in 37^{0}C water bath at the dark. Then, cells were stained for HSCs markers Sca-1-PE/Cy5.5, C-Kit-APC, CD34-PE and Flk2-PE and assayed by flow cytometer.

N-acetyl-L-cysteine (NAC) Administration *in vivo*

Six-week-old Meis1$^{f/f}$;Scl-Cre-ER^{T}+ mice were injected intraperitoneally with Tamoxifen (40 mg/kg) daily for 14 days. Following Tamoxifen injections, animals were treated daily for 2 weeks with NAC (100 mg/kg; Sigma) by subcutaneous administration or provided in drinking water (500 mg · kg^{-1} · d^{-1} in drinking water as described previously (Li et al., 2011; Pio et al., 2003)) and were subsequently analyzed as above. We used age-matched Tamoxifen injected

$Meis1^{+/+}$;Scl-Cre-ER^T (+) or $Meis1^{f/f}$;Scl-Cre-ER^T(-) mice as controls ($Meis1^{+/+}$ mice).

Chromatin Immunoprecipitation Assay (ChIP)

ChIP assays were performed to evaluate the *in vivo* binding of Meis1 to its consensus sequence in the *Hif-2α* gene. The assays were done in Kasumi-1 cells, a hematopoietic progenitor cell line, using the ChIP kit (Upstate, cat#17-295) as described previously (Simsek et al., 2010). Meis1 antibody (Santa Cruz Biotechnology, sc-10599) and normal goat IgG (Santa Cruz Biotechnology, sc-2028) were used. The DNA isolated from input chromatin fragments and from the precipitated chromatin fragments by anti-Meis1 antibody or control IgG was subjected to real time PCR using primers flanking the consensus Meis1 binding sites on Hif-2α promoter: 5'-GTTCCTCCCAGTCACCTTTCTCC-3' and 5'-TCTCCCAACCACTCTCGGTC-3'.

Measurement of blood cell counts (CBC/Differential)

About 50 ul of peripheral blood collected by retro orbital bleeding from $Meis1^{+/+}$ and $Meis1^{-/-}$ mice post 1 month and 3 months of Tamoxifen injections in K_3-EDTA tubes. Samples are submitted to UTSW ARC Diagnostic Lab and analyzed

with HemaVet 950FS analyzer. The following parameters are reported for the sample submitted: White blood count (WBC), Neutrophil count, Lymphocyte count, Monocyte count, Eosinophil count, Basophil count, Red blood cell count, Hemoglobin, HCT, MCV, MCH, MCHC, Platelet count, and MPV.

Statistical Analysis

Results are expressed as mean ± SEM and a 2-tailed Student *t* test was used to determine the level of significance. $p<0.05$ was considered statistically different.

RESULTS

Deletion of Meis1 in long-term (LT)-HSCs

Since the global loss of Meis1 is embryonic lethal (Azcoitia et al., 2005; Hisa et al., 2004; Imamura et al., 2002), we sought to pursue an inducible deletion of Meis1 to study the role of Meis1 in adult HSCs. $Meis1^{fl/fl}$ mice with loxp flanking exon 8 were crossed with transgenic mice expressing the Tamoxifen-inducible Cre recombinase under the control of stem cell leukemia (Scl) HSC enhancer, which warrants the deletion in HSCs (Gothert et al., 2005). Upon Tamoxifen treatment, exon 8 is deleted which results in the loss of Meis1 expression in HSCs (Figure 20A). To verify deletion of Meis1, we performed genotyping analysis and quantitative RT-PCR in peripheral blood cells and phenotypic LT-HSCs (Lin^- $Sca1^+Kit^+Flk2^-CD34^-$) in the bone marrow after Tamoxifen treatment. Meis1 in peripheral blood cells was deleted 14 days after Tamoxifen treatment, and Meis1 mRNA level in LT-HSCs was markedly decreased to around 10% of control values (Figure 20B).

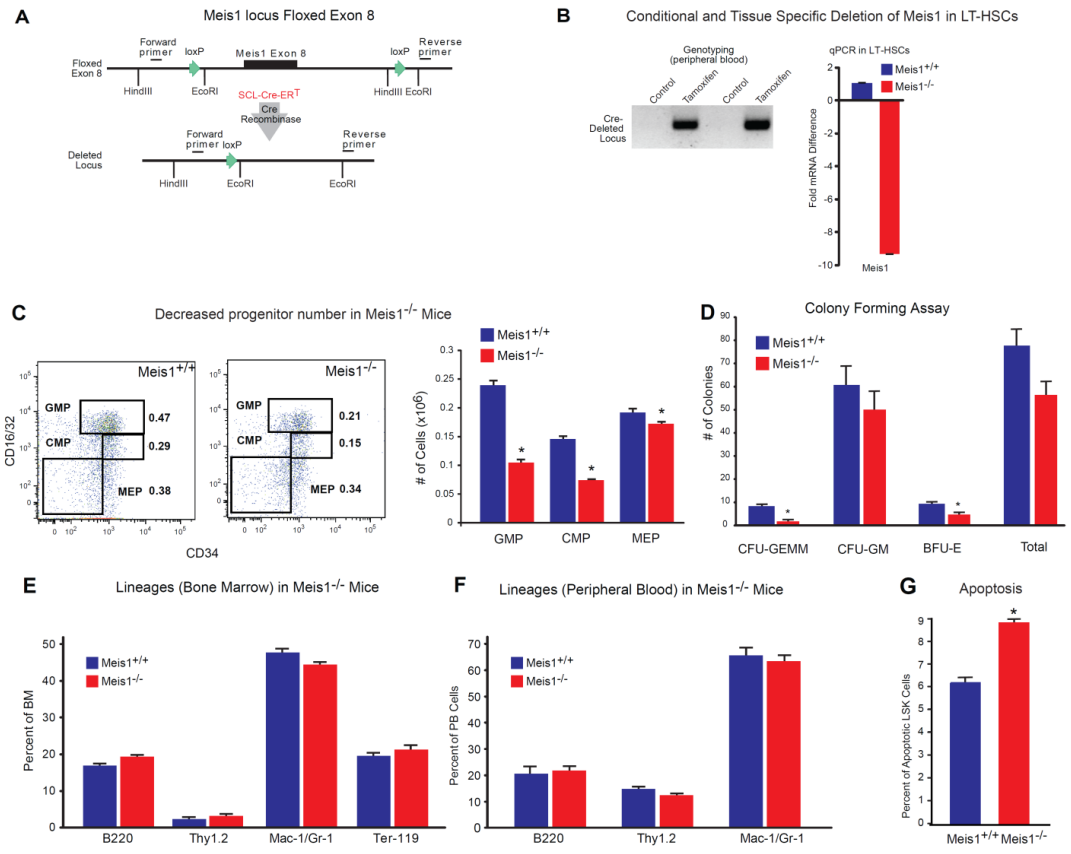

Figure 20. Conditional Deletion of Meis1 in LT-HSCs: A) Schematic of Meis1 floxed allele showing deletion of floxed Exon 8 following Cre recombinase activity. Scl-CreER^{T} allows specific deletion of Meis1 gene in hematopoietic stem cells following Tamoxifen injections. B) Left panel: Deletion of Meis1 was detected in peripheral blood following Tamoxifen injections by PCR. Right panel: Real Time PCR demonstrates deletion of Meis1 in the great majority LT-HSCs following 14 days of Tamoxifen injections (n=3). **Progenitors** C) Left: Representative FACS plots for hematopoietic progenitors. FACS plots are referred to Lin^{-}Sca-1^{-}Kit^{+} gate where GMPs are defined as CD34^{+}CD16/32^{+}, CMPs as CD34$^{+/lo}$CD16/32^{int}, and MEPs as CD34^{-}CD16/31^{-}. Right: Quantification of hematopoietic progenitor (GMP, CMP, MEP) number in the

bone marrow of control and Meis1$^{-/-}$ mice (n=3). **Colony Forming Assay** D) Quantification of number of colonies formed from Control Meis1$^{+/+}$ and Meis1$^{-/-}$ following 12 days of culture in methocult media (n=3). **Lineages in Meis1$^{-/-}$ mice** E) Quantification of specific lineages (B220, Thy1.2, Mac-1/Gr-1, and Ter-119) in the bone marrow of control Meis1$^{+/+}$ and Meis1$^{-/-}$ mice (n=5). F) Quantification of specific lineages (B220, Thy1.2, and Mac-1/Gr-1) in the peripheral blood of Control Meis1$^{+/+}$ and Meis1$^{-/-}$ mice (n=5). G) Quantification of apoptosis in Meis1$^{+/+}$ and Meis1$^{-/-}$ LSK Cells (n=3) *p<0.05.

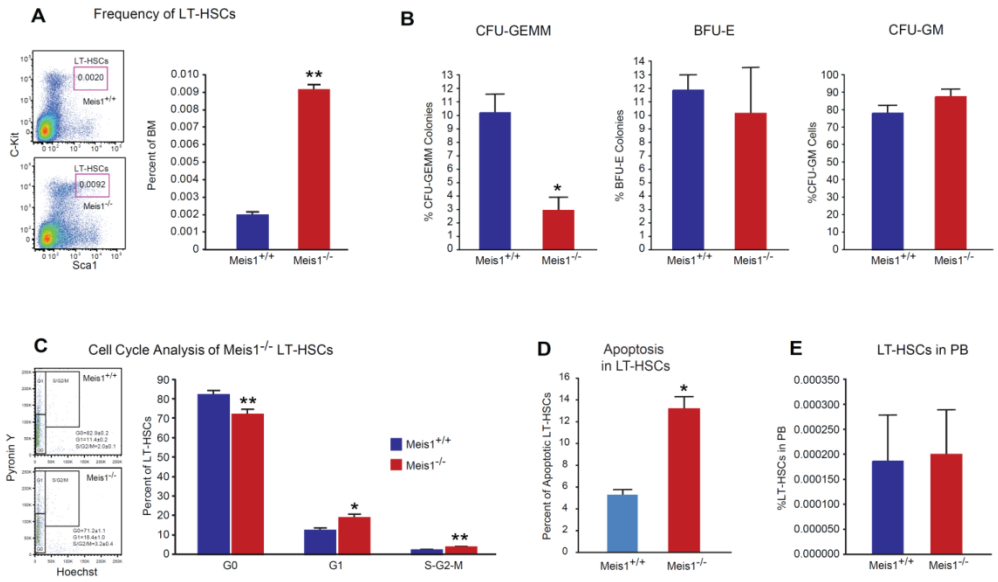

Figure 21. Meis1 Deletion in LT-HSCs results in Apoptosis and Loss of Quiescence: A) Left panel: Representative flow cytometry profile of LT-HSCs (Lin^{-}Sca-1^{+}Kit^{+}Flk2^{-}CD34^{-}) of bone marrow (BM) cells are shown for control

Meis1$^{+/+}$ and mutant Meis1$^{-/-}$ mice. Numbers in the FACS plots indicate percentages among total BM cells. Right panel: Quantification of LT-HSCs demonstrates significantly higher number of hematopoietic stem cells in Meis1$^{-/-}$ BM (n=6) B) *In vitro* methylcellulose colony formation assay were performed at the time of sacrifice following tamoxifen injections with BM cells of control and Meis1$^{-/-}$ mice. CFU-GEMM colonies representing most undifferentiated progenitors type of colonies derived from Meis1$^{+/+}$ and Meis1$^{-/-}$ BM cells demonstrates decreased percentage of CFU-GEMM. Quantification of BFU-E and CFU-GM colonies derived from Meis1$^{-/-}$ cells shows no differences (n=3) C) Left panel demonstrates representative FACS analysis of Pyronin Y/Hoecst staining on LT-HSCs (Lin^{-}Sca-1^{+}Kit^{+}CD150^{+}CD48^{-}) of Meis1$^{+/+}$ and Mesi1$^{-/-}$ mice. Numbers in the FACS plots indicate percentages among LT-HSCs. Right panel is the quantification of G_0, G_1, or S/G_2/M phase in Meis1$^{+/+}$ and Meis1$^{-/-}$ LT-HSCs (n=6) D) Quantification of apoptosis in Meis1$^{+/+}$ and Meis1$^{-/-}$ LT-HSCs (n=3) E) Quantification of LT-HSCs in peripheral blood (PB) of Meis1$^{+/+}$ and Meis1$^{-/-}$ mice (n=3). *p<0.05, **p<0.01.

Meis1 is required for the maintenance of LT-HSCs

To explore the role of Meis1 in LT-HSCs, we first examined the frequencies of phenotypic LT-HSCs in control (Meis1$^{+/+}$) and Meis1 conditional KO (Meis1$^{-/-}$) mice. As shown in Figure 21A, 7 days after Tamoxifen treatment, there was a 4.5-

fold increase of HSC frequency in Meis1$^{-/-}$ mice compared to Meis1$^{+/+}$ controls (0.0092% *vs* 0.002%). FACS analysis revealed robust reduction of granulocyte-monocyte progenitors (GMPs) and common myeloid progenitors (CMPs) and mild reduction in the total number of megakaryocyte/erythroid progenitors (MEPs)(Figure 20C). Meanwhile, by using colony-forming assay, we demonstrated that Meis1$^{-/-}$ mice had much lower primitive myeloid progenitor cells (CFU-GEMM), but no change in percentage of differentiated myeloid progenitor cells (CFU-GM), or erythroid progenitor cells (BFU-E) (Figure 21B and Figure 20D). No difference was detected in the distribution of T, B, myeloid, and erythroid lineages either in BM or peripheral blood of Meis1$^{-/-}$ (Figure 20E-F).

The increase of HSC frequency may result from cell-autonomously accelerated proliferation or the compensatory effect of increased apoptosis or mobilization in Meis1$^{-/-}$ HSCs. To address this concern, we first examined the cell cycle of HSCs by using Hoechest 33342 and pyronin Y staining, and we found that only around 71% of Meis1$^{-/-}$ LT-HSCs were in G_0 compartment, which is much lower than that of Meis1$^{+/+}$LT-HSCs (around 83%) (Figure 21C). This indicated that Meis1$^{-/-}$ HSCs were much less quiescent and prone to proliferation. Next, we examined apoptosis status in LT-HSCs (Lin^{-}Sca1^{+}Kit^{+}Flk2^{-}CD34^{-}) by using Annexin V. We detected more apoptotic cells in Meis1$^{-/-}$ LT-HSCs compared to Meis1$^{+/+}$ counterpart (Figure 21D and Figure 20G for LSK cells). Finally, to examine HSC

mobilization, we performed LT-HSC staining in peripheral blood in $Meis1^{+/+}$ and $Meis1^{-/-}$ mice, which did not show any difference in HSC frequency (Figure 21 E). These data suggest that the increased apoptosis in *Meis1*$^{-/-}$ LT-HSCs may result in increase of HSC frequency and decrease of quiescence in BM.

To further evaluate the function of Meis1 in HSCs *in vivo*, we performed competitive bone marrow transplantation with $Meis1^{+/+}$ and $Meis1^{-/-}$ HSCs. Two weeks after Tamoxifen treatment, 150 $Lin^{-}Sca1^{+}Kit^{+}Flk2^{-}CD34^{-}$ $Meis1^{+/+}$ or $Meis1^{-/-}$ CD45.2 HSCs, together with 1 x 10^5 CD45.1 competitors, were injected into CD45.1 recipients through retro-orbital complex. Repopulation was examined at 4, 10, 16 weeks post-transplant. Strikingly, as shown in Figure 22A, we couldn't detect any engraftment with $Meis1^{-/-}$ HSC donors, indicating a severe impairment of HSC repopulation ability after loss of Meis1. A repeat transplantation experiment with total BM cells showed similar results (Figure 22B). The impaired repopulation of Meis1 deficient LT-HSCs (Figure 22A) and progressive decline in repopulation of Meis1 deficient cells in primary transplant recipients (Figure 22B) suggested a defect in self-renewal. Therefore, we performed secondary transplant experiments to confirm the reduction of function Meis1 deficient LT-HSCs in the bone marrow of primary transplant recipients. 8 weeks after primary transplant, total bone marrow from primary recipients from whole transplanted mice were harvested and transplanted into secondary

recipients. Meis1 deficient cells from primary recipients (0.5-1x10^6 cells) were unable to repopulate secondary recipients (Figure 22C). The decreased repopulation may result from defects in HSC maintenance, or homing, or increased apoptosis. To exclude the possibility that the decreased engraftment is caused by defect of homing in Meis1$^{-/-}$ HSCs, we labeled Meis1$^{+/+}$ or Meis1$^{-/-}$ Lin$^-$ cells with 5-(and-6) carboxyfluorescein succinimidyl ester (CFSE) and injected into lethally irradiated recipients. Sixteen hours later, we examined CFSE$^+$ or LSK CFSE$^+$ cells in spleen, liver and BM. No significant difference in homed total CFSE$^+$ or LSK CFSE$^+$ cells was detected between Meis1$^{+/+}$and Meis1$^{-/-}$ donors (Figure 22D-E). In addition, quantification of lineage repopulation of Meis1$^{+/+}$ and Meis1$^{-/-}$ donors demonstrates no lineage specific defects (Figure 22F). Taken together, these data provide strong evidence that Meis1 plays a crucial role in the maintenance of HSCs and prevention of apoptosis in HSCs.

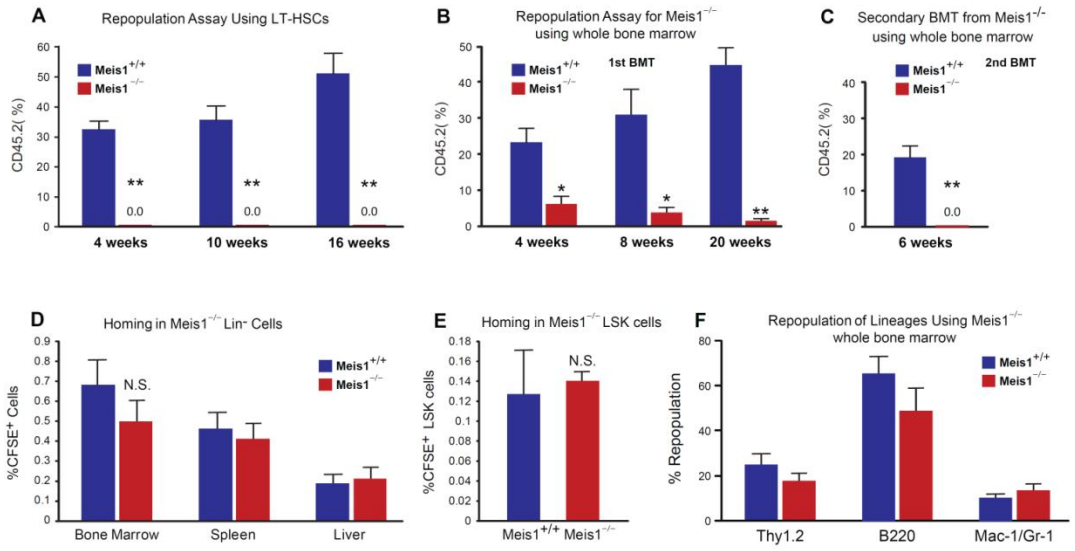

Figure 22. Impaired repopulation in Meis1$^{-/-}$ LT-HSCs: Repopulation assays: A) LT-HSCs ($Lin^-Sca1^+Kit^+Flk2^-CD34^-$) (150 cells) from either control ($Meis1^{+/+}$) or mutant $Meis1^{-/-}$ CD45.2 mice were transplanted into irradiated CD45.1 hosts in competition with BM from CD45.1 mice (1×10^5 cells). Quantification of flow cytometry profile of peripheral blood of bone marrow recipient mice up to 16 weeks for percentage of $CD45.2^+$ cells demonstrates total loss of bone marrow reconstitution of $Meis1^{-/-}$ LT-HSCs (n=5) B) Repopulation assay with whole bone marrow from either control $Meis1^{+/+}$ or mutant $Meis1^{-/-}$ CD45.2 mice were transplanted into irradiated CD45.1 mice demonstrates significantly impaired repopulation in mice transplanted with $Meis1^{-/-}$ cells (n=5) C) Analysis of repopulation following 2nd bone marrow transplantation (BMT)

from 1st BMT mice demonstrates complete loss of repopulation (n=5). **Homing assays:** D) BM Lin^- cells ($3x10^6$ cells) were transplanted into irradiated mice and quantified for $CFSE^+$ cells in different tissues. Quantification of percentage of $CFSE^+$ cells in BM, spleen and liver show no difference between $Meis1^{+/+}$ and $Meis1^{-/-}$ mice (n=5). E) Quantification of percentage of $CFSE^+$ LSK cells in BM of $Meis1^{+/+}$ and $Meis1^{-/-}$ mice (n=5). F) Quantification of repopulation of lineages for $Meis1^{-/-}$ using whole bone marrow from 1st BMT mice demonstrates no defects in lineage repopulation (n=5). *$p<0.05$, **$p<0.01$

Role of Meis1 in regulating Hif-1α for glycolytic metabolism of LT-HSCs

We have shown previously that Meis1 gene acts upstream of Hif-1α by regulating its transcriptional activity by an enhancer located in the first intron of Hif-1α (Simsek et al., 2010). We further examined if hypoxia inducible factors (Hif-1α, Hif-2α, and Hif-3α) are regulated by Meis1 in LT-HSCs. Quantitative real time PCR analysis demonstrated that mRNA levels of both Hif-1α and Hif-2α were downregulated but no change in Hif-3α levels observed in $Meis1^{-/-}$ LT-HSCs (Figure 23A). To explore the role of Hif-1α in the regulation of metabolism of LT-HSCs, we used the same inducible Cre-system to delete Hif-1α specifically in HSCs (Figure 24A). $Hif\text{-}1\alpha^{fl/fl}$ mice with loxp flanking exon 2 were crossed with transgenic mice expressing the Tamoxifen-inducible Cre recombinase under the control of stem cell leukemia (Scl) HSC enhancer. Upon Tamoxifen treatment,

exon 2 is deleted resulting in the loss of Hif-1α expression in HSCs (Figure 24A). To verify deletion of Hif-1α, we performed quantitative RT-PCR in LT-HSCs ($Lin^{-}Sca1^{+}Kit^{+}$ $Flk2^{-}CD34^{-}$) in bone marrow after Tamoxifen treatment. Hif-1α mRNA level in LT-HSCs was dramatically decreased, about 400 fold lower than that of control ($Hif\text{-}1^{+/+}$) following 14 days of Tamoxifen treatment (Figure 24B). We showed previously that LT-HSCs primarily rely on cytoplasmic glycolysis rather than mitochondrial oxidative phosphorylation (Simsek et al., 2010). However, the role of Hif-1α in HSC metabolism was not examined before. Here we demonstrate that HSC specific deletion of Hif-1α results in increased mitochondrial respiration as shown by increased oxygen consumption (Figure 24C), and decreased glycolytic flux measured by the rate of glucose-drived ^{13}C lactate production (Figure 24D). These results clearly demonstrates that deletion of Hif-1α results in a switch from anaerobic glycolytic metabolism to oxidative phosphorylation which may lead to increased reactive oxygen species and eventually loss of stemness in HSCs.

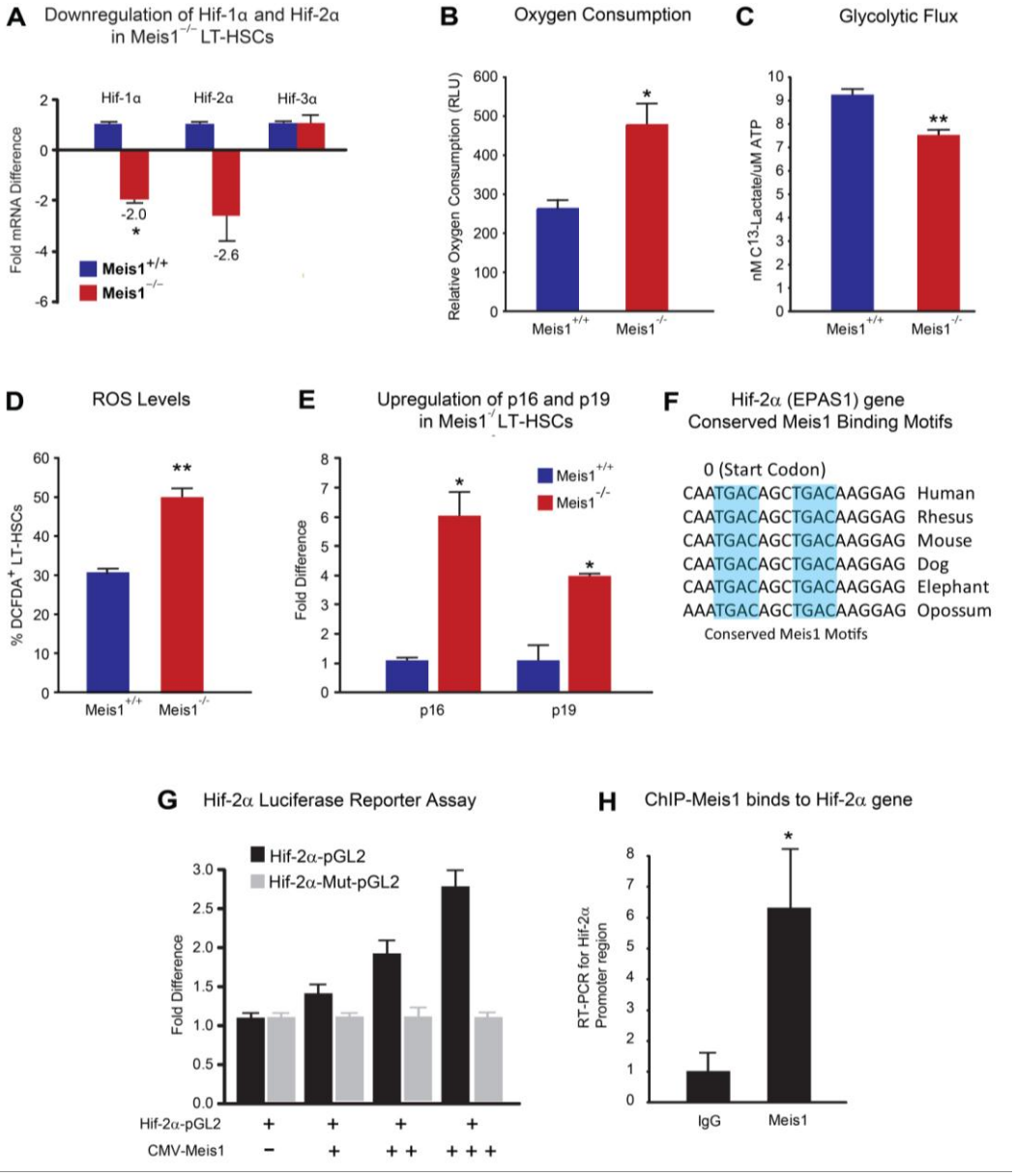

Figure 23. Metabolic regulation of LT-HSCs by Meis1: A) RT-PCR histogram demonstrates the significant downregulation of Hif-1α and Hif-2α (EPAS1), but not Hif-3α following Meis1 deletion in LT-HSCs (n=3) B) Measurement of oxygen consumption rate for 6 hours demonstrates significantly higher aerobic phosphorylation in Meis1$^{-/-}$ LT-HSCs compared to Meis1$^{+/+}$ LT-HSCs (n=3) C)

Quantification of labeled lactated in glycolytic flux assay demonstrates that Meis1$^{-/-}$ LT-HSCs are less glycolytic (n=3). D) Measurement of reactive oxygen species (ROS) in LT-HSCs as determined by quantification of %DCFDA^{+} LT-HSCs in Meis1$^{+/+}$ and Meis1$^{-/-}$ mice (n=3) E) RT-PCR of p16 and p19 demonstrates association of higher level of ROS with upregulation of p16 and p19 in Meis1$^{-/-}$ LT-HSCs (n=3). F) Figure shows conserved consensus Meis1 motifs found on Hif-2α (EPAS1) gene. Note the duplex Meis1 binding motifs found next to each other and conserved till Opossum. G) Luciferase reporter assays demonstrate dose-dependent transcriptional activation of Hif-2α by Meis1 (n=3) H) Real-time PCR with primers flanking the consensus Meis1 binding sequence following ChIP assay demonstrating *in vivo* binding of Meis1 to Hif-2α promoter (n=3) . *$p<0.05$, **$p<0.01$

To further examine the role of Hif-1α in HSCs, we examined expression of Hif-2α (a master regulator of oxidant stress response) and Hif-3α in Hif-1α$^{-/-}$ LT-HSCs. We found that deletion of Hif-1α in LT-HSCs results in a profound increase in Hif-2α mRNA levels (>120 fold), with no significant change in the levels of Hif-3α mRNA (Figure 24E). This marked compensatory upregulation of Hif-2α in Hif-1α$^{-/-}$ LT-HSCs is in stark contrast to the downregulation of Hif-2α in the Meis1$^{-/-}$ LT-HSCs.

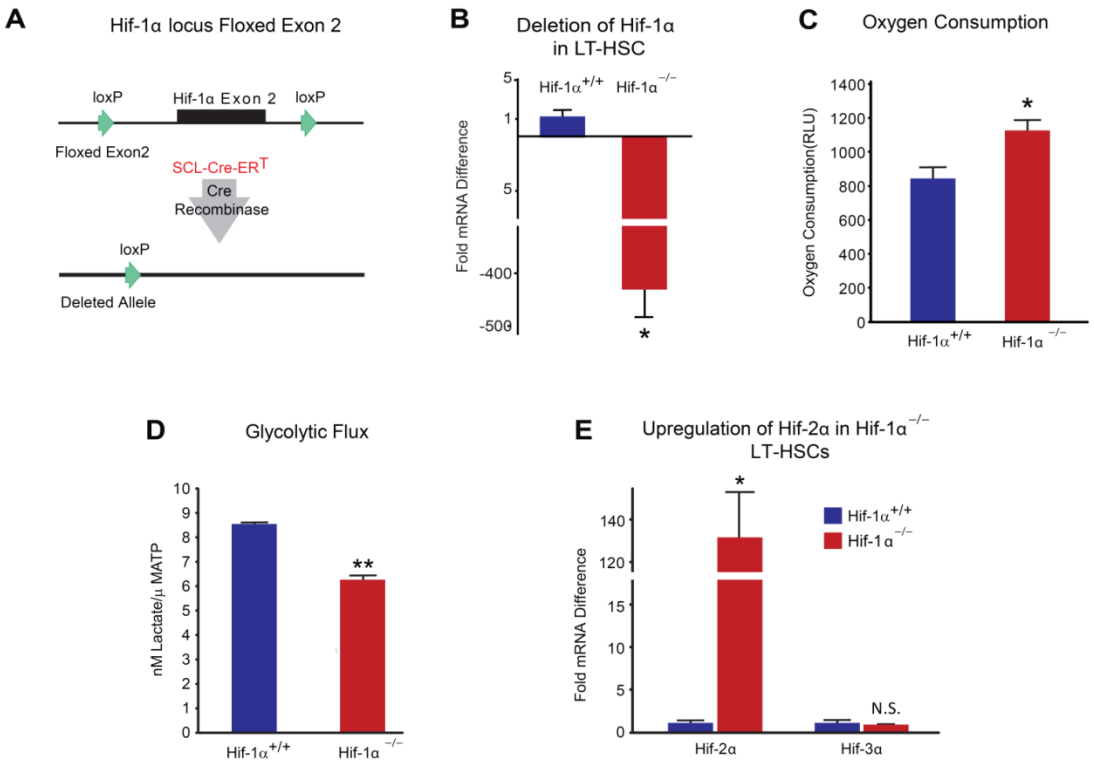

Figure 24. Metabolic Phenotype of Hif-1α KO HSCs: A) Schematic of Hif-1α floxed allele showing deletion of floxed Exon 2 following Cre recombinase activity. B) RT-PCR demonstrates more than 400 fold downregulation of Hif-1α in the LT-HSCs following 14 days of Tamoxifen injections. Note that Scl-CreER^{T} allows specific deletion of Hif-1α gene in hematopoietic stem cells following Tamoxifen injections (n=3). C) Oxygen consumption assay demonstrates significantly higher oxygen consumption rates in Hif-1α$^{-/-}$ LT-HSCs compared to Hif-1α$^{+/+}$ (n=3) D) Quantification of labeled lactate in glycolytic flux assay demonstrates that Hif-1α$^{-/-}$ LT-HSCs have lower levels of lactate, indicating decreased cytoplasmic glycolysis in Hif-1α$^{-/-}$ LT-HSCs (n=3) E) RT-PCR of Hif-2α and Hif-3α in Hif-1α$^{-/-}$ LT-HSCs demonstrates robust upregulation of Hif-2α

mRNA levels in Hif-1$\alpha^{-/-}$ LT-HSCs (n=3). N.S.=no significance, *$p<0.05$, **$p<0.01$

HSC specific deletion of Hif-1α also demonstrated hematopoietic defects similar (Figure 25) to global deletion (Mx-1-Cre) in the bone marrow shown by Takubo and colleagues (Takubo et al., 2010), including the increased frequency of HSCs (Figure 25A), decreased myeloid progenitors (Figure 25B), loss of quiescence (Figure 25C), and similar multilineage defects (Figure 25F-G).

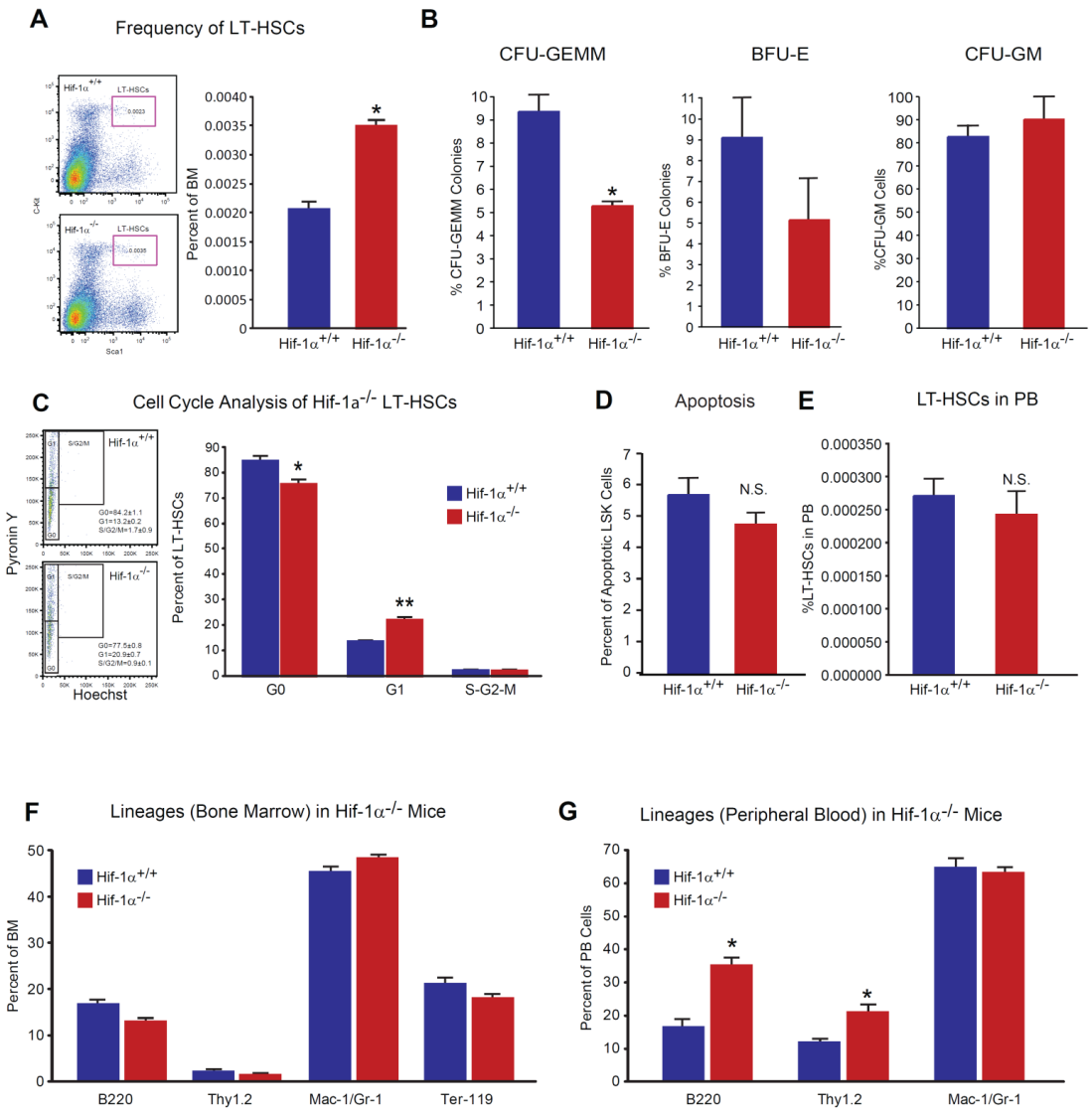

Figure 25. Characterization of Hif-1α$^{-/-}$ HSCs: A) Left panel: Representative flow-cytometry profile of LT-HSCs (Lin^{-}Sca1^{+}Kit^{+}Flk2^{-}CD34^{-}) of Control Hif-1α$^{+/+}$ and Hif-1α$^{-/-}$ mice. Right panel: Quantification of LT-HSCs (n=6). B) Quantification of CFU-GEMM colonies after 12 days of methocult assay demonstrates significantly lower numbers of CFU-GEMM colonies from Hif-1α$^{-/-}$

bone marrow. Quantification of BFU-E and CFU-GM colonies derived from Hif-1α$^{-/-}$ cells shows no significant difference (n=3). C) Left panel demonstrates representative Pyronin Y/Hoechst images of flow cytometric analysis of cell cycle of Hif-1α$^{+/+}$ and Hif-1α$^{-/-}$ LT-HSCs. Right panel is the quantification of different stages of cells in control and Hif-1α$^{-/-}$ cells . The lower percentage of G_0 cells in Hif-1α$^{-/-}$ LT-HSCs indicates impaired quiescence of LT-HSCs (n=3). D) Quantification of apoptosis in control Hif-1α$^{+/+}$ and Hif-1α$^{-/-}$ LSK Cells. E) Quantification of LT-HSCs in peripheral blood (PB) in Hif-1α$^{+/+}$ and Hif-1α$^{-/-}$ mice (n=5). **Lineages in Hif-1α$^{-/-}$ mice** F) Quantification of specific lineages (B220, Thy1.2, Mac-1/Gr-1, and Ter-119) in the bone marrow of Control Hif-1α$^{+/+}$ and Hif-1α$^{-/-}$ Mice (n=5). G) Quantification of specific lineages (B220, Thy1.2, and Mac-1/Gr-1) in the peripheral blood of Control Hif-1α$^{+/+}$ and Hif-1α$^{-/-}$ Mice. Observed defects are similar to global deletion observed in Hif-1α Mx-1 Cre mice as previously demonstrated by Takuba et al, 2010, Cell Stem Cells. (n=5). N.S.=no significance, *p<0.05, **p<0.01.

Meis1 is a Transcriptional Activator of Hif-2α

Downregulation of Hif-1α and Hif-2α in Meis1$^{-/-}$ LT-HSCs (Figure 23A) led us to examine their metabolic profile and ROS levels. Here we show that Meis1$^{-/-}$ LT-HSCs have increased levels of oxygen consumption (Figure 23B) and decreased glycolytic flux (Figure 23C). In addition, Meis1$^{-/-}$ LT-HSCs showed significantly

higher ROS levels compared to control Meis1$^{+/+}$ LT-HSCs (Figure 23D). This increased ROS was associated with increased expression of p16^{Ink4a} and p19^{Arf} in Meis1$^{-/-}$ LT-HSCs, which are known to induce HSC-senescence and apoptosis, respectively (Figure 23E). Therefore, the increased ROS production in Meis1$^{-/-}$ LT-HSCs is compounded by the downregulation of the master antioxidant gene Hif-2α. To determine the mechanism of downregulation of Hif-2α in Meis1$^{-/-}$ LT-HSCs, we identified two Meis1 consensus binding motifs in the promoter of Hif-2α gene (Figure 23F). Using a Hif-2α–pGL2 reporter which includes conserved Meis1 binding site, we demonstrate a dose-dependent activation of Hif-2α by Meis1 expression vector (CMV-Meis1) (Figure 23G). In addition, this activation demonstrates dependence on binding of Meis1 to its consensus binding sequences in the Hif-2α promoter because mutation of the seed sequences (Hif-2α–Mut-pGL2) completely abolished the activation of Hif-2α by Meis1. Given down regulation of Hif-2α in Meis1$^{-/-}$ LT-HSCs (Figure 23A), these results indicate that Meis1 is required for optimal transcriptional activation of Hif-2α in LT-HSCs. We also confirmed the *in vivo* binding of Meis1 to its conserved sequences in the Hif-2α gene by chromatin immuno-precipitation (ChIP) assays in Kasumi1 cells as determined by real-time PCR following immunoprecipitation with Meis1 antibody (Figure 3H).

Effect of ROS Scavenging on the Meis1$^{-/-}$ Phenotype

In order to study effects of ROS observed in Meis1$^{-/-}$ mice, we used NAC, an antioxidant, in an attempt to rescue the Meis1 phenotype by scavenging of ROS in Meis1 HSCs. Following 14 days of Tamoxifen injection, we administered NAC intraperitoneally for 12 days (Figure 26A). Mice where then harvested and HSCs were isolated for analysis of HSC frequency, HSC cell cycle status, apoptosis rate, ROS levels and expression of redox sensitive cell cycle regulators p16^{Ink4a} and p19^{Arf}. Here we show that NAC administration rescues the Meis1$^{-/-}$ phenotype. We found that frequency of hematopoietic stem cells in Meis1$^{-/-}$ mice become similar to Meis1$^{+/+}$ mice (Figure 26B). Flow cytometric analysis of cell cycle of Meis1$^{+/+}$ and Mesi1$^{-/-}$ LT-HSCs, which were both injected with NAC, show a similar numbers of G_0 cells in Meis1$^{-/-}$ LT-HSCs (Figure 26C). Quantification of apoptosis in Meis1$^{+/+}$ and Meis1$^{-/-}$ mice show an increased apoptosis in Meis1$^{-/-}$ mice, however this increase in number of apoptotic cells was not statistically significant (p=0.051) (Figure 26D). In addition, quantification of ROS following NAC treatments restored ROS to Meis1$^{+/+}$ control levels in Meis1$^{-/-}$ LT-HSCs (Figure 26E). Finally, scavenging ROS restored the transcript levels of p16^{Ink4a} and p19^{Arf} in HSC to Meis1$^{+/+}$ control levels (Figure 26F). Additional studies on the measurement of peripheral blood counts of Meis1$^{-/-}$ mice post 1 month and 3 months of Tamoxifen treatments demonstrated decreased red blood cells, white blood cells as well as plateletes (Figure 27).

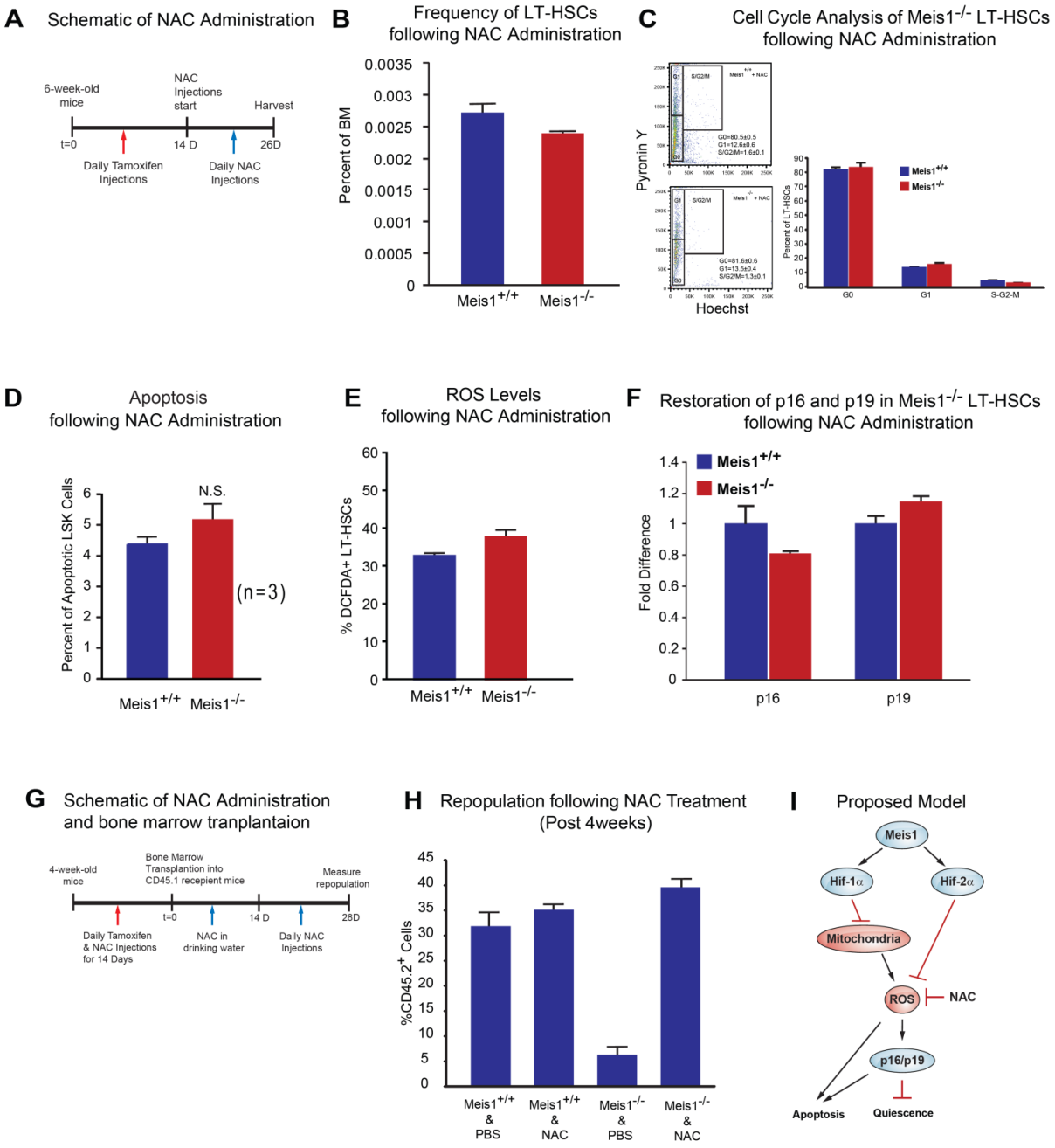

Figure 26. Effect of ROS Scavenging on the Meis1$^{-/-}$ Phenotype: A) Schematic of NAC administration. We performed daily I.P. injections for Tamoxifen for 14 days followed by daily NAC injections upto 12 days. B) Flow cytometry profile

of LT-HSCs ($Lin^-Sca\text{-}1^+Kit^+Flk2^-CD34^-$) of $Meis1^{+/+}$ and $Meis1^{-/-}$ mice following 12 days NAC administration. Note the number of hematopoietic stem cells in $Meis1^{-/-}$ mice is now similar to $Meis1^{+/+}$ values (n=3). C) Left, FACS plot of Pyronin Y/Hoechst staining of LT-HSCs. Right, quantification of Flow cytometric analysis of cell cycle of $Meis1^{+/+}$ and $Mesi1^{-/-}$ LT-HSCs demonstrates restored numbers of G_0 cells in $Meis1^{-/-}$ cells which indicates restored quiescence of LT-HSCs (n=3). D) Quantification of apoptosis in $Meis1^{+/+}$ and $Meis1^{-/-}$ LSK Cells ($Lin^-Sca\text{-}1^+Kit^+$) showing persistent trend towards an increase in the number of apoptotic cells, which was not statistically significant (p=0.059) (n=3). E) Quantification of ROS in $Meis1^{+/+}$ and $Meis1^{-/-}$ LT-HSCs ($Lin^-Sca\text{-}1^+Kit^+Flk2^-CD34^-$) following NAC treatment showing only a modest increase in ROS in $Meis1^{-/-}$ HSCs (n=3) F) Real time PCR of HSC isolated from $Meis1^{+/+}$ and $Meis1^{-/-}$ HSCs following NAC treatment demonstrating no change in p16 and p19 transcripts (n=3). G) Schematic of NAC administration and bone marrow transplantations. We performed daily I.P. injections for Tamoxifen and NAC for 14 days followed by bone marrow transplantation. Then, NAC is provided in drinking water for 2 weeks and administrated another 2 weeks. Repopulation was examined at 4 weeks post-transplant. H) Analysis of repopulation following NAC treatments of BMTs from $Meis1^{+/+}$ and $Meis1^{-/-}$ mice demonstrates restoration of repopulation defect following Meis1 deletion (n=5) I) Schematic of proposed

model is demonstrating how Meis1 regulates metabolism and maintenance of hematopoietic stem cells through its role on Hif-1α and Hif-2α.

To further evaluate the effect of ROS in engraftment defect observed following Meis1 deletion, we performed another bone marrow transplantation from $Meis1^{+/+}$ and $Meis1^{-/-}$ mice treated with and without NAC. Two weeks after Tamoxifen treatment and NAC administration, 1 x 10^5 BM cells from Meis1+/+ or Meis1-/- CD45.2 , together with 1 x 10^5 CD45.1 competitors, were injected into CD45.1 recipients through retro-orbital complex (Figure 26G). Following bone marrow transplantation, NAC is provided in drinking water for 2 weeks and injected daily for 2 more weeks. Repopulation was examined at 4 weeks post-transplant. As shown in Figure 26H, scavenging of ROS by NAC administration restored engraftment defects in Meis1-/- donors. In conclusion, scavenging ROS, through administration of NAC, rescues the Meis1 phenotype in HSC by decreasing levels of ROS, thereby normalizing $p16^{Ink4a}$ and $p19^{Arf}$ expression and restoring HSC quiescence and repopulation defects.

Post 1 month TM	Meis1$^{+/+}$	Meis1$^{-/-}$	p-value
WBC (K/uL)	11.120±1.503	7.016±1.478	0.036
Neutrophil (K/uL)	2.882±0.479	1.366±0.233	0.006
Lymphocyte (K/uL)	7.852±1.065	5.358±1.213	0.081
Monocyte (K/uL)	0.276±0.042	0.23±0.065	0.467
Eosinophil (K/uL)	0.084±0.040	0.048±0.014	0.309
Basophil (K/uL)	0.022±0.014	0.016±0.005	0.637
RBC (M/uL)	8.742±0.538	8.822±0.214	0.863
HB (g/dL)	12.64±0.61	12.82±0.50	0.778
HCT (%)	37.94±1.74	38.14±1.09	0.903
MCV(fL)	43.52±0.95	43.22±0.27	0.707
MCH (Pg)	14.5±0.19	14.52±0.43	0.958
MCHC (g/dL)	33.3±0.43	33.62±1.03	0.721
RDW (%)	19.38±1.74	18.94±0.38	0.759
PLT (K/uL)	691.6±112.3	554.4±99.6	0.272
MPV (fL)	4.82±0.13	4.98±0.11	0.277

Post 3 months TM	Meis1$^{+/+}$	Meis1$^{-/-}$	p-value
WBC (K/uL)	10.036±1.554	10.625±0.846	0.4798
Neutrophil (K/uL)	2.450±0.45	2.492±0.174	0.7045
Lymphocyte (K/uL)	7.138±1.092	7.6325±0.556	0.4527
Monocyte (K/uL)	0.272±0.022	0.350±0.061	0.1417
Eosinophil (K/uL)	0.138±0.033	0.1275±0.064	0.5612
Basophil (K/uL)	0.038±0.009	0.025±0.020	0.7952
RBC (M/uL)	10.426±0.179	9.057±0.225	0.0015
HB (g/dL)	14.10±0.16	13.07±0.40	0.0121
HCT (%)	43.86±0.46	40.72±0.95	0.0095
MCV(fL)	42.12±0.58	44.95±0.12	0.0041
MCH (Pg)	13.52±0.10	14.47±0.12	0.0003
MCHC (g/dL)	32.18±0.41	32.12±0.30	0.9166
RDW (%)	17.7±0.34	17.77±0.17	0.8619
PLT (K/uL)	895.8±56.6	565.2±32.4	0.001
MPV (fL)	4.72±0.07	4.82±0.03	0.2598

Figure 27. Peripheral Blood Counts of Meis1$^{-/-}$ Mice: Quantification of peripheral blood counts of Meis1$^{-/-}$ mice post 1 month and post 3 month of Tamoxifen injections demonstrate various defects in blood cells (mean ± SEM, n=5)

In summary, we demonstrate that Meis1 regulates both HSC metabolism and oxidant stress response through transcriptional activation of Hif-1α and Hif-2α, respectively. Meis1 deletion results in a shift in HSC metabolism toward oxygen consumption, with the resultant increase in ROS production. This phenotype is compounded by downregulation of the oxidant stress response gene Hif-2α, and as a result Meis1 deletion results in HSC dysfunction and apoptosis.

DISCUSSION

In the current report, we demonstrate that Meis1 functions upstream of a transcriptional network that regulates HSC metabolism, and oxidant defense. The Meis1 deletion-induced metabolic shift, and oxidant injury is compounded by the downregulation of Hif-2α, which is in stark contrast to the marked upregulation of Hif-2α in HSC following Hif-1α deletion. This phenotype is associated with upregulation of $p16^{Ink4a}$ and $p19^{Arf}$, loss of quiescence, increased apoptosis, and marked HSC dysfunction.

Endothelial PAS domain protein 1 (EPAS1), also known as Hif-2α (Tian et al., 1997), is closely related to Hif-1α in structure and is likewise activated during hypoxia(Wang et al., 1995b). While Hif-1α is a master regulator of metabolism, Hif-2α is a master regulator of oxidant stress response (Scortegagna et al., 2003a), and is induced by ROS (Wiesener et al., 1998). It is involved in regulation of numerous antioxidant genes that minimize the oxidant damage that results from mitochondrial respiration (Scortegagna et al., 2003a). Hif-$2\alpha^{-/-}$ mice are pancytopenic (Scortegagna et al., 2005; Scortegagna et al., 2003b), and have high levels of oxidative stress (Scortegagna et al., 2003a), which suggests that Hif-2α is required for normal hematopoiesis. Our results indicate that Hif-2α is markedly upregulated following Hif-1α deletion (over 100 fold), which is an indication of a robust antioxidant response to Hif-1α deletion, likely secondary to a shift toward

oxidative metabolism, with the subsequent increase in ROS (Wiesener et al., 1998). In stark contrast, we show that Hif-2α is downregulated following Meis1 KO in HSC, which may partially explain the severity of the Meis1$^{-/-}$ phenotype compared to the Hif-1α$^{-/-}$ phenotype.

Delicate control of ROS levels in HSCs is crucial for HSC maintenance, where elevated ROS levels in HSCs is associated with defects in HSC self-renewal and increased apoptosis. Regulation of ROS in HSCs is likely a highly complex process that involves regulation of the metabolic phenotype of HSCs, as well as regulation of antioxidant defense mechanisms. The contribution of oxidative metabolism to ROS production has been extensively studied (Orrenius et al., 2007). It is estimated that 2% of all electrons flowing through the mitochondrial respiratory chain result in the formation of oxygen free radicals. Electrons leaking of from the respiratory chain interact with oxygen, partially reducing it to superoxide anion ($O2^{-}$•) (Orrenius et al., 2007). Even though $O2^{-}$• itself is not a strong oxidant, it is the precursor of most other ROS (Beckman and Koppenol, 1996; Turrens, 2003). ROS overwhelm the natural antioxidant defense mechanisms overtime, and result in wide spread cellular damage, and stimulation of apoptosis (Orrenius et al., 2007). ROS can also induce the cell cycle regulators p16^{Ink4a} and p19^{Arf}, which cause loss of quiescence and apoptosis of HSCs (Ito et al., 2006). Our results indicate that Meis1 regulates ROS production in HSC

through regulation of both the metabolic phenotype (through Hif-1α) and oxidant defense mechanisms (through Hif-2 α). Finally, our scavenger studies indicate that the effect of loss of Meis1 on HSC cell cycle and engraftment defect are mediated through an increase in ROS production.

In the current report, we highlight the role of Meis1 in a transcriptional network that regulates HSC metabolism and antioxidant defense. Our findings suggest that HSCs are endowed with redundant mechanisms for regulation of their metabolic phenotype, rather than being solely dependent on environmental signals, such as the hypoxic microenvironment. Deciphering the role of these transcriptional networks in regulating HSC fate and function may provide valuable clues for understanding HSC disease and malignancies.

PART 2

MEIS1 IS A TRANSCRIPTIONAL REGULATOR OF CARDIOMYOCYTE CELL CYCLE

INTRODUCTION

Heart failure is a costly and deadly disease affecting over 5 million Americans. At the core of the pathophysiology of heart failure is the inability of the adult mammalian heart to regenerate after injury, leading to replacement of lost cardiomyocytes with non-contractile fibrous tissue. Despite the grossly non-regenerative nature of the mammalian heart, limited myocyte turnover does occur, however it is insufficient to cause any meaningful functional recovery after injury (Bergmann et al., 2009; Bergmann et al., 2012; Laflamme et al., 2002; Nadal-Ginard, 2001; Quaini et al., 2002). This adult phenotype is in stark contrast to the highly regenerative neonatal heart, which has a remarkable regenerative capacity mediated by cardiomyocyte proliferation, reminiscent of lower vertebrates, and is lost by 7 days post-natally (Porrello et al., 2011).

These findings suggest that the key to unlocking the regenerative potential of the adult mammalian heart may lie within the early post-natal cardiomyocytes. Conceivably, identifying subtle changes in transcription factor expression in the

neonatal heart may help identify the mechanism of post-natal cardiomyocytes cell cycle arrest. Therefore, we examined the transcriptional profile of injured and non-injured neonatal mouse heart, and we found that the TALE domain transcription factor Meis1 (Myeloid Ecotropic Integration site 1) was differentially expressed in the post-natal heart in a pattern that suggests its involvement in myocyte cell cycle arrest.

Meis1 is a BHLH transcription factor, which was first identified due to its expression in acute myeloid leukemia (Imamura et al., 2002; Moskow et al., 1995; Rozovskaia et al., 2001). Although Meis1 has not been previously studied in the heart, global knockout studies demonstrate defects in cardiac development including overriding aorta and ventral septal defect in Meis1 knockout embryos, which die around E11.5-14.5 (Azcoitia et al., 2005; Hisa et al., 2004; Imamura et al., 2002). Despite the association of Meis1 with cardiac growth, the precise function of Meis1 in cardiomyocytes is not determined.

Here, we show that Meis1 expression is activated in cardiomyocytes at the onset of postnatal cell cycle arrest. We generated cardiomyocyte-specific Meis1 knockout mice and found that loss of Meis1 resulted in robust cardiomyocyte proliferation in the adult heart. Moreover, conditional deletion of Meis1 in the adult heart resulted in re-activation of cardiomyocyte proliferation in the adult

heart. Finally, we demonstrate that Meis1 is required for transcriptional activation of INK4A-ARF-INK4B locus and p21 $^{(CIP1/WAF1)}$ in cardiomyocytes. These results identify Meis1 as a key regulator of postnatal cardiomyocyte cell cycle arrest and as a potential therapeutic target for cardiac regeneration.

METHODS

Mouse breeding and genotyping

The Meis1 floxed mice were kindly provided by Dr. R. Keith Humphries, University of British Columbia, Canada. Mice were genotyped as described previously (Simsek et al., 2010) using Meis1 sense (5'-CCAAAGTAGCCACCAATATCATGA-3') and Meis1 antisense (5'-AGCGTCACTTGGAAAAGCAATGAT-3') primers. The wild-type (WT) allele was identified as a 332bp-long PCR product and the mutant allele was determined by a 440bp long PCR product on a 1.2% agarose gel. Cardiac-specific deletion of Meis1 (Meis1 KO) was achieved by crossing *Meis1*$^{f/f}$ mice with αMHC-Cre mice (McFadden et al., 2005). αMHC-Cre mice were genotyped using αMHC-Cre sense (5'-GATTTCCGTCTCTGGTGTAGCTGATGATCC-3) and αMHC-Cre antisense (5'-GCCAGGTATCTCTGACCAGAGTCATCC-3) primers. Age-matched Meis1$^{+/+}$;αMHC-Cre(+) mice were used as controls. Inducible cardiomyocyte-specific deletion of Meis1 (Meis1 iKO) was achieved by crossing Meis1$^{f/f}$ mice with *Myh6*-MerCreMer (tamoxifen-inducible Cre recombinase under control of *Myh6* cardiomyocyte-specific promoter) mice (Sohal et al., 2001). Homologous recombination in cardiomyocytes was achieved by administering 3 doses of Tamoxifen injections by I.P. (1 mg/day/mice) to 5-6 week-old Meis1 iKO mice. *Myh6*-MerCreMer mice were genotyped using *Myh6*-MerCreMer sense (5'-GATTTCCGTCTCTGGTGTAGCTGATGATCC-3) and

Myh6-MerCreMer antisense (5'-GCCAGGTATCTCTGACCAGAGTCATCC-3) primers. Age-matched Meis1$^{+/+}$;*Myh6*-MerCreMer(+) mice were used as controls and received same dose of Tamoxifen.

Myocardial Infarction (MI)

Myocardial infarction on neonatal mice was performed at post-natal day 1 (P1) following anesthetization by cooling on an ice bed (Porrello et al., 2011). Following skin incision and dissection of the intercostal muscles, 6-0 prolene suture (Ethicon, NJ) was tied through the mid-ventricle below the origin of the left anterior descending (LAD) coronary artery. Sham-operated mice underwent the same procedure without LAD ligation. Myocardial infarctions on adult mice (5-6 weeks old) were done following anesthetization with isoflurane with endotracheal intubation for ventilation using the mouse ventilator (Harvard Apparatus, MA).

Cardiomyocyte isolation from adult mouse heart

Whole adult mouse hearts (5-6 weeks old) were anticoagulated with 10 IU/kg of IP heparin sodium and digested using a Langendorff retrograde perfusion-digestion system using collagenase as previously described (O'Connell et al.,

2007). Cardiomyocytes in the pellet were collected following centrifugation at 50g for 5 minutes.

Immunostaining for Mesi1 and Cardiac Troponin

Following antigen retrieval with EDTA Buffer (1 mM EDTA, 0.05% Tween 20, pH 8.0) in boiling water for 40 min, paraffin sections were permeabilized with 0.3% triton X/PBS for 10 minutes and then blocked with 10% goat serum for 30 minutes. Primary antibodies against Meis1 (Santa Cruz Biotechnology, sc-10599) and cardiac troponin T (Tnnt) (Thermoscientific, MS-295-P1, 1:100 dilution) were incubated overnight at 4^{o}C. Sections were subsequently washed with PBS and incubated with corresponding secondary antibodies conjugated to Alexa Fluor 488 and Alexa Fluor 555 (Invitrogen).

Immunostaining for PH3 and Aurora B

Immunostaining on paraffin embedded sections for PH3 and Aurora B were performed as described previously (Porrello et al., 2011). Following antigen retrieval with 10 mM Na-Citrate (pH6.1) in boiling water for 20 min, sections were blocked with 10% goat serum, and incubated with PH3 or Aurora B (1:100 dilution) and Tnnt (Thermoscientific, MS-295-P1, 1:100 dilution) antibodies

overnight at 4^{o}C. Sections were subsequently washed with PBS and incubated with corresponding secondary antibodies conjugated to Alexa Fluor 488 and Alexa Fluor 555 (Invitrogen).

Wheat germ agglutinin (WGA) staining

Following deparaffinization, slides were rinsed 3 times in PBS and then incubated for 1 hour at room temperature with a primary antibody against WGA conjugated to Alexa Fluor 488 (50 µg/ml, Invitrogen, CA). Slides were then rinsed in PBS and mounted in Vectashield containing DAPI (Vector Labs, CA). To quantify size of cells, images at 40 X zoom were captured and ImageJ was used to determine the area of each cell. Quantitative analyses involved counting of multiple fields from three independent samples per group (~50 cells per field assessed, total ~250 cells per group).

Hematoxylin/eosin and Trichrome staining

Hematoxylin/eosin and Masson's trichrome staining were performed according to standard procedures on paraffin sections.

TUNEL staining

Paraffin embedded heart sections were deparaffinized and permeabilized with 0.2% Triton-PBS at room temperature for 10 minutes. Following 1 hour blocking with 1%BSA, 1%normal goat serum, 0.025%Tween-20, slides were incubated with Desmin (1/100 in PBS) overnight at 4^{o}C. Following incubation with a corresponding secondary antibody conjugated to Alexa Fluor 488 (Invitrogen), TUNEL staining was performed according to manufacturer's recommendations (In Situ Cell Death Detection Kit, Fluorescein, Cat# 11684795910, Roche).

Meis-1 knockdown:

Meis-1 siRNA knockdown was carried out *in vitro* on cultured rat neonatal cardimyocytes. Cardiomyocytes were cultured on 6-well plates at 70% confluency. 12 ul of lipofectamine (invitrogen) and siRNA (50 nM of siRNA) were incubated in 200 ul of OPTIMEM (Invitrogen) for 20 min at RT. Silencer Select Pre-designed siRNAs (Applied Biosystems, Ambion) for Meis1 (siRNA ID# s8662) and negative control were diluted into 50nM stocks: siRNA ID# s8662: 5'-GGCAUCUACUCGUUCAGGAtt-3' and 5'-UCCUGAACGAGUAGAUGCCgt-3'. siRNA were added to cells dropwise and incubated for 6 hours. After 6 hours incubation, cardiomyocyte growth medium

was added and plates were incubated under normal growth conditions for 48 hours.

Immunostaining on neonatal cardiomyocytes following Meis1 siRNA treatment

Control siRNA or Meis1 siRNA transfected neonatal cardiomyocytes were fixed on coverslips with 4% PFA for 5 min at room temperature. Following permeabilization with 0.1% Triton X in PBS for 2 min at room temperature, cells were blocked with 3% normal goat serum for 30 minutes. Coverslips were incubated with PH3(1:100) and TnnT (1:100) primary antibodies in humid chamber for one hour at room temperature. This was followed by incubation with corresponding secondary antibodies conjugated to Alexa Fluor 488 and Alexa Fluor 555, Hoechst 33342 staining and fluorescent imaging.

Real-Time PCR:

Total RNA was isolated using Qiagen`s RNeasy Mini Kit (cat# 74104) according to manufacturer's instructions. cDNA was synthesized from 2 µg of RNA using SuperScript II RT (Invitrogen). Predesigned primers (Table 4) from NIH mouse primer depot (http://mouseprimerdepot.nci.nih.gov/) were ordered from Integrated DNA Technologies unless otherwise stated. Real time PCR was performed with

SyberGreen (Applied Biosystems) on ABI Prism 7700 Sequence Detector (Applied Biosystems). GAPDH was used as a housekeeping control to normalize gene expression using the ΔΔCt method.

Table 4: List of primers used for real time PCR

Gene	Forward Primer	Reverse Primer
GAPDH	GAACCCTAAGGCCAACCGTGAAAGAT	ACCGCTCGTTGCCAATAGTGATG
Meis1	GTTGTCCAAGCCATCACCTT	ATCCACTCGTTCAGGAGGAA
$p15^{INK4b}$ (CDKN2B)	CAGTTGGGTTCTGCTCCGT	AGATCCCAACGCCCTGAAC
$p16^{INK4a}$ (Xu et al., 2011)	GGGTTTCGCCCAACGCCCCGA	TGCAGCACCACCAGCGTGTCC
p21(CDKN1A)	ATCACCAGGATTGGACATGG	CGGTGTCAGAGTCTAGGGGA
$p19^{ARF}$(Xu et al., 2011)	GTTTTCTTGGTGAAGTTCGTGC	TCATCACCTGGTCCAGGATTC
p18(CDKN2C)	CTCCGGATTTCCAAGTTTCA	GGGGGACCTAGAGCAACTTAC
p27(CDKN1B)	GGGGAACCGTCTGAAACATT	AGTGTCCAGGGATGAGGAAG
p57(CDKN1C)	TTCTCCTGCGCAGTTCTCTT	CTGAAGGACCAGCCTCTCTC
p19(CDKN2D)	GTCCTGGACATTGGGGCT	AACCGCTTCGGCAAGAC

Generation of INK4b–ARF–INK4a locus ($p16^{INK4a}$/$p19^{ARF}$/$p15^{INK4b}$) and p21 Reporter vectors

A 691 bp long DNA fragment (chr9:22,010,169-22,010,227) from the promoter region of INK4b–ARF–INK4a locus and a 987 bp long DNA fragment (chr6:36,650,803-36,650,829) from the promoter region of p21 (Cdkn1a) containing conserved Meis-1 binding sites were amplified from mouse genomic

DNA. PCR primers for cloning include INK4b–ARF–INK4a-pGL2-F 5'-CCCTTGAGCTTTGGTTGTAATCC-3' and INK4b–ARF–INK4a-pGL2-R5'-GGAATCTGACACACGTACTACC-3' for generation of INK4b–ARF–INK4a luciferase reporter, p21-pGL-F 5'-GTATGTGTGTGGTAGTGTATGTGG-3' and p21-pGL-R 5'-GCCAGCCTGGTCTACAAAGTG-3' for generation of p21 luciferase reporter. PCR products were subsequently subcloned into the E1b-pGL2 vector to generate INK4b–ARF–INK4a and p21 luciferase reporter vectors. To test for Meis1 binding site specificity, the Meis1 binding site (TGAC) was mutated using IProof (Bio-rad) with the following primers: INK4b–ARF–INK4a del(NotI)-F 5'-agtgcggccgcCCCAGCACCACACCCGAGT-3' and INK4b–ARF–INK4a del(NotI)-R 5'-agtgcggccgcTTAAAGCCCTCTCTGAACGT-3'. p21mut (NotI)-F 5'-agtgcggccgcAGTGGGAGGGAGGGAGGG-3' and p21mut (NotI)-R 5'-agtgcggccgcCAGGTGCTCCAGGCTGGAGG-3'.

Luciferase reporter assays:

Transcriptional activation of INK4b–ARF–INK4a locus and p21 by Meis1 was evaluated using INK4b–ARF–INK4a-pGL2 and p21-pGL2 vectors as described previously (Simsek et al., 2010). 0.8 μg of INK4b–ARF–INK4a-pGL2 or p21-pGL2 was co-transfected with 50 ng, 100 ng, 200 ng and 400 ng of the Meis-1 expression vector pCMV-SPORT6-Meis1 (OpenBiosystems) and 0.2 μg of pCMV-LacZ (internal control) into COS cells in 6-well plates using lipofectamine

transfection reagent (Invitrogen). Forty-eight hours after transfection, the cell lysate was processed for luciferase activity using the luciferase reporter system (Promega), according to the manufacturer's instructions. Luciferase measurements were calculated as firefly luciferase units normalized to β-gal units.

Echocardiography

Left ventricular systolic function was determined echocardiographically on conscious mice using the Visual Sonics Vevo 2100, equipped with a 40 MHz mouse ultrasound probe. Ejection fraction and fractional shortening were calculated based on end diastolic and end systolic dimensions obtained from M-mode ultrasound.

Chromatin Immunoprecipitation Assay (ChIP)

ChIP assays were performed to evaluate the in vivo binding of Meis1 to its consensus sequence in the INK4b–ARF–INK4a and p21 promoter. The assays were done in whole mouse hearts using the ChIP kit (Upstate, cat#17-295) as described previously (Simsek et al., 2010). Meis1 antibody (Santa Cruz Biotechnology, sc-10599) and normal goat IgG (Santa Cruz Biotechnology, sc-2028) were used. The DNA isolated from input chromatin fragments and from the precipitated chromatin fragments by anti-Meis1 antibody or control IgG was subjected to PCR using primers flanking the consensus Meis1 binding sites on

INK4b–ARF–INK4a and p21 promoters: p21-Chip-F 5'-GCTACTGCCTCCTCCCAGG-3' and p21-Chip-R5'-TAGGCAATCCTGAGAAACAGAAGC-3', INK4b–ARF–INK4a -ChIP-For5'-TCTTAGTTTGCCCTCTTACTGG-3' and INK4b–ARF–INK4a -ChIP-Rev5'-AGCAGTATGTTCCTTCGCTTGG-3'

Statistical Analysis

Results are expressed as mean ± SEM. A 2-tailed Student's *t* test was used to determine statistical significance and $p<0.05$ was considered statistically different.

RESULTS

Meis1 is required for post-natal mitotic arrest of cardiomyocytes

We have recently demonstrated that the neonatal mouse heart can regenerate following surgical amputation of the ventricular apex (Porrello et al., 2011) and myocardial infarction (unpublished). The molecular mechanisms that lead to loss of cardiac regenerative capacity in mammals after birth are poorly understood. We performed microarray analysis at day 7 following myocardial infarction surgeries in neonatal mice during the regenerative window (at P1) and outside the regenerative window (at P7) and identified as Meis1 a putative regulator in cardiac regeneration. Interestingly, Meis1 is required for normal hematopoiesis and is essential for embryonic heart development, but the potential roles of Meis1 in postnatal heart maturation and heart regeneration have not been explored.

To outline the expression profile of Meis1 during neonatal heart development and regeneration, we performed qPCR and immunostaining on neonatal hearts at different postnatal time points and following myocardial infarction at postnatal day 1 (P1). qPCR analysis demonstrated higher levels of Meis1 expression at P7 (Figure 28A). Myocardial infarction at P1 was associated with a modest decrease in the expression of the homeobox transcription factor Meis1 at day 7 post-MI, whereas Meis1 was significantly increased at day 7 following MI at P7 (Figure 28B). Moreover, Meis1

protein was undetectable by immunohistochemistry in neonatal cardiomyocytes at P1 but becomes readily detectable in the nucleus of cardiomyocytes by P7 (Figure 28C). Furthermore, following myocardial infarction at P1, which induces a robust proliferative response in neonatal cardiomyocytes, Meis1 was undetectable in the vast majority of cardiomyocyte nuclei at day 7 post-MI (Figure 28C). To elucidate the role Meis1 cardiomyocyte proliferation, we performed siRNA knowdown *in vitro* in rat neonatal cardiomyocytes and confirmed knockdown of Meis1 as shown by real time PCR at Figure 28D. siRNA-mediated knockdown of Meis1 in cultured rat neonatal cardiomyocytes led to a significant increase in myocyte proliferation (Figure 28E). Taken together, these results suggest that Meis1 plays an important role in inducing postnatal mitotic arrest of cardiomyocytes. These results suggest that Meis1 expression in cardiomyocytes is associated with mitotic arrest.

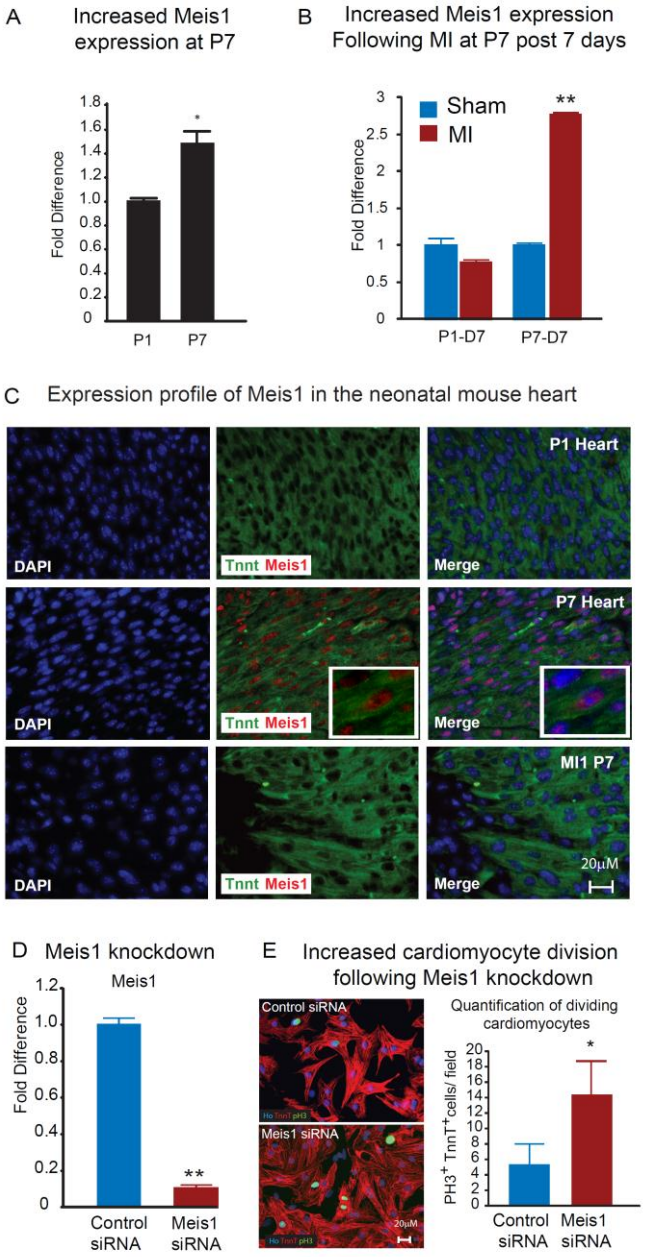

Figure 28. A) Real time PCR showing increased expression of Meis1 at p7. B) Real time PCR showing expression pattern of Meis1 following Myocardial Infarctions at P1 and P7. Note the downregulation of Meis1 in surgeries in regenerative window and upregulation outside of regenerative window C) Expression profile of Meis1 in the Heart: Meis1 immunostaining demonstrating

localization of Meis1 to the nucleus of the uninjured heart cells at P7. DAPI (blue), Meis1 (red) and TnnT (green). Note the absence of Meis1 staining at P1 and following myocardial infarction in neonates at P7 (MI1 P7). D) Real time PCR showing knockdown of Meis1 in rat neonatal cardiomyocytes by Meis1 siRNA E) Cardiomyocyte division following Meis1 knockdown: Left Panel: Immunostaining showing co-localization of PH3, TnnT and Hoechst at rat neonatal cardiomyocytes following control and Meis1 siRNA treatment. Scale bar, 20 μm. Right Panel: Quantification of the $PH3^{+}TnnT^{+}$ nuclei in Control and Meis1 siRNA treated cardiomyocytes. Quantitative analysis represents counting of multiple fields from three independent samples per group. Note increased cardiomyocyte division following Meis1 knockdown.

To elucidate the role of Meis1 in postnatal cardiomyocyte cell cycle arrest *in vivo*, we crossed $Meis1^{f/f}$ mice with αMHC-Cre mice to specifically delete Meis1 in cardiomyocytes (CMs) (Figure 29A). Real-time PCR (Figure 29B) of isolated cardiomyocytes and immunostaining (Figure 29C) of $Meis1^{f/f}$; αMHC-Cre (Meis1 KO) compared to αMHC-Cre (Control) mice heart confirmed Meis1 deletion in CMs. Phenotypic characterization of Meis1 KO mice demonstrated a modest increase in heart-to-body weight ratio (Figure 29D). Meis1 KO mice exhibit a normal cardiac function as indicated by ejection fraction (EF) and fractional shortening (FS) following echocardiography at 6 weeks of age (Figure 29E).

Here, we show that Meis1 KO CMs are smaller compared to Control CMs *in vivo* (Figure 29F). Given that cardiac enlargement was associated with smaller cardiomyocyte size in Meis1 KO hearts, these findings imply that Meis1 KO hearts have an increased number of cardiomyocytes.

To determine if Meis1 deletion in cardiomyocytes *in vivo* increases cardiomyocyte proliferation, we performed immunostaining on Meis1 KO and control heart sections using the mitosis marker PH3 and the cytokinesis marker Aurora B. Meis1 deletion resulted in a robust induction of cardiomyocyte proliferation as quantified by an increase in the number of $PH3^{+}TnnT^{+}$ (>9 fold) (Figure 29G) and Aurora B^{+} $TnnT^{+}$ (>5 fold) (Figure 29H) cardiomyocytes.

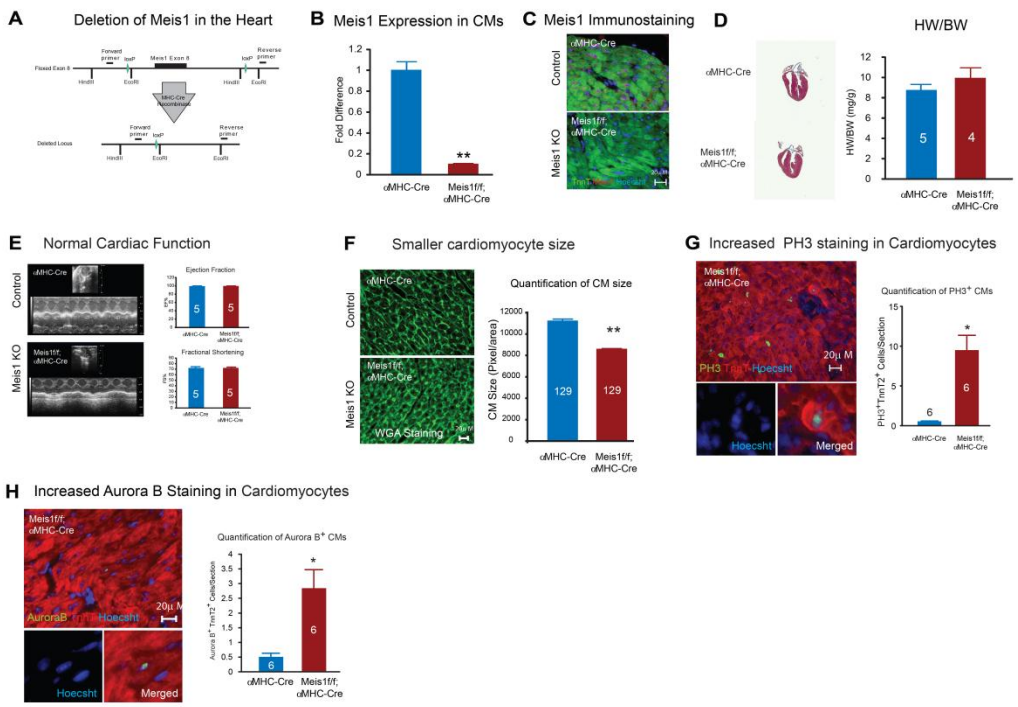

Figure 29. Cardiomyocyte proliferation in Meis1-/- Heart: A) Schematic of Meis1 floxed allele showing deletion of floxed Exon 8 following Cre recombinase activity. αMHC-Cre recombinase allows specific deletion of Meis1 gene in cardiomyocytes. B) Real Time PCR demonstrates deletion of Meis1 in the isolated cardiomyocytes (n=3). C) Immunostaining demonstrates deletion of Meis1 in Meis1 KO hearts. D) Heart weight-to-body weight ratio in Control and Meis1 KO mice E) Left ventricular systolic function quantified by ejection fraction (EF) and fractional shortening (FS) showing normal systolic function at baseline in Meis1 KO hearts at p28 (n= 4-7 per group). F) Wheat germ agglutinin staining (WGA) (left panel) and cell size quantification (right panel) showing

significant smaller cardiomyocyte size in Meis1 KO hearts (at P21). Quantitative analyses represent counting of multiple fields from three independent samples per group (~total of 129 cells assessed). Scale bar, 20 μm. G) Left Panel: Immunostaining showing co-localization of PH3, TnnT and Hoechst at Meis1 KO heart (at P21). Scale bar, 20 μm. A closer look of $PH3^{+}TnnT^{+}$ nucleus was noted (bottom boxes). Right Panel: Quantification of the number of PH3+TnnT+ nuclei at Control and Meis1 KO hearts. Quantitative analysis represents counting of multiple sections from three independent samples per group (~3 sections per heart). H) Left Panel: Immunostaining showing co-localization of Aurora B, TnnT and Hoechst at Meis1 KO heart (at P21). Scale bar, 20 μm. A closer look of Aurora $B^{+}TnnT^{+}$ nucleus was noted (bottom boxes). Right Panel: Quantification of the number of $PH3^{+}TnnT^{+}$ nuclei at Control and Meis1 KO hearts. Quantitative analysis represents counting of multiple sections from three independent samples per group (~3 sections per heart). Values presented as mean ± SEM; *P<0.05.

We next investigated whether conditional deletion of Meis1 in the adult heart could induce cardiomyocyte cell cycle re-entry. Thus, we crossed $Meis1^{f/f}$ mice with αMHC-MerCreMer mice, which allowed for specific deletion of Meis1 in cardiomyocytes following Tamoxifen (TM) injections. Following administration of 3 doses of TM to 6 week old mice, Meis1 was deleted in the majority of cardiomyocytes (Figure 30A and 31B). Characterization of Inducible Meis1

knockout mice (Meis1 iKO) demonstrated a similar cardiac output and a normal cardiac function compared to controls (Figure 30C). Heart-to-body weight ratio (Figure 30D) and overall heart size (Figure 30E) were increased in Meis1 iKO mice at D28. Cardiomyocyte size was similar in Meis1 iKO hearts (Figure 30F), while the number of mitotic cardiomyocytes was higher (Figure 30G). Meis1 has been associated with increased apoptosis in hematopoietic stem cells as we have shown previously (Chapter 5, Figure 21D). However, we don't see any significant change in the apoptosis in Meis1 KO hearts (Figure 31). Collectively, these results demonstrate that Meis1 plays an essential role in maintaining the post-mitotic state of adult cardiomyocytes.

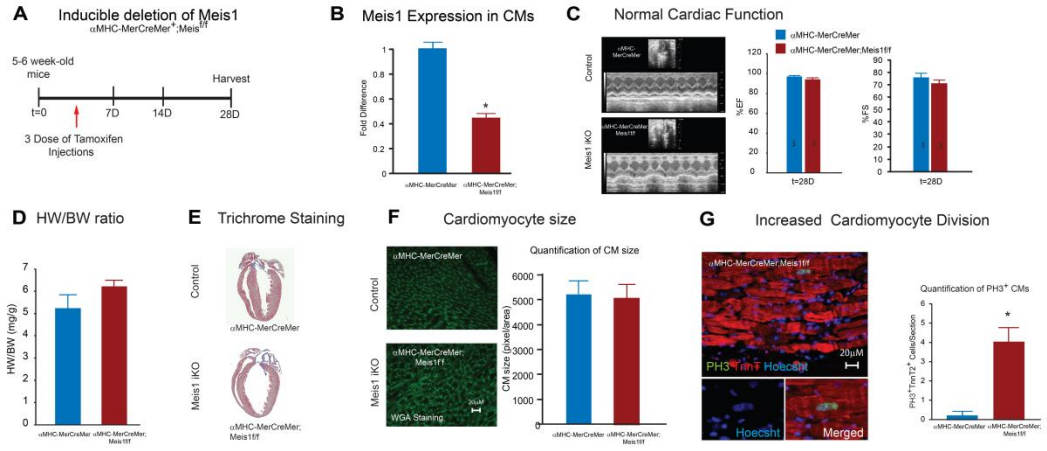

Figure 30. Inducible deletion of Meis1 in cardiomyocytes: A) Schematic of Tamoxifen administration protocol. αMHC-MerCreMer recombinase allows specific deletion of Meis1 in cardiomyocytes following TM injections. B) Real Time PCR demonstrates deletion of Meis1 in the isolated cardiomyocytes (n=3).

C) Left ventricular systolic function quantified by ejection fraction (EF) and fractional shortening (FS) showing normal systolic function following TM injection in αMHC-MerCreMer^{+};Meis$^{f/f}$ (Meis1 iKO) hearts (n= 4 per group). D) Heart weight-to-body weight ratio in Control and Meis1 iKO mice E) Trichrome stained sections at D28 following Tamoxifen injections. F) Wheat germ agglutinin staining (WGA) (left panel) and cell size quantification (right panel) showing significant cardiomyocyte hypertrophy at day 28. Quantitative analyses represent counting of multiple fields from three independent samples per group (~50 cells per field assessed, total ~250 cells per group). Scale bar, 20 μm. G) Left Panel: Immunostaining showing co-localization of PH3, TnnT and Hoechst post 7 days in Meis1 iKO heart. Scale bar, 20 μm. A closer look of PH3^{+}TnnT^{+} nucleus was noted (bottom boxes). Right Panel: Quantification of the number of PH3^{+}TnnT^{+} nuclei post 7 days of TM in Control and Meis1 KO hearts. n=6. Values presented as mean ± SEM; *P<0.05.

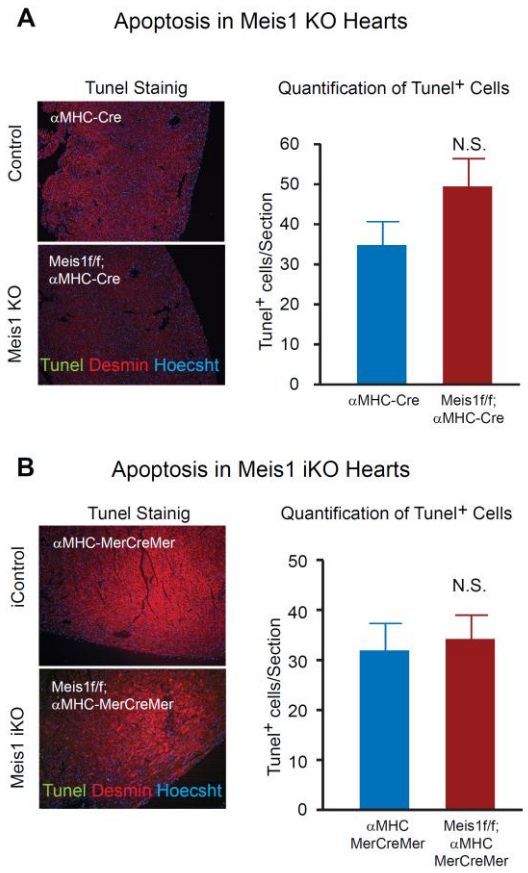

Figure 31. Apoptosis in Meis1 KO hearts. A) Left Panel: Immunostaining showing co-localization of Tunel, Desmin, and Hoechst at Control and Meis1 KO heart. Right Panel: Quantification of the number of Tunel^{+} cells at Control and Meis1 KO hearts (n=3). B) A) Left Panel: Immunostaining showing co-localization of Tunel, Desmin, and Hoechst at Control and Meis1 inducible KO heart. Right Panel: Quantification of the number of Tunel^{+} cells at Control and Meis1 inducible KO hearts (n=3).

Regulation of cyclin-dependent kinase inhibitors by Meis1

In order to determine the molecular mechanism by which Meis1 governs cardiomyocyte proliferation and cardiac regenerative capacity, we performed myocardial infarctions in regenerative window where heart could regenerate completely about three weeks and at outside of the regeneration window where myocardial injury results in scar formation and lack of complete regeneration (Figure 32A). We found that Meis1 expression goes down once heart injured at p1 while it goes up if heart injured at p7. Since cardiomyocytes exit cell cycle around P7, we determined the pattern of expression of cyclin dependent kinase inhibitors if they demonstrate a similar pattern of expression with Meis1 (Figure 32B). Notably, cyclin-dependent kinase inhibitors including members of INK4b-ARF-INK4a locus (p16, p15 and $p19^{ARF}$) and p21 demonstrate a robust and similar expression pattern compared to Meis1 (Figure 28B) following myocardial infarctions at P1 and P7 (Figure 28 B and Figure 32B). Moreover, we found that deletion of Meis1 *in vivo* results in significant downregulation of a number of cyclin-dependent kinase inhibitors in isolated cardiomyocytes including members of the INK4b-ARF-INK4a locus (p16, p15 and $p19^{ARF}$) and CIP/KIP family(p21 and p57) (Figure 32C). Therefore, Meis1 is associated with the regulation of a number of cyclin-dependent kinase inhibitors belonging to the INK4b-ARF-INK4a and CIP/KIP family.

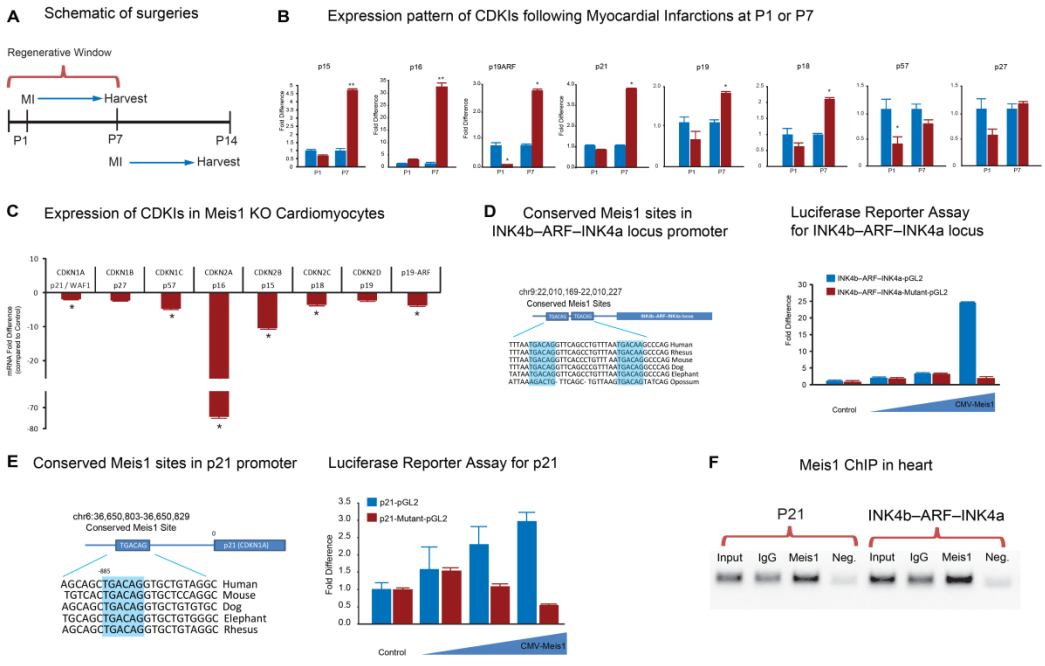

Figure 32. Regulation of cyclin-dependent kinase inhibitors by Meis1 A) Schematic of myocardial infarctions in neonates. Note neonatal heart heals completely following myocardial infarction in the regenerative window B) Real time PCR showing expression pattern of cyclin-dependent kinase inhibitors following myocardial infarctions at P1 and P7. Note the downregulation of CDKIs in surgeries in regenerative window and upregulation outside of regenerative window C) Real time PCR of Cyclin Dependent Kinase Inhibitors (CDKIs) in Meis1 KO cardiomyocytes demonstrates significant down regulation of CDKN1A (p21), CDKN2B (p15), CDKN2A (p16), $p19^{ARF}$, CDKN2C (p18), and CDKN1C (p57) D) Left panel: Highly conserved Meis1 motifs located in $p16^{INK4a}/p19^{ARF}/p15^{INK4b}$ promoter. Right Panel: Luciferase reporter assay for

INK4b–ARF–INK4a promoter demonstrating induction of INK4b–ARF–INK4a-pGL2 reporter by Meis1 and loss of reporter activity following mutation of Meis1 motifs (INK4b–ARF–INK4a-Mutant-pGL2). E) Left panel: Highly conserved Meis1 motif located in p21 promoter. Right Panel: Luciferase reporter assay for p21 demonstrating induction of p21-pGL2 reporter by Meis1 and loss of reporter activity following mutation of Meis1 motifs (p21Mutant-pGL2). F) In vivo confirmation of Meis1 interaction with INK4a/ARF/INK4b and p21 promoters is done by chromatin immunoprepitation assay.Values presented as mean ± SEM; *P<0.05.

We have located highly conserved Meis1 binding sites only in the promoter region of the INK4b–ARF–INK4a locus (which expresses $p16^{INK4a}$/$p19^{ARF}$/$p15^{INK4b}$) (Figure 32E) and p21 locus (Figure 32F) from the database of Genome browser (http://genome.ucsc.edu) conserved predicted transcriptional binding sites. To test if Meis1 can transcriptionally activate INK4b–ARF–INK4a and p21 locus, we generated luciferase reporters from conserved Meis1 binding motifs. Luciferase reporter assays with INK4b–ARF–INK4a-pGL2 reporter (Figure 32D) and p21-pGL2 reporter constructs (Figure 32E) demonstrated a dose-dependent activation by Meis1. In addition, mutation of the putative Meis1 binding site in these promoters (NK4b–ARF–INK4a-Mutant-pGL2 and p21-Mutant-pGL2 reporters) diminished Meis1-dependent activation of

the luciferase reporter (Figure 32D-E). Moreover, we demonstrate *in vivo* interaction of Meis1 with INK4a/ARF/INK4b and p21 promoters in the adult mouse heart as determined by chromatin immunoprepitation assay (Figure 32F).

In conclusion, these studies show that Meis1 plays a critical role in cardiomyocyte cell cycle arrest by targeting multiple cyclin-dependent kinase inhibitors belonging to the INK4b-ARF-INK4a and p21 locus (Proposed Model: Figure 33). Given that deletion of Meis1 in adult mice resulted in cardiomyocyte proliferation, Meis1 may be a potential therapeutic target for cardiac regeneration.

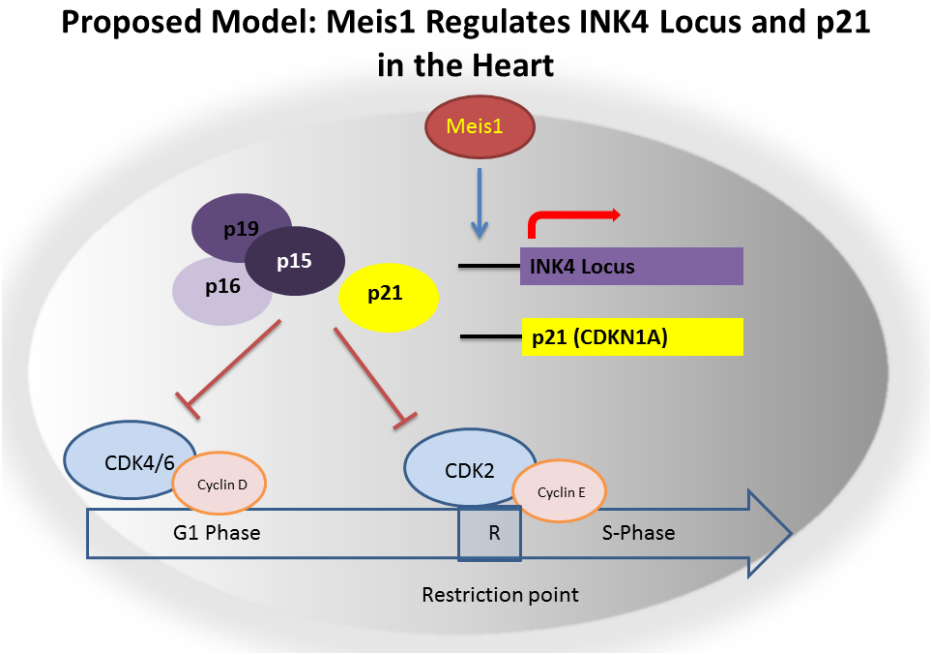

Figure 33. Proposed Model of Cardiomyocyte Cell Cycle Arrest by Meis1

Meis1 involves in regulation of cardiomyocyte cell cycle arrest through

transcriptional activation of Cyclin Dependent Kinase Inhibitors (CDKIs); INK4b-ARF-INK4a locus and p21 genes. Activation of CDKIs leads to cell cycle arrest at G1 by inhibiting CDKs.

DISCUSSION

Myocardial infarction, which leads to loss of substantial amount of cardiomyocytes, is the most common antecedent of heart failure. At the core of the pathophysiology of heart failure is the inability of the adult mammalian heart to regenerate following injury. This is in sharp contrast to the early post-natal heart that harbors a robust regenerative capacity, mediated by proliferation of pre-existing cardiomyocytyes (Porrello et al., 2011). However, this proliferative potential of neonatal cardiomyocytes is lost within a week after birth, afterwhich cardiomyocyte hypertrophy becomes the default mechanism of cardiac growth. To date, the molecular mechanisms that regulate this switch from hyperplastic to hypertrophic phenotype are not well understood. Therefore, we set out to identify transcription factors that regulate the post-natal cell cycle exit of cardiomyocyte, in an effort to re-activate mitotic entry in the adult heart.

Our results demonstrate that expression of Meis1 in post-natal cardiomyocytes coincides with cell cycle arrest. Knockout studies confirm the role of Meis1 in cardiomyocyte cell cycle regulation where loss of Meis1 results in global cardiomyocyte proliferation in the adult heart. Remarkably, inducible Meis1 deletion in the adult heart results in widespread reactivation of cardiomyocyte

proliferation without evidence of myocyte death or loss of contractile function of the heart.

Cardiomyocyte cell cycle exit is associated with downregulation of positive cell cycle regulators (CDK2, CDK3, CDK4, CCND1, and CDK cofactors) as well induction of cell cycle inhibitors (p21, TSC2) (Pasumarthi and Field, 2002; Poolman et al., 1998; Walsh et al., 2010). Consistently, cardiomyocyte specific overexpression of Cyclin D2, which is a Cdk cofactor that positively regulates cell cycle progression, leads to cardiomyocyte cell cycle entry (Pasumarthi et al., 2005). In addition, deletion of CDKI $p27^{Kip1}$ or immunodepletion of $p21^{Cip1}$ in cardiomyocytes is associated with a trend towards progression to S-phase (Poolman et al., 1998; Poolman et al., 1999). Our results indicate that the effect of loss of Meis1 on cardiomyocyte cell cycle is mediated by downregulation of a number of cyclin dependent kinase inhibitors (CDKIs), where we demonstrate that Meis1 is required for transcriptional activation of the synergistic CDK inhibitors $p15^{INK4B}$, $p16^{INK4A}$, $p19^{ARF}$ and $p21^{CIP1}$. While there certainly may be other downstream targets of Meis1 at play, our results clearly implicate these CDK inhibitors in the Meis1 phenotype.

The cardiac regeneration field has evolved rapidly over the past two decades. Although it was previously thought that the heart is a post mitotic organ, it is now

clear that there is measurable myocyte turnover that occurs in the adult mouse (Hsieh et al., 2007; Nadal-Ginard, 2001) and human (Beltrami et al., 2001; Bergmann et al., 2009; Laflamme et al., 2002; Quaini et al., 2002) hearts. While the mechanism of myocyte turnover in the adult mammalian heart is not well understood, a plausible strategy to achieve the elusive goal of cardiac regeneration may very well lie within cardiomyocytes themselves. Our results indicate that this goal may be achievable though careful analysis of events that induce cell cycle arrest of cardiomyocytes soon after birth. The current study identifies Meis1 is a key regulator of cardiomyocyte proliferation, and sets the stage for future studies to determine the role of Meis1 in heart regeneration.

PART 3 - DISCUSSION AND FUTURE DIRECTIONS

Hematopoietic Stem Cell Metabolism

Hematopoietic stem cells (HSCs) are characterized by their ability to self-renew and provide lifelong supply of blood cells. They reside primarily in the endosteal regions of the bone marrow (Arai et al., 2004; Calvi et al., 2003; Zhang et al., 2003). This zone has unique vasculature with the arteriols arising from the small arteries which divide into capillaries. Perfusion of oxygen is further limited where the blood from these capillaries reaches into sinusoids, thus results in very low oxygen tension in the endoestreal region described as "hypoxic niche" of HSCs. While this hypoxic niche provides protective mechanisms against oxidative damage, HSCs require certain metabolic adaptations for self-renewal and survival in this microenvironment. Since HSCs are mainly kept quiescent and reside in hypoxic microenvironment, we hypothesized that HSCs have lower rates of metabolism, thus might utilize glycolytic metabolism instead of mitochondrial respiration. Therefore, we determined the metabolic characteristics of mouse and human HSCs. Using flow cytometry, we demonstrated that mouse LT-HSCs and human HPSCs are localized to a distinct population of cells characterized by low MP. This population represents only a small fraction of the total bone marrow or mobilized periperal human blood, but contains the vast majortiy of HSCs. We

showed that both HSCs and low MP cells have low ATP levels and utilize primarily cytoplasmic glycolysis instead of mitochondrial oxidative phosphorylation. This unique metabolic profile of HSCs and low MP cells is associated with upregulation of Hif-1α and Meis1. Hif-1 is the key transcription factor for response to the hypoxia and mediates metabolic switch from mitochondrial oxidative phosphorylation to glycolysis (Semenza, 2007b, 2009b, 2010). Hif-1 consist of oxygen regulated Hif-1α and constitutively expressed Hif-1β subunits. Hif-1α could be regulated either by protein stabilization (Li et al., 2005; Nakayama et al., 2004; Semenza, 2001, 2004, 2007a) or transcriptional activation (Gorlach and Bonello, 2008; Hirota et al., 2004; Laughner et al., 2001; Rius et al., 2008). Our studies showed Meis1 as a transcriptional regulator of Hif-1α in HSCs. Additional characterization of Meis1 binding site in Hif-1α gene provided evidence that cofactors of Meis1, Pbx1 and HoxA9 contribute to activation of Hif-1α in a cooperative manner.

Flow cytometry has been extensively used for HSC isolation and mostly relies on the expression of combination of a number of surface markers or transporters (Goodell et al., 1996; Huynh et al.; Kiel et al., 2005; Osawa et al., 1996; Wilson et al., 2008; Yilmaz et al., 2006). We developed a flow cytometry protocol that allows us to enrich HSCs based on their metabolic profile. We showed that separation of cells solely based on this metabolic footprint markedly enriches

HSCs as determined by *in vitro* colony forming assays (both mouse and human Low MP cells) and *in vivo* long-term repopulation assays (mouse low MP cells). Importantly, we found human HSCs are localized to the low MP gate even after G-CSF mobilization to the peripheral blood, which supports the notion of intrinsic transcriptional regulation of HSC metabolism irrespective of their hypoxic niche. In addition, the transcriptional regulation of Hif-1α by Meis1, Pbx1 and HoxA9 in HSCs highlights the involvement of stem cell-associated transcription factors in the regulation of the glycolytic phenotype of HSCs and suggest that HSCs have intrinsic mechanisms for regulation of their metabolic properties.

Meis1, myeloid ecotrophic insertion site 1, was first identified in a spontaneous mouse leukemia model (BXH-2) as a common integration site of B-ecotropic provirus (Moskow et al., 1995). Meis1 belongs to three-amino-acid loop extension (TALE) class transcriptions factors, which specifically bind and activate transcription via TGACAG motifs (Cesselli et al., 2001; Okada et al., 2003). High levels of Meis1 expression were found in bone marrow of acute myeloid leukemia patients and in the primitive hematopoietic cells (Argiropoulos et al., 2007; Fischbach et al., 2005; Imamura et al., 2002; Pineault et al., 2004; Pineault et al., 2003; Rozovskaia et al., 2001). Meis1 expression is crucial to suppress differentiation of hematopoietic cells by G-CSF stimulated differentiation, whereas Meis1 expression decreases in differentiated

cells(Argiropoulos and Humphries, 2007; Argiropoulos et al., 2007; Calvo et al., 2001; Imamura et al., 2002; Pineault et al., 2002a). Mice lacking Meis1 shows various hematopoietic and cardiac defects and die around E11.5-14.5 (Azcoitia et al., 2005; Hisa et al., 2004; Imamura et al., 2002). Meis1$^{-/-}$ embryos have decreased number of colony-forming cells. In addition, fetal liver cells fail to radioprotect following transplantation into irradiated host and show poor competition in repopulation assays.

Meis1 represents an important cofactor for Pbx1 and HoxA9 (Argiropoulos et al., 2007; Calvo et al., 1999; Cvejic et al., 2011; Ferrell et al., 2005; Ficara et al., 2008; Gwin et al., 2010; Hu et al., 2009; Huang et al., 2011; Kirito et al., 2004; Lawrence et al., 2005; Pillay et al., 2010; Pineault et al., 2002a; Thorsteinsdottir et al., 2002; Yan et al., 2006). Meis1 and other TALE family proteins cooperate and form dimeric or trimeric complexes with Hox proteins thus increase DNA binding specificity and affinity (Shen et al., 1997; Shen et al., 1999). Meis1-Pbx-Hox trimer demonstrate higher stability suggesting the role of Meis1 in stabilization of DNA bound complex (Shanmugam et al., 1999). In addition, the Pbx interaction domain, the homeodomain and transactivating C-terminal domain of Meis1 are required for interaction with Pbx proteins and HoxA9 (Wong et al., 2007). Pbx1 knockdown in Zebrafish show similar hematopoietic defects with Meis1 knockdown (Cvejic et al., 2011). Moreover, Pbx1 regulates self-renewal of

mouse HSCs by maintaining their quiescence (Ficara et al., 2008). In spite of clear association of Meis1 with hematopoiesis, the function of Meis1 in adult HSCs was unknown. Our initial studies on the HSC metabolism suggested the involvement of Meis1-Hif-glycolysis axis in HSC function (Part I- Chapter 2, and (Simsek et al., 2010)).

HSC fate is tightly regulated between self-renewal, quiescence, apoptosis and differentiation. Growing evidence indicates that not only environmental cues provided by the HSC niche but also intrinsic stem cell factors govern HSC fate decision (Warr et al., 2011). Therefore, we sought to determine the role of metabolic regulators in HSC fate and function. Utilizing conditional and tissue specific deletion of *Hif-1α* and *Meis1* in HSCs *in vivo*, we showed that Hif-1α and Meis1 are required for proper HSC function and metabolism. Similarly, studies by Takubo et al. (2010) also demonstrated that conditional deletion of Hif-1α in bone marrow leads to loss of HSC quiescence, increased HSC cycling and loss of long-term repopulation(Takubo et al., 2010). Despite the importance of Hif-1α, which is considered the master regulator of metabolism, the role of Hif-1α and its upstream regulators in HSC metabolism are not understood. Our studies show that HSCs lacking *Hif-1α* or *Meis1* shows a metabolic shift from cytoplasmic glycolysis to mitochondrial oxidative phosphorylation with markedly higher rates

of oxygen consumption, lower rates of glycolysis, and increased ROS, which resulted in loss of HSC quiescence and apoptosis.

In addition, we found that Meis1 not only regulates HSC metabolism but also oxidative stress response through transcriptional regulation of Hif-2α. While Hif-1α and Hif-2α are highly homologous and target similar genes such as GLUT1 and VEGF, they have distinct targets. For instance, Hif-1α uniquely stimulates glycolytic enzymes (PGK, LDHA) while Hif-2α regulates expression of antioxidant enzymes such as catalase, superoxide dismutase and glutathione peroxide ((Scortegagna et al., 2003a) and reviewed in (Patel and Simon, 2008)). Mitochondrial oxidative phosphorylation is accompanied by the generation of ROS and if excessive, it could lead to senescence or apoptosis. Hif-2α null mice demonstrate increased oxidative stress with multiorgan dysfunction including cardiac hypertrophy, hepatic steatosis, defects in spermatogenesis and hematopoiesis (Gruber et al., 2010; Scortegagna et al., 2003a; Scortegagna et al., 2005; Scortegagna et al., 2003b). Our results clearly demonstrate that Meis1 deletion results in downregulation of Hif-2α and increased ROS in HSCs. Moreover, we showed that adverse effects of ROS in Meis1 KO mice can be completely reversed by treatment of N-acetyl-L-cysteine (NAC), a ROS scavenger. These findings highlight an important transcriptional network which regulates HSC metabolism, ROS and HSC function, which Meis1 at its core.

Meis1 and its cofactors are overexpressed in a wide variety of leukemias (Ernst et al., 2004; Horton et al., 2005; Milne et al., 2005; Zeisig et al., 2004) and found to modulate maintenance of leukemia cells (Argiropoulos et al., 2007; Wong et al., 2007). In addition, it has been reported that cancer cells demonstrate metabolic adaptations and preferential use of glycolysis (Denko, 2008; Kim et al., 2007; Semenza, 2009a). Although the clear association of metabolic adaptation and overexpression of Meis1 in cancer cells, the involvement of Meis1 and its cofactors in the transformation and regulation of cancer cell metabolism remain to be determined. Furthermore, we showed that stem cells could be enriched solely based on metabolic profiling. Similarly, metabolic profiling of cancer cells could provide novel approaches to identify cancers stem cells.

Hypoxic Cardiac Stem Cell Niche

Knowledge from HSC biology has been extensively used for the identification of cardiac progenitor/stem cells, which lead to discovery of a number of resident cardiac progenitor/stem cells (Martin-Puig et al., 2008). Metabolic profiling of hematopoietic stem cells provided us with a functional approach to asses if there is any resident cardiac progenitor/stem cell population that can be isolated based on metabolic footprint without the use of surface markers. Based on metabolic

profiling, we identified glycolytic cardiac progenitors (GCPs) that mainly use glycolysis, express Hif-1α and display a multilineage differentiation potential. Furthermore, similar to HSCs, Hif-1α regulates the metabolic phenotype, differentiation and proliferation of GCPs. These findings raised an obvious question: Is there a hypoxic niche that GCPs are maintained?

Our quest to find where GCPs might reside in adult mouse heart led us to identify the epicardium and subepicardium as the cardiac hypoxic niche. We demonstrated that epicardium and supepicardium have lower capillary densities and house Hif-1α expressing cells, including numerous cardiomyocytes. Further evidence is provided by the colocalization of epicardial marker expressing GCPs with the lowest Hoechst perfusion in the heart. Future studies will focus on whether these hypoxic epicardial and subepicardial cells give rise to all cardiac lineages in vivo after myocardial injury. This will require generation of an inducible Hif-1α reporter mouse line, which is technically very difficult since Hif-1α is regulated by protein stabilization and is ubiquitously transcribed in all cells. For this purpose we have generated a fusion protein where Hif-1α is fused to the inducible reporter. This will allow us to determine whether these Hif-1α expressing epicardial and subepicardial cells are true cardiac progenitors. It is intriguing to ponder whether these Hif-1α^{+} cardiomyocytes differ from other cardiomyocytes reside in well-perfused myocardium. For example, are these cardiomyocyte

mononucleated or bi-nucleated? Are they arrested in G0/G1 phase of cell cycle like the majority of cardiomyocytes in the adult heart? Or are they able to cycle in response to injury? Further studies are also required to determine the role of hypoxia signaling in cell fate decision of cardiac progenitors as well as for cell cycle regulation of cardiomyocytes that reside in the cardiac hypoxic niche.

Reactivating Cardiomyocyte Cell Cycle

We demonstrated that deletion of Meis1 in HSCs results in loss of quiescence and a marked increased proliferation. Given mice lacking Meis1 shows various development defects including in heart development (Azcoitia et al., 2005; Hisa et al., 2004; Imamura et al., 2002), Meis1 is likely to play important role in cardiomyocyte proliferation.

Cardiomyocytes have developmentally different forms of growth such as rapid proliferation during fetal life, binucleation postnatally in the first week of life and increase in cell size, or hypertrophy in adult heart. Mouse cardiomyocytes undergo dramatic changes at the first week of life as marked with the expression of adult isoforms of contractile proteins, and induction of DNA synthesis without cytokinesis resulting in binucleation and cell cycle arrest at G_0/G_1. Adult cardiomyocytes show increased levels of CDKIs and decreased activity of

positive regulators of cell cycle(Brooks et al., 1998; Brooks et al., 1997; Li et al., 1998; Poolman and Brooks, 1998; Poolman et al., 1998; Poolman et al., 1999). It has been postulated that the primary limiting factor for cardiac regeneration following myocardial injury is the inability of adult mammalian myocardium to reactivate cardiomyocyte cell cycle. Several studies demonstrated feasibility of the induction of cardiomyocte cell cycle by administration of growth factors such as periostin, neurogulin, and FGF1 (Bersell et al., 2009; Braun and Dimmeler, 2009; Engel et al., 2006; Kuhn et al., 2007), expression of cell cycle regulator Cyclin D2 (Pasumarthi et al., 2005), or induction of the Hippo pathway(Heallen et al., 2011; Xin et al., 2011)

Neonatal heart differs from adult heart in virtue of ability to regenerate following injury at P1 with a profound and global cardiomyocyte proliferation (Porrello et al., 2011). In search for the transcription factors that regulate this remarkable regenerative capacity of the neonatal heart, we found that Meis1 expression pattern in the post natal heart corresponded with post natal cell cycle arrest. Given the role of Meis1 in regulation of HSC cell cycle, we hypothesized that Meis1 expression in cardiomyocytes could be associated with the postnatal myocyte cell cycle arrest. We found that knockdown or cardiomyocyte specific deletion of Meis1 in the cardiomyocytes lead to profound cardiomyocyte proliferation. More importantly, we demonstrate that inducible Meis1 KO in the adult heart is

associated with reactivation of cardiomyocyte cell cycle, a finding that has never been reported in the literature before. Finally, our studies *in vitro* and *in vivo* demonstrated that Meis1 regulates all three checkpoints of cardiomyocyte cell cycle by transcriptional activation of synergistic cyclin-dependent kinase inhibitors; $p15^{INK4B}$, $p16^{INK4A}$, $p19^{ARF}$ and $p21^{CIP1}$. Further studies to understand how Meis1 cardiomyocyte expression is regulated could provide new approaches to cardiac regeneration therapies following myocardial infarction.

Our studies provide new insights into the interplay between metabolism and cell cycle regulation. These findings can have far reaching impacts on regenerative medicine as well as cancer biology. While we clearly demonstrate that Meis1 is an integral part of the transcriptional network that regulates metabolism and cell cycle, we have only begun to understand how these complex processes may be linked. It is crucial for future studies to determine other links between metabolism and cell cycle regulation, and more importantly, understand how these master transcription factors are regulated, either by epigenetic, systemic, or environmental factors.

BIBLIOGRAPHY

Abramson, S., Miller, R.G., and Phillips, R.A. (1977). The identification in adult bone marrow of pluripotent and restricted stem cells of the myeloid and lymphoid systems. J Exp Med *145*, 1567-1579.

Aguilar, V., and Fajas, L. (2010). Cycling through metabolism. EMBO Mol Med *2*, 338-348.

Arai, F., Hirao, A., Ohmura, M., Sato, H., Matsuoka, S., Takubo, K., Ito, K., Koh, G.Y., and Suda, T. (2004). Tie2/angiopoietin-1 signaling regulates hematopoietic stem cell quiescence in the bone marrow niche. Cell *118*, 149-161.

Argiropoulos, B., and Humphries, R.K. (2007). Hox genes in hematopoiesis and leukemogenesis. Oncogene *26*, 6766-6776.

Argiropoulos, B., Yung, E., and Humphries, R.K. (2007). Unraveling the crucial roles of Meis1 in leukemogenesis and normal hematopoiesis. Genes Dev *21*, 2845-2849.

Arminan, A., Gandia, C., Garcia-Verdugo, J.M., Lledo, E., Mullor, J.L., Montero, J.A., and Sepulveda, P. (2010). Cardiac Transcription Factors Driven Lineage-Specification of Adult Stem Cells. J Cardiovasc Transl *3*, 61-65.

Azcoitia, V., Aracil, M., Martinez, A.C., and Torres, M. (2005). The homeodomain protein Meis1 is essential for definitive hematopoiesis and vascular patterning in the mouse embryo. Dev Biol *280*, 307-320.

Barile, L., Messina, E., Giacomello, A., and Marban, E. (2007). Endogenous cardiac stem cells. Prog Cardiovasc Dis *50*, 31-48.

Bearzi, C., Rota, M., Hosoda, T., Tillmanns, J., Nascimbene, A., De Angelis, A., Yasuzawa-Amano, S., Trofimova, I., Siggins, R.W., Lecapitaine, N., *et al.* (2007). Human cardiac stem cells. Proc Natl Acad Sci U S A *104*, 14068-14073.

Becker, M.W., and Jordan, C.T. (2011). Leukemia Stemness Signatures Step toward the Clinic. Cell Stem Cell *9*, 185-186.

Beckman, J.S., and Koppenol, W.H. (1996). Nitric oxide, superoxide, and peroxynitrite: the good, the bad, and ugly. The American journal of physiology *271*, C1424-1437.

Belaiba, R.S., Bonello, S., Zahringer, C., Schmidt, S., Hess, J., Kietzmann, T., and Gorlach, A. (2007). Hypoxia up-regulates hypoxia-inducible factor-1alpha transcription by involving phosphatidylinositol 3-kinase and nuclear factor kappaB in pulmonary artery smooth muscle cells. Mol Biol Cell *18*, 4691-4697.

BelAiba, R.S., Bonello, S., Zharinger, C., Schmidt, S., Hess, J., Kietzmann, T., and Gorlach, A. (2006). Transcriptional regulation of HIF-1alpha by NFkappaB in response to hypoxia. Circulation *114*, 182-183.

Beltrami, A.P., Barlucchi, L., Torella, D., Baker, M., Limana, F., Chimenti, S., Kasahara, H., Rota, M., Musso, E., Urbanek, K., *et al.* (2003). Adult cardiac stem cells are multipotent and support myocardial regeneration. Cell *114*, 763-776.

Beltrami, A.P., Urbanek, K., Kajstura, J., Yan, S.M., Finato, N., Bussani, R., Nadal-Ginard, B., Silvestri, F., Leri, A., Beltrami, C.A., *et al.* (2001). Evidence that human cardiac myocytes divide after myocardial infarction. N Engl J Med *344*, 1750-1757.

Bergmann, O., Bhardwaj, R.D., Bernard, S., Zdunek, S., Barnabe-Heider, F., Walsh, S., Zupicich, J., Alkass, K., Buchholz, B.A., Druid, H., *et al.* (2009). Evidence for cardiomyocyte renewal in humans. Science *324*, 98-102.

Bergmann, O., Zdunek, S., Frisen, J., Bernard, S., Druid, H., and Jovinge, S. (2012). Cardiomyocyte renewal in humans. Circ Res *110*, e17-18; author reply e19-21.

Bersell, K., Arab, S., Haring, B., and Kuhn, B. (2009). Neuregulin1/ErbB4 signaling induces cardiomyocyte proliferation and repair of heart injury. Cell *138*, 257-270.

Bhatia, M., Bonnet, D., Kapp, U., Wang, J.C., Murdoch, B., and Dick, J.E. (1997). Quantitative analysis reveals expansion of human hematopoietic repopulating cells after short-term ex vivo culture. J Exp Med *186*, 619-624.

Blank, U., Karlsson, G., and Karlsson, S. (2008). Signaling pathways governing stem-cell fate. Blood *111*, 492-503.

Blouin, C.C., Page, E.L., Soucy, G.M., and Richard, D.E. (2004). Hypoxic gene activation by lipopolysaccharide in macrophages: implication of hypoxia-inducible factor 1alpha. Blood *103*, 1124-1130.

Bradley, T.R., Hodgson, G.S., and Rosendaal, M. (1978). The effect of oxygen tension on haemopoietic and fibroblast cell proliferation in vitro. J Cell Physiol *97*, 517-522.

Braun, T., and Dimmeler, S. (2009). Breaking the silence: stimulating proliferation of adult cardiomyocytes. Dev Cell *17*, 151-153.

Brooks, G., Poolman, R.A., and Li, J.M. (1998). Arresting developments in the cardiac myocyte cell cycle: role of cyclin-dependent kinase inhibitors. Cardiovasc Res *39*, 301-311.

Brooks, G., Poolman, R.A., McGill, C.J., and Li, J.M. (1997). Expression and activities of cyclins and cyclin-dependent kinases in developing rat ventricular myocytes. J Mol Cell Cardiol *29*, 2261-2271.

Bruick, R.K., and McKnight, S.L. (2001). A conserved family of prolyl-4-hydroxylases that modify HIF. Science *294*, 1337-1340.

Buchakjian, M.R., and Kornbluth, S. (2010). The engine driving the ship: metabolic steering of cell proliferation and death. Nat Rev Mol Cell Biol *11*, 715-727.

Bunn, H.F., and Poyton, R.O. (1996). Oxygen sensing and molecular adaptation to hypoxia. Physiol Rev *76*, 839-885.

Cai, C.L., Martin, J.C., Sun, Y., Cui, L., Wang, L., Ouyang, K., Yang, L., Bu, L., Liang, X., Zhang, X., *et al.* (2008). A myocardial lineage derives from Tbx18 epicardial cells. Nature *454*, 104-108.

Calvi, L.M., Adams, G.B., Weibrecht, K.W., Weber, J.M., Olson, D.P., Knight, M.C., Martin, R.P., Schipani, E., Divieti, P., Bringhurst, F.R., *et al.* (2003). Osteoblastic cells regulate the haematopoietic stem cell niche. Nature *425*, 841-846.

Calvo, K.R., Knoepfler, P., McGrath, S., and Kamps, M.P. (1999). An inhibitory switch derepressed by pbx, hox, and Meis/Prep1 partners regulates DNA-binding by pbx1 and E2a-pbx1 and is dispensable for myeloid immortalization by E2a-pbx1. Oncogene *18*, 8033-8043.

Calvo, K.R., Knoepfler, P.S., Sykes, D.B., Pasillas, M.P., and Kamps, M.P. (2001). Meis1a suppresses differentiation by G-CSF and promotes proliferation by SCF: potential mechanisms of cooperativity with Hoxa9 in myeloid leukemia. Proc Natl Acad Sci U S A *98*, 13120-13125.

Camargo, F.D., Green, R., Capetanaki, Y., Jackson, K.A., and Goodell, M.A. (2003). Single hematopoietic stem cells generate skeletal muscle through myeloid intermediates. Nat Med *9*, 1520-1527.

Caro, J. (2001). Hypoxia regulation of gene transcription. High Alt Med Biol *2*, 145-154.

Cesselli, D., Jakoniuk, I., Barlucchi, L., Beltrami, A.P., Hintze, T.H., Nadal-Ginard, B., Kajstura, J., Leri, A., and Anversa, P. (2001). Oxidative stress-mediated cardiac cell death is a major determinant of ventricular dysfunction and failure in dog dilated cardiomyopathy. Circ Res *89*, 279-286.

Challen, G.A., Boles, N., Lin, K.K., and Goodell, M.A. (2009). Mouse hematopoietic stem cell identification and analysis. Cytometry A *75*, 14-24.

Chong, J.J., Chandrakanthan, V., Xaymardan, M., Asli, N.S., Li, J., Ahmed, I., Heffernan, C., Menon, M.K., Scarlett, C.J., Rashidianfar, A., *et al.* (2011). Adult cardiac-resident MSC-like stem cells with a proepicardial origin. Cell Stem Cell *9*, 527-540.

Chow, D.C., Wenning, L.A., Miller, W.M., and Papoutsakis, E.T. (2001). Modeling pO(2) distributions in the bone marrow hematopoietic compartment. I. Krogh's model. Biophys J *81*, 675-684.

Chowdhury, R., Hardy, A., and Schofield, C.J. (2008). The human oxygen sensing machinery and its manipulation. Chem Soc Rev *37*, 1308-1319.

Cipolleschi, M.G., Dello Sbarba, P., and Olivotto, M. (1993). The role of hypoxia in the maintenance of hematopoietic stem cells. Blood *82*, 2031-2037.

Conneally, E., Cashman, J., Petzer, A., and Eaves, C. (1997). Expansion in vitro of transplantable human cord blood stem cells demonstrated using a quantitative assay of their lympho-myeloid repopulating activity in nonobese diabetic-scid/scid mice. Proc Natl Acad Sci U S A *94*, 9836-9841.

Covello, K.L., Kehler, J., Yu, H., Gordan, J.D., Arsham, A.M., Hu, C.J., Labosky, P.A., Simon, M.C., and Keith, B. (2006). HIF-2alpha regulates Oct-4: effects of hypoxia on stem cell function, embryonic development, and tumor growth. Genes Dev *20*, 557-570.

Crisan, M., Yap, S., Casteilla, L., Chen, C.W., Corselli, M., Park, T.S., Andriolo, G., Sun, B., Zheng, B., Zhang, L., *et al.* (2008). A perivascular origin for mesenchymal stem cells in multiple human organs. Cell Stem Cell *3*, 301-313.

Cvejic, A., Serbanovic-Canic, J., Stemple, D.L., and Ouwehand, W.H. (2011). The role of meis1 in primitive and definitive hematopoiesis during zebrafish development. Haematologica *96*, 190-198.

Danet, G.H., Pan, Y., Luongo, J.L., Bonnet, D.A., and Simon, M.C. (2003). Expansion of human SCID-repopulating cells under hypoxic conditions. The Journal of clinical investigation *112*, 126-135.

De Filippis, L., and Delia, D. Hypoxia in the regulation of neural stem cells. Cell Mol Life Sci *68*, 2831-2844.

DeBerardinis, R.J., Mancuso, A., Daikhin, E., Nissim, I., Yudkoff, M., Wehrli, S., and Thompson, C.B. (2007). Beyond aerobic glycolysis: transformed cells can engage in glutamine metabolism that exceeds the requirement for protein and nucleotide synthesis. Proc Natl Acad Sci U S A *104*, 19345-19350.

Denko, N.C. (2008). Hypoxia, HIF1 and glucose metabolism in the solid tumour. Nat Rev Cancer *8*, 705-713.

Dettman, R.W., Denetclaw, W., Jr., Ordahl, C.P., and Bristow, J. (1998). Common epicardial origin of coronary vascular smooth muscle, perivascular fibroblasts, and intermyocardial fibroblasts in the avian heart. Dev Biol *193*, 169-181.

Doetsch, F., Caille, I., Lim, D.A., Garcia-Verdugo, J.M., and Alvarez-Buylla, A. (1999a). Subventricular zone astrocytes are neural stem cells in the adult mammalian brain. Cell *97*, 703-716.

Doetsch, F., Garcia-Verdugo, J.M., and Alvarez-Buylla, A. (1999b). Regeneration of a germinal layer in the adult mammalian brain. Proc Natl Acad Sci U S A *96*, 11619-11624.

Draenert, K., and Draenert, Y. (1980). The vascular system of bone marrow. Scan Electron Microsc, 113-122.

Eliasson, P., and Jonsson, J.I. The hematopoietic stem cell niche: low in oxygen but a nice place to be. J Cell Physiol *222*, 17-22.

Elvidge, G.P., Glenny, L., Appelhoff, R.J., Ratcliffe, P.J., Ragoussis, J., and Gleadle, J.M. (2006). Concordant regulation of gene expression by hypoxia and 2-oxoglutarate-dependent dioxygenase inhibition: the role of HIF-1alpha, HIF-2alpha, and other pathways. J Biol Chem *281*, 15215-15226.

Engel, F.B., Hsieh, P.C., Lee, R.T., and Keating, M.T. (2006). FGF1/p38 MAP kinase inhibitor therapy induces cardiomyocyte mitosis, reduces scarring, and

rescues function after myocardial infarction. Proc Natl Acad Sci U S A *103*, 15546-15551.
Eppert, K., Takenaka, K., Lechman, E.R., Waldron, L., Nilsson, B., van Galen, P., Metzeler, K.H., Poeppl, A., Ling, V., Beyene, J., *et al.* (2011). Stem cell gene expression programs influence clinical outcome in human leukemia. Nat Med *17*, 1086-1093.
Epstein, A.C., Gleadle, J.M., McNeill, L.A., Hewitson, K.S., O'Rourke, J., Mole, D.R., Mukherji, M., Metzen, E., Wilson, M.I., Dhanda, A., *et al.* (2001). C. elegans EGL-9 and mammalian homologs define a family of dioxygenases that regulate HIF by prolyl hydroxylation. Cell *107*, 43-54.
Ergen, A.V., and Goodell, M.A. (2010). Mechanisms of hematopoietic stem cell aging. Exp Gerontol *45*, 286-290.
Ernst, P., Mabon, M., Davidson, A.J., Zon, L.I., and Korsmeyer, S.J. (2004). An Mll-dependent Hox program drives hematopoietic progenitor expansion. Curr Biol *14*, 2063-2069.
Ferrell, C.M., Dorsam, S.T., Ohta, H., Humphries, R.K., Derynck, M.K., Haqq, C., Largman, C., and Lawrence, H.J. (2005). Activation of stem-cell specific genes by HOXA9 and HOXA10 homeodomain proteins in CD34+ human cord blood cells. Stem Cells *23*, 644-655.
Ficara, F., Murphy, M.J., Lin, M., and Cleary, M.L. (2008). Pbx1 regulates self-renewal of long-term hematopoietic stem cells by maintaining their quiescence. Cell Stem Cell *2*, 484-496.
Fischbach, N.A., Rozenfeld, S., Shen, W., Fong, S., Chrobak, D., Ginzinger, D., Kogan, S.C., Radhakrishnan, A., Le Beau, M.M., Largman, C., *et al.* (2005). HOXB6 overexpression in murine bone marrow immortalizes a myelomonocytic precursor in vitro and causes hematopoietic stem cell expansion and acute myeloid leukemia in vivo. Blood *105*, 1456-1466.
Fuchs, E., Tumbar, T., and Guasch, G. (2004). Socializing with the neighbors: stem cells and their niche. Cell *116*, 769-778.
Funk, J.O. (1999). Cancer cell cycle control. Anticancer Res *19*, 4772-4780.
Gatenby, R.A., and Gillies, R.J. (2004). Why do cancers have high aerobic glycolysis? Nat Rev Cancer *4*, 891-899.
Goodell, M.A., Brose, K., Paradis, G., Conner, A.S., and Mulligan, R.C. (1996). Isolation and functional properties of murine hematopoietic stem cells that are replicating in vivo. J Exp Med *183*, 1797-1806.
Gorlach, A., and Bonello, S. (2008). The cross-talk between NF-kappaB and HIF-1: further evidence for a significant liaison. Biochem J *412*, e17-19.
Gothert, J.R., Gustin, S.E., Hall, M.A., Green, A.R., Gottgens, B., Izon, D.J., and Begley, C.G. (2005). In vivo fate-tracing studies using the Scl stem cell enhancer: embryonic hematopoietic stem cells significantly contribute to adult hematopoiesis. Blood *105*, 2724-2732.

Gruber, M., Mathew, L.K., Runge, A.C., Garcia, J.A., and Simon, M.C. (2010). EPAS1 Is Required for Spermatogenesis in the Postnatal Mouse Testis. Biol Reprod *82*, 1227-1236.
Gwin, K., Frank, E., Bossou, A., and Medina, K.L. (2010). Hoxa9 regulates Flt3 in lymphohematopoietic progenitors. J Immunol *185*, 6572-6583.
Hagg, M., and Wennstrom, S. (2005). Activation of hypoxia-induced transcription in normoxia. Exp Cell Res *306*, 180-191.
Harman, D. (1972). The biologic clock: the mitochondria? Journal of the American Geriatrics Society *20*, 145-147.
Harrison, J.S., Rameshwar, P., Chang, V., and Bandari, P. (2002). Oxygen saturation in the bone marrow of healthy volunteers. Blood *99*, 394.
He, S., Nakada, D., and Morrison, S.J. (2009). Mechanisms of stem cell self-renewal. Annu Rev Cell Dev Biol *25*, 377-406.
Heallen, T., Zhang, M., Wang, J., Bonilla-Claudio, M., Klysik, E., Johnson, R.L., and Martin, J.F. (2011). Hippo pathway inhibits Wnt signaling to restrain cardiomyocyte proliferation and heart size. Science *332*, 458-461.
Hermitte, F., Brunet de la Grange, P., Belloc, F., Praloran, V., and Ivanovic, Z. (2006). Very low O2 concentration (0.1%) favors G0 return of dividing CD34+ cells. Stem Cells *24*, 65-73.
Hirota, K., Fukuda, R., Takabuchi, S., Kizaka-Kondoh, S., Adachi, T., Fukuda, K., and Semenza, G.L. (2004). Induction of hypoxia-inducible factor 1 activity by muscarinic acetylcholine receptor signaling. J Biol Chem *279*, 41521-41528.
Hisa, T., Spence, S.E., Rachel, R.A., Fujita, M., Nakamura, T., Ward, J.M., Devor-Henneman, D.E., Saiki, Y., Kutsuna, H., Tessarollo, L., *et al.* (2004). Hematopoietic, angiogenic and eye defects in Meis1 mutant animals. EMBO J *23*, 450-459.
Horton, S.J., Grier, D.G., McGonigle, G.J., Thompson, A., Morrow, M., De Silva, I., Moulding, D.A., Kioussis, D., Lappin, T.R., Brady, H.J., *et al.* (2005). Continuous MLL-ENL expression is necessary to establish a "Hox Code" and maintain immortalization of hematopoietic progenitor cells. Cancer Res *65*, 9245-9252.
Hsieh, P.C., Segers, V.F., Davis, M.E., MacGillivray, C., Gannon, J., Molkentin, J.D., Robbins, J., and Lee, R.T. (2007). Evidence from a genetic fate-mapping study that stem cells refresh adult mammalian cardiomyocytes after injury. Nat Med *13*, 970-974.
Hu, Y.L., Fong, S., Ferrell, C., Largman, C., and Shen, W.F. (2009). HOXA9 modulates its oncogenic partner Meis1 to influence normal hematopoiesis. Mol Cell Biol *29*, 5181-5192.
Huang, Y., Sitwala, K., Bronstein, J., Sanders, D., Dandekar, M., Collins, C., Robertson, G., Macdonald, J., Cezard, T., Bilenky, M., *et al.* (2011).

Identification and characterization of Hoxa9 binding sites in hematopoietic cells. Blood.

Huynh, H., Zheng, J., Umikawa, M., Zhang, C., Silvany, R., Iizuka, S., Holzenberger, M., Zhang, W., and Zhang, C.C. IGF binding protein 2 supports the survival and cycling of hematopoietic stem cells. Blood *118*, 3236-3243.

Imamura, T., Morimoto, A., Takanashi, M., Hibi, S., Sugimoto, T., Ishii, E., and Imashuku, S. (2002). Frequent co-expression of HoxA9 and Meis1 genes in infant acute lymphoblastic leukaemia with MLL rearrangement. Br J Haematol *119*, 119-121.

Ito, K., Hirao, A., Arai, F., Takubo, K., Matsuoka, S., Miyamoto, K., Ohmura, M., Naka, K., Hosokawa, K., Ikeda, Y., *et al.* (2006). Reactive oxygen species act through p38 MAPK to limit the lifespan of hematopoietic stem cells. Nature medicine *12*, 446-451.

Ivan, M., Kondo, K., Yang, H., Kim, W., Valiando, J., Ohh, M., Salic, A., Asara, J.M., Lane, W.S., and Kaelin, W.G., Jr. (2001). HIFalpha targeted for VHL-mediated destruction by proline hydroxylation: implications for O2 sensing. Science *292*, 464-468.

Ivanovic, Z., Hermitte, F., Brunet de la Grange, P., Dazey, B., Belloc, F., Lacombe, F., Vezon, G., and Praloran, V. (2004). Simultaneous maintenance of human cord blood SCID-repopulating cells and expansion of committed progenitors at low O2 concentration (3%). Stem Cells *22*, 716-724.

Iyer, N.V., Kotch, L.E., Agani, F., Leung, S.W., Laughner, E., Wenger, R.H., Gassmann, M., Gearhart, J.D., Lawler, A.M., Yu, A.Y., *et al.* (1998). Cellular and developmental control of O2 homeostasis by hypoxia-inducible factor 1 alpha. Genes & development *12*, 149-162.

Jaakkola, P., Mole, D.R., Tian, Y.M., Wilson, M.I., Gielbert, J., Gaskell, S.J., Kriegsheim, A., Hebestreit, H.F., Mukherji, M., Schofield, C.J., *et al.* (2001). Targeting of HIF-alpha to the von Hippel-Lindau ubiquitylation complex by O2-regulated prolyl hydroxylation. Science *292*, 468-472.

Jang, Y.Y., and Sharkis, S.J. (2007). A low level of reactive oxygen species selects for primitive hematopoietic stem cells that may reside in the low-oxygenic niche. Blood *110*, 3056-3063.

Jewell, U.R., Kvietikova, I., Scheid, A., Bauer, C., Wenger, R.H., and Gassmann, M. (2001). Induction of HIF-1alpha in response to hypoxia is instantaneous. FASEB J *15*, 1312-1314.

Jiang, B.H., Agani, F., Passaniti, A., and Semenza, G.L. (1997). V-SRC induces expression of hypoxia-inducible factor 1 (HIF-1) and transcription of genes encoding vascular endothelial growth factor and enolase 1: involvement of HIF-1 in tumor progression. Cancer Res *57*, 5328-5335.

Jordan, C.T., McKearn, J.P., and Lemischka, I.R. (1990). Cellular and developmental properties of fetal hematopoietic stem cells. Cell *61*, 953-963.

Kaelin, W.G., Jr., and Ratcliffe, P.J. (2008). Oxygen sensing by metazoans: the central role of the HIF hydroxylase pathway. Mol Cell *30*, 393-402.
Kamura, T., Sato, S., Iwai, K., Czyzyk-Krzeska, M., Conaway, R.C., and Conaway, J.W. (2000). Activation of HIF1alpha ubiquitination by a reconstituted von Hippel-Lindau (VHL) tumor suppressor complex. Proc Natl Acad Sci U S A *97*, 10430-10435.
Katahira, J., and Mizoguchi, H. (1987). Improvement of culture conditions for human megakaryocytic and pluripotent progenitor cells by low oxygen tension. Int J Cell Cloning *5*, 412-420.
Kawagoe, H., Humphries, R.K., Blair, A., Sutherland, H.J., and Hogge, D.E. (1999). Expression of HOX genes, HOX cofactors, and MLL in phenotypically and functionally defined subpopulations of leukemic and normal human hematopoietic cells. Leukemia *13*, 687-698.
Kiel, M.J., Radice, G.L., and Morrison, S.J. (2007). Lack of evidence that hematopoietic stem cells depend on N-cadherin-mediated adhesion to osteoblasts for their maintenance. Cell Stem Cell *1*, 204-217.
Kiel, M.J., Yilmaz, O.H., Iwashita, T., Terhorst, C., and Morrison, S.J. (2005). SLAM family receptors distinguish hematopoietic stem and progenitor cells and reveal endothelial niches for stem cells. Cell *121*, 1109-1121.
Kikuchi, K., Holdway, J.E., Werdich, A.A., Anderson, R.M., Fang, Y., Egnaczyk, G.F., Evans, T., Macrae, C.A., Stainier, D.Y., and Poss, K.D. (2010). Primary contribution to zebrafish heart regeneration by gata4(+) cardiomyocytes. Nature *464*, 601-605.
Kim, C.G., Lee, J.J., Jung, D.Y., Jeon, J., Heo, H.S., Kang, H.C., Shin, J.H., Cho, Y.S., Cha, K.J., Kim, C.G., *et al.* (2006a). Profiling of differentially expressed genes in human stem cells by cDNA microarray. Mol Cells *21*, 343-355.
Kim, J.W., Gao, P., and Dang, C.V. (2007). Effects of hypoxia on tumor metabolism. Cancer Metastasis Rev *26*, 291-298.
Kim, J.W., Tchernyshyov, I., Semenza, G.L., and Dang, C.V. (2006b). HIF-1-mediated expression of pyruvate dehydrogenase kinase: a metabolic switch required for cellular adaptation to hypoxia. Cell Metab *3*, 177-185.
Kim, M., Turnquist, H., Jackson, J., Sgagias, M., Yan, Y., Gong, M., Dean, M., Sharp, J.G., and Cowan, K. (2002). The multidrug resistance transporter ABCG2 (breast cancer resistance protein 1) effluxes Hoechst 33342 and is overexpressed in hematopoietic stem cells. Clin Cancer Res *8*, 22-28.
Kimble, J.E., and White, J.G. (1981). On the control of germ cell development in Caenorhabditis elegans. Dev Biol *81*, 208-219.
Kirito, K., Fox, N., and Kaushansky, K. (2004). Thrombopoietin induces HOXA9 nuclear transport in immature hematopoietic cells: potential mechanism by which the hormone favorably affects hematopoietic stem cells. Mol Cell Biol *24*, 6751-6762.

Koller, M.R., Bender, J.G., Miller, W.M., and Papoutsakis, E.T. (1992). Reduced oxygen tension increases hematopoiesis in long-term culture of human stem and progenitor cells from cord blood and bone marrow. Exp Hematol *20*, 264-270.

Kubota, Y., Takubo, K., and Suda, T. (2008). Bone marrow long label-retaining cells reside in the sinusoidal hypoxic niche. Biochem Biophys Res Commun *366*, 335-339.

Kuhn, B., del Monte, F., Hajjar, R.J., Chang, Y.S., Lebeche, D., Arab, S., and Keating, M.T. (2007). Periostin induces proliferation of differentiated cardiomyocytes and promotes cardiac repair. Nat Med *13*, 962-969.

Laflamme, M.A., and Murry, C.E. (2011). Heart regeneration. Nature *473*, 326-335.

Laflamme, M.A., Myerson, D., Saffitz, J.E., and Murry, C.E. (2002). Evidence for cardiomyocyte repopulation by extracardiac progenitors in transplanted human hearts. Circulation research *90*, 634-640.

LaIuppa, J.A., Papoutsakis, E.T., and Miller, W.M. (1998). Oxygen tension alters the effects of cytokines on the megakaryocyte, erythrocyte, and granulocyte lineages. Exp Hematol *26*, 835-843.

Laughner, E., Taghavi, P., Chiles, K., Mahon, P.C., and Semenza, G.L. (2001). HER2 (neu) signaling increases the rate of hypoxia-inducible factor 1alpha (HIF-1alpha) synthesis: novel mechanism for HIF-1-mediated vascular endothelial growth factor expression. Mol Cell Biol *21*, 3995-4004.

Laugwitz, K.L., Moretti, A., Lam, J., Gruber, P., Chen, Y., Woodard, S., Lin, L.Z., Cai, C.L., Lu, M.M., Reth, M., *et al.* (2005). Postnatal isl1+ cardioblasts enter fully differentiated cardiomyocyte lineages. Nature *433*, 647-653.

Lawrence, H.J., Christensen, J., Fong, S., Hu, Y.L., Weissman, I., Sauvageau, G., Humphries, R.K., and Largman, C. (2005). Loss of expression of the Hoxa-9 homeobox gene impairs the proliferation and repopulating ability of hematopoietic stem cells. Blood *106*, 3988-3994.

Lepilina, A., Coon, A.N., Kikuchi, K., Holdway, J.E., Roberts, R.W., Burns, C.G., and Poss, K.D. (2006). A dynamic epicardial injury response supports progenitor cell activity during zebrafish heart regeneration. Cell *127*, 607-619.

Li, H.Y., Chien, Y., Chen, Y.J., Chen, S.F., Chang, Y.L., Chiang, C.H., Jeng, S.Y., Chang, C.M., Wang, M.L., Chen, L.K., *et al.* (2011). Reprogramming induced pluripotent stem cells in the absence of c-Myc for differentiation into hepatocyte-like cells. Biomaterials *32*, 5994-6005.

Li, J.M., Poolman, R.A., and Brooks, G. (1998). Role of G1 phase cyclins and cyclin-dependent kinases during cardiomyocyte hypertrophic growth in rats. Am J Physiol *275*, H814-822.

Li, Z., and Li, L. (2006). Understanding hematopoietic stem-cell microenvironments. Trends Biochem Sci *31*, 589-595.

Li, Z., Wang, D., Messing, E.M., and Wu, G. (2005). VHL protein-interacting deubiquitinating enzyme 2 deubiquitinates and stabilizes HIF-1alpha. EMBO Rep *6*, 373-378.
Lilly, A.J., Johnson, W.E., and Bunce, C.M. (2011). The haematopoietic stem cell niche: new insights into the mechanisms regulating haematopoietic stem cell behaviour. Stem Cells Int *2011*, 274564.
Limana, F., Zacheo, A., Mocini, D., Mangoni, A., Borsellino, G., Diamantini, A., De Mori, R., Battistini, L., Vigna, E., Santini, M., *et al.* (2007). Identification of myocardial and vascular precursor cells in human and mouse epicardium. Circulation research *101*, 1255-1265.
Liu, Q., Moller, U., Flugel, D., and Kietzmann, T. (2004). Induction of plasminogen activator inhibitor I gene expression by intracellular calcium via hypoxia-inducible factor-1. Blood *104*, 3993-4001.
Lo Celso, C., Wu, J.W., and Lin, C.P. (2009). In vivo imaging of hematopoietic stem cells and their microenvironment. Journal of biophotonics *2*, 619-631.
Loffredo, F.S., Steinhauser, M.L., Gannon, J., and Lee, R.T. (2011). Bone marrow-derived cell therapy stimulates endogenous cardiomyocyte progenitors and promotes cardiac repair. Cell Stem Cell *8*, 389-398.
Majeti, R., Park, C.Y., and Weissman, I.L. (2007). Identification of a hierarchy of multipotent hematopoietic progenitors in human cord blood. Cell Stem Cell *1*, 635-645.
Malumbres, M., and Barbacid, M. (2009). Cell cycle, CDKs and cancer: a changing paradigm. Nat Rev Cancer *9*, 153-166.
Marin-Hernandez, A., Gallardo-Perez, J.C., Ralph, S.J., Rodriguez-Enriquez, S., and Moreno-Sanchez, R. (2009). HIF-1alpha Modulates Energy Metabolism in Cancer Cells by Inducing Over-expression of Specific Glycolytic Isoforms. Mini Rev Med Chem.
Martin-Puig, S., Wang, Z., and Chien, K.R. (2008). Lives of a heart cell: tracing the origins of cardiac progenitors. Cell Stem Cell *2*, 320-331.
Martin, C.M., Ferdous, A., Gallardo, T., Humphries, C., Sadek, H., Caprioli, A., Garcia, J.A., Szweda, L.I., Garry, M.G., and Garry, D.J. (2008). Hypoxia-inducible factor-2alpha transactivates Abcg2 and promotes cytoprotection in cardiac side population cells. Circ Res *102*, 1075-1081.
Martin, C.M., Meeson, A.P., Robertson, S.M., Hawke, T.J., Richardson, J.A., Bates, S., Goetsch, S.C., Gallardo, T.D., and Garry, D.J. (2004). Persistent expression of the ATP-binding cassette transporter, Abcg2, identifies cardiac SP cells in the developing and adult heart. Dev Biol *265*, 262-275.
Mastrogiannaki, M., Matak, P., Keith, B., Simon, M.C., Vaulont, S., and Peyssonnaux, C. (2009). HIF-2alpha, but not HIF-1alpha, promotes iron absorption in mice. J Clin Invest *119*, 1159-1166.

Matsuura, K., Nagai, T., Nishigaki, N., Oyama, T., Nishi, J., Wada, H., Sano, M., Toko, H., Akazawa, H., Sato, T., *et al.* (2004). Adult cardiac Sca-1-positive cells differentiate into beating cardiomyocytes. Journal of Biological Chemistry *279*, 11384-11391.

Maxwell, P.H., Wiesener, M.S., Chang, G.W., Clifford, S.C., Vaux, E.C., Cockman, M.E., Wykoff, C.C., Pugh, C.W., Maher, E.R., and Ratcliffe, P.J. (1999). The tumour suppressor protein VHL targets hypoxia-inducible factors for oxygen-dependent proteolysis. Nature *399*, 271-275.

Maxwell, P.J., Gallagher, R., Seaton, A., Wilson, C., Scullin, P., Pettigrew, J., Stratford, I.J., Williams, K.J., Johnston, P.G., and Waugh, D.J. (2007). HIF-1 and NF-kappaB-mediated upregulation of CXCR1 and CXCR2 expression promotes cell survival in hypoxic prostate cancer cells. Oncogene *26*, 7333-7345.

McCune, J.M., Namikawa, R., Kaneshima, H., Shultz, L.D., Lieberman, M., and Weissman, I.L. (1988). The SCID-hu mouse: murine model for the analysis of human hematolymphoid differentiation and function. Science *241*, 1632-1639.

McFadden, D.G., Barbosa, A.C., Richardson, J.A., Schneider, M.D., Srivastava, D., and Olson, E.N. (2005). The Hand1 and Hand2 transcription factors regulate expansion of the embryonic cardiac ventricles in a gene dosage-dependent manner. Development *132*, 189-201.

Meissner, K., Heydrich, B., Jedlitschky, G., Meyer Zu Schwabedissen, H., Mosyagin, I., Dazert, P., Eckel, L., Vogelgesang, S., Warzok, R.W., Bohm, M., *et al.* (2006). The ATP-binding cassette transporter ABCG2 (BCRP), a marker for side population stem cells, is expressed in human heart. J Histochem Cytochem *54*, 215-221.

Mikawa, T., and Gourdie, R.G. (1996). Pericardial mesoderm generates a population of coronary smooth muscle cells migrating into the heart along with ingrowth of the epicardial organ. Dev Biol *174*, 221-232.

Milne, T.A., Martin, M.E., Brock, H.W., Slany, R.K., and Hess, J.L. (2005). Leukemogenic MLL fusion proteins bind across a broad region of the Hox a9 locus, promoting transcription and multiple histone modifications. Cancer Res *65*, 11367-11374.

Miquel, J., Economos, A.C., Fleming, J., and Johnson, J.E., Jr. (1980). Mitochondrial role in cell aging. Experimental gerontology *15*, 575-591.

Mohyeldin, A., Garzon-Muvdi, T., and Quinones-Hinojosa, A. (2010). Oxygen in stem cell biology: a critical component of the stem cell niche. Cell Stem Cell *7*, 150-161.

Morrison, S.J., and Spradling, A.C. (2008). Stem cells and niches: mechanisms that promote stem cell maintenance throughout life. Cell *132*, 598-611.

Morrison, S.J., Uchida, N., and Weissman, I.L. (1995). The biology of hematopoietic stem cells. Annu Rev Cell Dev Biol *11*, 35-71.

Moskow, J.J., Bullrich, F., Huebner, K., Daar, I.O., and Buchberg, A.M. (1995). Meis1, a PBX1-related homeobox gene involved in myeloid leukemia in BXH-2 mice. Molecular and Cellular Biology *15*, 5434-5443.
Murray, L., Chen, B., Galy, A., Chen, S., Tushinski, R., Uchida, N., Negrin, R., Tricot, G., Jagannath, S., Vesole, D., *et al.* (1995). Enrichment of human hematopoietic stem cell activity in the CD34+Thy-1+Lin- subpopulation from mobilized peripheral blood. Blood *85*, 368-378.
Nadal-Ginard, B. (2001). [Generation of new cardiomyocytes in the adult heart: Prospects of myocardial regeneration as an alternative to cardiac transplantation]. Rev Esp Cardiol *54*, 543-550.
Nakada, D., Levi, B.P., and Morrison, S.J. (2011). Integrating physiological regulation with stem cell and tissue homeostasis. Neuron *70*, 703-718.
Nakayama, K., Frew, I.J., Hagensen, M., Skals, M., Habelhah, H., Bhoumik, A., Kadoya, T., Erdjument-Bromage, H., Tempst, P., Frappell, P.B., *et al.* (2004). Siah2 regulates stability of prolyl-hydroxylases, controls HIF1alpha abundance, and modulates physiological responses to hypoxia. Cell *117*, 941-952.
Nohl, H., and Hegner, D. ((1978)). Eur J Biochem *82*, 563−567.
O'Connell, T.D., Rodrigo, M.C., and Simpson, P.C. (2007). Isolation and culture of adult mouse cardiac myocytes. Methods Mol Biol *357*, 271-296.
Oh, H., Bradfute, S.B., Gallardo, T.D., Nakamura, T., Gaussin, V., Mishina, Y., Pocius, J., Michael, L.H., Behringer, R.R., Garry, D.J., *et al.* (2003). Cardiac progenitor cells from adult myocardium: homing, differentiation, and fusion after infarction. Proc Natl Acad Sci U S A *100*, 12313-12318.
Okada, Y., Nagai, R., Sato, T., Matsuura, E., Minami, T., Morita, I., and Doi, T. (2003). Homeodomain proteins MEIS1 and PBXs regulate the lineage-specific transcription of the platelet factor 4 gene. Blood *101*, 4748-4756.
Olivey, H.E., and Svensson, E.C. (2010). Epicardial-myocardial signaling directing coronary vasculogenesis. Circulation research *106*, 818-832.
Orrenius, S., Gogvadze, V., and Zhivotovsky, B. (2007). Mitochondrial oxidative stress: implications for cell death. Annu Rev Pharmacol Toxicol *47*, 143-183.
Osawa, M., Hanada, K., Hamada, H., and Nakauchi, H. (1996). Long-term lymphohematopoietic reconstitution by a single CD34-low/negative hematopoietic stem cell. Science *273*, 242-245.
Panchision, D.M. (2009). The role of oxygen in regulating neural stem cells in development and disease. J Cell Physiol *220*, 562-568.
Papandreou, I., Cairns, R.A., Fontana, L., Lim, A.L., and Denko, N.C. (2006). HIF-1 mediates adaptation to hypoxia by actively downregulating mitochondrial oxygen consumption. Cell Metab *3*, 187-197.
Park, M.S., and Koff, A. (2001). Overview of the cell cycle. Curr Protoc Cell Biol *Chapter 8*, Unit 8 1.

Park, M.T., and Lee, S.J. (2003). Cell cycle and cancer. J Biochem Mol Biol *36*, 60-65.
Parmar, K., Mauch, P., Vergilio, J.A., Sackstein, R., and Down, J.D. (2007). Distribution of hematopoietic stem cells in the bone marrow according to regional hypoxia. Proc Natl Acad Sci U S A *104*, 5431-5436.
Pasarica, M., Sereda, O.R., Redman, L.M., Albarado, D.C., Hymel, D.T., Roan, L.E., Rood, J.C., Burk, D.H., and Smith, S.R. (2009). Reduced adipose tissue oxygenation in human obesity: evidence for rarefaction, macrophage chemotaxis, and inflammation without an angiogenic response. Diabetes *58*, 718-725.
Passier, R., van Laake, L.W., and Mummery, C.L. (2008). Stem-cell-based therapy and lessons from the heart. Nature *453*, 322-329.
Pasumarthi, K.B., and Field, L.J. (2002). Cardiomyocyte cell cycle regulation. Circ Res *90*, 1044-1054.
Pasumarthi, K.B., Nakajima, H., Nakajima, H.O., Soonpaa, M.H., and Field, L.J. (2005). Targeted expression of cyclin D2 results in cardiomyocyte DNA synthesis and infarct regression in transgenic mice. Circ Res *96*, 110-118.
Patel, S.A., and Simon, M.C. (2008). Biology of hypoxia-inducible factor-2alpha in development and disease. Cell Death Differ *15*, 628-634.
Peault, B., Weissman, I., and Baum, C. (1993). Analysis of candidate human blood stem cells in "humanized" immune-deficiency SCID mice. Leukemia *7 Suppl 2*, S98-101.
Pedersen, M., Lofstedt, T., Sun, J., Holmquist-Mengelbier, L., Pahlman, S., and Ronnstrand, L. (2008). Stem cell factor induces HIF-1alpha at normoxia in hematopoietic cells. Biochem Biophys Res Commun *377*, 98-103.
Perry, J.M., and Li, L. (2012). To be or not to be a stem cell: dissection of cellular and molecular components of haematopoietic stem cell niches. EMBO J *31*, 1060-1061.
Pietras, E.M., Warr, M.R., and Passegue, E. (2011). Cell cycle regulation in hematopoietic stem cells. J Cell Biol *195*, 709-720.
Pillay, L.M., Forrester, A.M., Erickson, T., Berman, J.N., and Waskiewicz, A.J. (2010). The Hox cofactors Meis1 and Pbx act upstream of gata1 to regulate primitive hematopoiesis. Dev Biol *340*, 306-317.
Pineault, N., Abramovich, C., Ohta, H., and Humphries, R.K. (2004). Differential and common leukemogenic potentials of multiple NUP98-Hox fusion proteins alone or with Meis1. Molecular and Cellular Biology *24*, 1907-1917.
Pineault, N., Buske, C., Feuring-Buske, M., Abramovich, C., Rosten, P., Hogge, D.E., Aplan, P.D., and Humphries, R.K. (2003). Induction of acute myeloid leukemia in mice by the human leukemia-specific fusion gene NUP98-HOXD13 in concert with Meis1. Blood *101*, 4529-4538.

Pineault, N., Helgason, C.D., Lawrence, H.J., and Humphries, R.K. (2002a). Differential expression of Hox, Meis1, and Pbx1 genes in primitive cells throughout murine hematopoietic ontogeny. Exp Hematol *30*, 49-57.

Pineault, N., Helgason, C.D., Lawrence, H.J., and Humphries, R.K. (2002b). Differential expression of Hox, Meis1, and Pbx1 genes in primitive cells throughout murine hematopoietic ontogeny. Experimental Hematology *30*, 49-57.

Pio, B.S., Byrne, F.R., Aranda, R., Boulay, G., Spicher, K., Song, M.H., Birnbaumer, L., Phelps, M.E., Czernin, J., and Silverman, D.H. (2003). Noninvasive quantification of bowel inflammation through positron emission tomography imaging of 2-deoxy-2-[18F]fluoro-D-glucose-labeled white blood cells. Mol Imaging Biol *5*, 271-277.

Poolman, R.A., and Brooks, G. (1998). Expressions and activities of cell cycle regulatory molecules during the transition from myocyte hyperplasia to hypertrophy. J Mol Cell Cardiol *30*, 2121-2135.

Poolman, R.A., Gilchrist, R., and Brooks, G. (1998). Cell cycle profiles and expressions of p21CIP1 AND P27KIP1 during myocyte development. Int J Cardiol *67*, 133-142.

Poolman, R.A., Li, J.M., Durand, B., and Brooks, G. (1999). Altered expression of cell cycle proteins and prolonged duration of cardiac myocyte hyperplasia in p27KIP1 knockout mice. Circ Res *85*, 117-127.

Popescu, L.M., Gherghiceanu, M., Manole, C.G., and Faussone-Pellegrini, M.S. (2009). Cardiac renewing: interstitial Cajal-like cells nurse cardiomyocyte progenitors in epicardial stem cell niches. J Cell Mol Med *13*, 866-886.

Porrello, E.R., Mahmoud, A.I., Simpson, E., Hill, J.A., Richardson, J.A., Olson, E.N., and Sadek, H.A. (2011). Transient regenerative potential of the neonatal mouse heart. Science *331*, 1078-1080.

Qi, J., Nakayama, K., Gaitonde, S., Goydos, J.S., Krajewski, S., Eroshkin, A., Bar-Sagi, D., Bowtell, D., and Ronai, Z. (2008). The ubiquitin ligase Siah2 regulates tumorigenesis and metastasis by HIF-dependent and -independent pathways. Proc Natl Acad Sci U S A *105*, 16713-16718.

Qian, Q., Qian, H., Zhang, X., Zhu, W., Yan, Y., Ye, S., Peng, X., Li, W., Xu, Z., Sun, L., *et al.* (2011). 5-Azacytidine induces cardiac differentiation of human umbilical cord derived mesenchymal stem cells by activating extracellular regulated kinaseERK. Stem Cells Dev.

Quaini, F., Urbanek, K., Beltrami, A.P., Finato, N., Beltrami, C.A., Nadal-Ginard, B., Kajstura, J., Leri, A., and Anversa, P. (2002). Chimerism of the transplanted heart. N Engl J Med *346*, 5-15.

Reimer, K.A., Lowe, J.E., Rasmussen, M.M., and Jennings, R.B. (1977). The wavefront phenomenon of ischemic cell death. 1. Myocardial infarct size vs duration of coronary occlusion in dogs. Circulation *56*, 786-794.

Rius, J., Guma, M., Schachtrup, C., Akassoglou, K., Zinkernagel, A.S., Nizet, V., Johnson, R.S., Haddad, G.G., and Karin, M. (2008). NF-kappaB links innate immunity to the hypoxic response through transcriptional regulation of HIF-1alpha. Nature *453*, 807-811.

Roitbak, T., Surviladze, Z., and Cunningham, L.A. (2010). Continuous expression of HIF-1alpha in neural stem/progenitor cells. Cell Mol Neurobiol *31*, 119-133.

Rozovskaia, T., Feinstein, E., Mor, O., Foa, R., Blechman, J., Nakamura, T., Croce, C.M., Cimino, G., and Canaani, E. (2001). Upregulation of Meis1 and HoxA9 in acute lymphocytic leukemias with the t(4 : 11) abnormality. Oncogene *20*, 874-878.

Ryan, H.E., Lo, J., and Johnson, R.S. (1998). HIF-1 alpha is required for solid tumor formation and embryonic vascularization. The EMBO journal *17*, 3005-3015.

Salceda, S., and Caro, J. (1997). Hypoxia-inducible factor 1alpha (HIF-1alpha) protein is rapidly degraded by the ubiquitin-proteasome system under normoxic conditions. Its stabilization by hypoxia depends on redox-induced changes. J Biol Chem *272*, 22642-22647.

Scharenberg, C.W., Harkey, M.A., and Torok-Storb, B. (2002). The ABCG2 transporter is an efficient Hoechst 33342 efflux pump and is preferentially expressed by immature human hematopoietic progenitors. Blood *99*, 507-512.

Schenke-Layland, K., Nsair, A., Van Handel, B., Angelis, E., Gluck, J.M., Votteler, M., Goldhaber, J.I., Mikkola, H.K., Kahn, M., and Maclellan, W.R. (2011). Recapitulation of the embryonic cardiovascular progenitor cell niche. Biomaterials *32*, 2748-2756.

Schofield, R. (1978). The relationship between the spleen colony-forming cell and the haemopoietic stem cell. Blood cells *4*, 7-25.

Scholz, H., and Kirschner, K.M. (2011). Oxygen-Dependent Gene Expression in Development and Cancer: Lessons Learned from the Wilms' Tumor Gene, WT1. Front Mol Neurosci *4*, 4.

Scortegagna, M., Ding, K., Oktay, Y., Gaur, A., Thurmond, F., Yan, L.J., Marck, B.T., Matsumoto, A.M., Shelton, J.M., Richardson, J.A., *et al.* (2003a). Multiple organ pathology, metabolic abnormalities and impaired homeostasis of reactive oxygen species in Epas1-/- mice. Nat Genet *35*, 331-340.

Scortegagna, M., Ding, K., Zhang, Q., Oktay, Y., Bennett, M.J., Bennett, M., Shelton, J.M., Richardson, J.A., Moe, O., and Garcia, J.A. (2005). HIF-2alpha regulates murine hematopoietic development in an erythropoietin-dependent manner. Blood *105*, 3133-3140.

Scortegagna, M., Morris, M.A., Oktay, Y., Bennett, M., and Garcia, J.A. (2003b). The HIF family member EPAS1/HIF-2alpha is required for normal hematopoiesis in mice. Blood *102*, 1634-1640.

Segers, V.F., and Lee, R.T. (2008). Stem-cell therapy for cardiac disease. Nature *451*, 937-942.
Semenza, G.L. (2001). HIF-1 and mechanisms of hypoxia sensing. Curr Opin Cell Biol *13*, 167-171.
Semenza, G.L. (2004). Hydroxylation of HIF-1: oxygen sensing at the molecular level. Physiology (Bethesda) *19*, 176-182.
Semenza, G.L. (2007a). Hypoxia-inducible factor 1 (HIF-1) pathway. Sci STKE *2007*, cm8.
Semenza, G.L. (2007b). Life with oxygen. Science *318*, 62-64.
Semenza, G.L. (2007c). Oxygen-dependent regulation of mitochondrial respiration by hypoxia-inducible factor 1. Biochem J *405*, 1-9.
Semenza, G.L. (2009a). Regulation of cancer cell metabolism by hypoxia-inducible factor 1. Semin Cancer Biol *19*, 12-16.
Semenza, G.L. (2009b). Regulation of oxygen homeostasis by hypoxia-inducible factor 1. Physiology (Bethesda) *24*, 97-106.
Semenza, G.L. (2010). Oxygen homeostasis. Wiley Interdiscip Rev Syst Biol Med *2*, 336-361.
Semenza, G.L., and Wang, G.L. (1992). A nuclear factor induced by hypoxia via de novo protein synthesis binds to the human erythropoietin gene enhancer at a site required for transcriptional activation. Mol Cell Biol *12*, 5447-5454.
Shanmugam, K., Green, N.C., Rambaldi, I., Saragovi, H.U., and Featherstone, M.S. (1999). PBX and MEIS as non-DNA-binding partners in trimeric complexes with HOX proteins. Mol Cell Biol *19*, 7577-7588.
Shen, W.F., Montgomery, J.C., Rozenfeld, S., Moskow, J.J., Lawrence, H.J., Buchberg, A.M., and Largman, C. (1997). AbdB-like Hox proteins stabilize DNA binding by the Meis1 homeodomain proteins. Mol Cell Biol *17*, 6448-6458.
Shen, W.F., Rozenfeld, S., Kwong, A., Kom ves, L.G., Lawrence, H.J., and Largman, C. (1999). HOXA9 forms triple complexes with PBX2 and MEIS1 in myeloid cells. Mol Cell Biol *19*, 3051-3061.
Shima, H., Takubo, K., Tago, N., Iwasaki, H., Arai, F., Takahashi, T., and Suda, T. (2010). Acquisition of G(0) state by CD34-positive cord blood cells after bone marrow transplantation. Exp Hematol *38*, 1231-1240.
Simsek, T., Kocabas, F., Zheng, J., Deberardinis, R.J., Mahmoud, A.I., Olson, E.N., Schneider, J.W., Zhang, C.C., and Sadek, H.A. (2010). The distinct metabolic profile of hematopoietic stem cells reflects their location in a hypoxic niche. Cell Stem Cell *7*, 380-390.
Slukvin, II (2011). Epicardial origin of cardiac CFU-Fs. Cell Stem Cell *9*, 492-493.
Smart, N., Bollini, S., Dube, K.N., Vieira, J.M., Zhou, B., Davidson, S., Yellon, D., Riegler, J., Price, A.N., Lythgoe, M.F., *et al.* (2011). De novo cardiomyocytes from within the activated adult heart after injury. Nature *474*, 640-644.

Smart, N., Risebro, C.A., Melville, A.A., Moses, K., Schwartz, R.J., Chien, K.R., and Riley, P.R. (2007). Thymosin beta4 induces adult epicardial progenitor mobilization and neovascularization. Nature *445*, 177-182.

Smith, R.R., Barile, L., Cho, H.C., Leppo, M.K., Hare, J.M., Messina, E., Giacomello, A., Abraham, M.R., and Marban, E. (2007). Regenerative potential of cardiosphere-derived cells expanded from percutaneous endomyocardial biopsy specimens. Circulation *115*, 896-908.

Sohal, D.S., Nghiem, M., Crackower, M.A., Witt, S.A., Kimball, T.R., Tymitz, K.M., Penninger, J.M., and Molkentin, J.D. (2001). Temporally regulated and tissue-specific gene manipulations in the adult and embryonic heart using a tamoxifen-inducible Cre protein. Circulation Research *89*, 20-25.

Spradling, A., Drummond-Barbosa, D., and Kai, T. (2001). Stem cells find their niche. Nature *414*, 98-104.

Spradling, A.C., de Cuevas, M., Drummond-Barbosa, D., Keyes, L., Lilly, M., Pepling, M., and Xie, T. (1997). The Drosophila germarium: stem cells, germ line cysts, and oocytes. Cold Spring Harb Symp Quant Biol *62*, 25-34.

Takubo, K., Goda, N., Yamada, W., Iriuchishima, H., Ikeda, E., Kubota, Y., Shima, H., Johnson, R.S., Hirao, A., Suematsu, M., *et al.* (2010). Regulation of the HIF-1alpha level is essential for hematopoietic stem cells. Cell Stem Cell *7*, 391-402.

Thorsteinsdottir, U., Mamo, A., Kroon, E., Jerome, L., Bijl, J., Lawrence, H.J., Humphries, K., and Sauvageau, G. (2002). Overexpression of the myeloid leukemia-associated Hoxa9 gene in bone marrow cells induces stem cell expansion. Blood *99*, 121-129.

Tian, H., McKnight, S.L., and Russell, D.W. (1997). Endothelial PAS domain protein 1 (EPAS1), a transcription factor selectively expressed in endothelial cells. Genes Dev *11*, 72-82.

Till, J.E., and Mc, C.E. (1961). A direct measurement of the radiation sensitivity of normal mouse bone marrow cells. Radiat Res *14*, 213-222.

Turrens, J.F. (1997). Superoxide production by the mitochondrial respiratory chain. Biosci Rep *17*, 3-8.

Turrens, J.F. (2003). Mitochondrial formation of reactive oxygen species. J Physiol *552*, 335-344.

Urbanek, K., Cesselli, D., Rota, M., Nascimbene, A., De Angelis, A., Hosoda, T., Bearzi, C., Boni, A., Bolli, R., Kajstura, J., *et al.* (2006). Stem cell niches in the adult mouse heart. Proc Natl Acad Sci U S A *103*, 9226-9231.

van Vliet, P., Roccio, M., Smits, A.M., van Oorschot, A.A., Metz, C.H., van Veen, T.A., Sluijter, J.P., Doevendans, P.A., and Goumans, M.J. (2008). Progenitor cells isolated from the human heart: a potential cell source for regenerative therapy. Neth Heart J *16*, 163-169.

Vander Heiden, M.G., Cantley, L.C., and Thompson, C.B. (2009). Understanding the Warburg effect: the metabolic requirements of cell proliferation. Science *324*, 1029-1033.
Wagner, K.D., Wagner, N., Bondke, A., Nafz, B., Flemming, B., Theres, H., and Scholz, H. (2002). The Wilms' tumor suppressor Wt1 is expressed in the coronary vasculature after myocardial infarction. FASEB J *16*, 1117-1119.
Wagner, K.D., Wagner, N., Wellmann, S., Schley, G., Bondke, A., Theres, H., and Scholz, H. (2003). Oxygen-regulated expression of the Wilms' tumor suppressor Wt1 involves hypoxia-inducible factor-1 (HIF-1). FASEB J *17*, 1364-1366.
Walker, M.R., Patel, K.K., and Stappenbeck, T.S. (2009). The stem cell niche. J Pathol *217*, 169-180.
Walsh, S., Ponten, A., Fleischmann, B.K., and Jovinge, S. (2010). Cardiomyocyte cell cycle control and growth estimation in vivo--an analysis based on cardiomyocyte nuclei. Cardiovasc Res *86*, 365-373.
Wang, G.G., Pasillas, M.P., and Kamps, M.P. (2005). Meis1 programs transcription of FLT3 and cancer stem cell character, using a mechanism that requires interaction with Pbx and a novel function of the Meis1 C-terminus. Blood *106*, 254-264.
Wang, G.G., Pasillas, M.P., and Kamps, M.P. (2006). Persistent transactivation by meis1 replaces hox function in myeloid leukemogenesis models: evidence for co-occupancy of meis1-pbx and hox-pbx complexes on promoters of leukemia-associated genes. Mol Cell Biol *26*, 3902-3916.
Wang, G.L., Jiang, B.H., Rue, E.A., and Semenza, G.L. (1995a). Hypoxia-inducible factor 1 is a basic-helix-loop-helix-PAS heterodimer regulated by cellular O2 tension. Proc Natl Acad Sci U S A *92*, 5510-5514.
Wang, G.L., Jiang, B.H., and Semenza, G.L. (1995b). Effect of altered redox states on expression and DNA-binding activity of hypoxia-inducible factor 1. Biochem Biophys Res Commun *212*, 550-556.
Wang, G.L., and Semenza, G.L. (1995). Purification and characterization of hypoxia-inducible factor 1. J Biol Chem *270*, 1230-1237.
Wang, L.D., and Wagers, A.J. (2011). Dynamic niches in the origination and differentiation of haematopoietic stem cells. Nat Rev Mol Cell Biol.
Warr, M.R., Pietras, E.M., and Passegue, E. (2011). Mechanisms controlling hematopoietic stem cell functions during normal hematopoiesis and hematological malignancies. Wiley Interdiscip Rev Syst Biol Med *3*, 681-701.
Weinberger, F., Mehrkens, D., Friedrich, F.W., Stubbendorff, M., Hua, X., Muller, J.C., Schrepfer, S., Evans, S.M., Carrier, L., and Eschenhagen, T. (2012). Localization of Islet-1-positive cells in the healthy and infarcted adult murine heart. Circ Res *110*, 1303-1310.

Weissman, I.L. (2000). Stem cells: units of development, units of regeneration, and units in evolution. Cell *100*, 157-168.
Wiesener, M.S., Jurgensen, J.S., Rosenberger, C., Scholze, C.K., Horstrup, J.H., Warnecke, C., Mandriota, S., Bechmann, I., Frei, U.A., Pugh, C.W., *et al.* (2003). Widespread hypoxia-inducible expression of HIF-2alpha in distinct cell populations of different organs. FASEB J *17*, 271-273.
Wiesener, M.S., Turley, H., Allen, W.E., Willam, C., Eckardt, K.U., Talks, K.L., Wood, S.M., Gatter, K.C., Harris, A.L., Pugh, C.W., *et al.* (1998). Induction of endothelial PAS domain protein-1 by hypoxia: characterization and comparison with hypoxia-inducible factor-1alpha. Blood *92*, 2260-2268.
Wilson, A., Laurenti, E., Oser, G., van der Wath, R.C., Blanco-Bose, W., Jaworski, M., Offner, S., Dunant, C.F., Eshkind, L., Bockamp, E., *et al.* (2008). Hematopoietic stem cells reversibly switch from dormancy to self-renewal during homeostasis and repair. Cell *135*, 1118-1129.
Wong, P., Iwasaki, M., Somervaille, T.C., So, C.W., and Cleary, M.L. (2007). Meis1 is an essential and rate-limiting regulator of MLL leukemia stem cell potential. Genes Dev *21*, 2762-2774.
Xie, T., and Spradling, A.C. (1998). decapentaplegic is essential for the maintenance and division of germline stem cells in the Drosophila ovary. Cell *94*, 251-260.
Xin, M., Kim, Y., Sutherland, L.B., Qi, X., McAnally, J., Schwartz, R.J., Richardson, J.A., Bassel-Duby, R., and Olson, E.N. (2011). Regulation of insulin-like growth factor signaling by Yap governs cardiomyocyte proliferation and embryonic heart size. Sci Signal *4*, ra70.
Xu, Y., Li, J., Zuo, Y., Deng, J., Wang, L.S., and Chen, G.Q. (2011). SUMO-specific protease 1 regulates the in vitro and in vivo growth of colon cancer cells with the upregulated expression of CDK inhibitors. Cancer Lett *309*, 78-84.
Yan, J., Chen, Y.X., Desmond, A., Silva, A., Yang, Y., Wang, H., and Hua, X. (2006). Cdx4 and menin co-regulate Hoxa9 expression in hematopoietic cells. PLoS One *1*, e47.
Yilmaz, O.H., Kiel, M.J., and Morrison, S.J. (2006). SLAM family markers are conserved among hematopoietic stem cells from old and reconstituted mice and markedly increase their purity. Blood *107*, 924-930.
Yu, A.Y., Frid, M.G., Shimoda, L.A., Wiener, C.M., Stenmark, K., and Semenza, G.L. (1998). Temporal, spatial, and oxygen-regulated expression of hypoxia-inducible factor-1 in the lung. Am J Physiol *275*, L818-826.
Zeisig, B.B., Milne, T., Garcia-Cuellar, M.P., Schreiner, S., Martin, M.E., Fuchs, U., Borkhardt, A., Chanda, S.K., Walker, J., Soden, R., *et al.* (2004). Hoxa9 and Meis1 are key targets for MLL-ENL-mediated cellular immortalization. Mol Cell Biol *24*, 617-628.

Zhang, C.C., and Lodish, H.F. (2005). Murine hematopoietic stem cells change their surface phenotype during ex vivo expansion. Blood *105*, 4314-4320.
Zhang, H., Gao, P., Fukuda, R., Kumar, G., Krishnamachary, B., Zeller, K.I., Dang, C.V., and Semenza, G.L. (2007). HIF-1 inhibits mitochondrial biogenesis and cellular respiration in VHL-deficient renal cell carcinoma by repression of C-MYC activity. Cancer Cell *11*, 407-420.
Zhang, J., Niu, C., Ye, L., Huang, H., He, X., Tong, W.G., Ross, J., Haug, J., Johnson, T., Feng, J.Q., *et al.* (2003). Identification of the haematopoietic stem cell niche and control of the niche size. Nature *425*, 836-841.
Zhao, C., Deng, W., and Gage, F.H. (2008). Mechanisms and functional implications of adult neurogenesis. Cell *132*, 645-660.
Zheng, J., Huynh, H., Umikawa, M., Silvany, R., and Zhang, C.C. (2011). Angiopoietin-like protein 3 supports the activity of hematopoietic stem cells in the bone marrow niche. Blood *117*, 470-479.
Zhong, J.F., Zhao, Y., Sutton, S., Su, A., Zhan, Y., Zhu, L., Yan, C., Gallaher, T., Johnston, P.B., Anderson, W.F., *et al.* (2005). Gene expression profile of murine long-term reconstituting vs. short-term reconstituting hematopoietic stem cells. Proc Natl Acad Sci U S A *102*, 2448-2453.
Zhou, B., Honor, L.B., He, H., Ma, Q., Oh, J.H., Butterfield, C., Lin, R.Z., Melero-Martin, J.M., Dolmatova, E., Duffy, H.S., *et al.* (2011). Adult mouse epicardium modulates myocardial injury by secreting paracrine factors. The Journal of clinical investigation *121*, 1894-1904.
Zhou, B., Ma, Q., Rajagopal, S., Wu, S.M., Domian, I., Rivera-Feliciano, J., Jiang, D., von Gise, A., Ikeda, S., Chien, K.R., *et al.* (2008). Epicardial progenitors contribute to the cardiomyocyte lineage in the developing heart. Nature *454*, 109-113.
Zhou, S., Huang, C., and Wei, Y. (2010). The metabolic switch and its regulation in cancer cells. Sci China Life Sci *53*, 942-958.
Zon, L.I. (2008). Intrinsic and extrinsic control of haematopoietic stem-cell self-renewal. Nature *453*, 306-313.